Time-Resolved Measurements of a Transonic Compressor During Surge and Rotating Stall

by

Denver Jackson Osborne, Jr.

Thesis submitted to the Faculty of the
Virginia Polytechnic Institute and State University
in partial fulfillment of the requirements for the degree of

Master of Science

in

Mechanical Engineering

APPROVED:

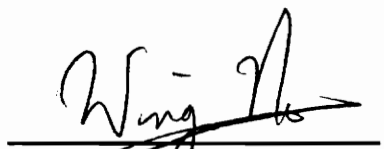

Dr. Wing F. Ng, Chairman

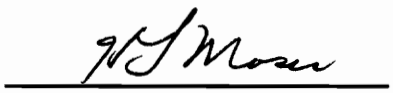

Dr. Hal L. Moses

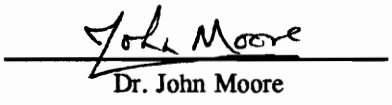

Dr. John Moore

August 1992

Blacksburg, Virginia

LD
5655
V855
1992
0836
C.2

Time-Resolved Measurements of a Transonic Compressor during Surge and Rotating Stall

by

Denver Jackson Osborne, Jr.

Dr. W. F. Ng, Chairman

Mechanical Engineering

(ABSTRACT)

This thesis presents the results from measurements taken during the transient unstable operation of an axial-flow transonic core-compressor rotor. The measurements were taken to better understand the unstable flow physics of transonic rotors. The rotor, commonly referred to as Rotor 37, was designed by NASA Lewis to be the first stage of an advanced, eight-stage, core-compressor having a high pressure ratio (about 20:1), good efficiency and sufficient stall margin. The rotor was tested without the presence of a stator (or any of the following seven stages) at the NASA Lewis single-stage, high-speed, core-compressor test-rig. The measurements were obtained with a single circumferential, high-response, total pressure and total temperature probe. The measurements were taken immediately after the machine was 'tripped' into unstable operation by slowly closing the downstream throttle valve. Measurements were obtained at several different spanwise locations and at two different operating speeds. The rotor was shown to exhibit many of the same characteristics typical of low-speed axial-flow machines. Both rotating stall cells and surge cycles were present during unstable operation. The surge cycles present immediately after the inception of unstable operation involved a large-extent single-cell

type rotating stall that was present only during the first half of the surge cycles (the second half of these surge cycles involved operation in the stable operating region). However, as the unstable operation progressed (approximately three to five surge cycles later), surge cycles were present that contained a multiple-cell smaller-extent type rotating stall that existed throughout the entire surge cycle with no partial operation in the stable operating region. Thus, compressor system recovery from single-cell large-extent rotating stall (partial operation in stable operating range during the surge cycle) is more probable than recovery from multiple-cell small-extent rotating stall (no operation in stable operating range during the surge cycle). Rotor wheel speed was shown to be an important variable in influencing the form of unstable operation. Surge and rotating stall were shown to be coupled during the unstable operation. Furthermore, the surge/stall coupling was shown to be related more by pressure interactions than by temperature or efficiency interactions. Also, this high hub-tip ratio transonic rotor was shown to exhibit instantaneous stalling across the entire blade span (typical of low-speed, high hub-tip ratio machines). Attempts to fit the data to Greitzer's one-dimensional lumped-parameter model are presented and the reasons for poor agreement are discussed.

Abstract

Acknowledgements

I wish to take this opportunity to express my appreciation for those who have contributed to the completion of this thesis. I would like to thank my family, in particular my sisters, Penny and Jackie and my parents, Mr. and Mrs. Denver J. Osborne Sr., for the support, encouragement and strength they have provided me throughout my school years. Without them, my education would not have been possible nor would it have had any meaning.

I would also like to thank professors Dr. John Moore, Dr. Hal L. Moses, and Dr. Wing F. Ng for the giving of their time to serve on my advisory committee. They have all willingly invested their valuable time towards my education by teaching several of my classes, answering my many questions, and by fostering my thought with new ideas. Furthermore, I am indeed sincerely grateful to my advisor and committee chair, Dr. Wing F. Ng, for the patience, support, and confidence he has given me through times of frustration and success. I simply could not have completed this work without his guidance. I would also like to express my gratitude to Dr. Albin Bölcs for his insightful comments and suggestions.

I would also like to thank those at the NASA Lewis Research Center in Cleveland, Ohio who contributed to this work. I thank Bob Gronski and Bob McCluskey for providing me with invaluable electronic and mechanical support. A special thanks goes out to Ken Suder for the tremendous all-around knowledge, help and support that he shared with me during my stay at NASA Lewis. A special thanks also goes out to Dr. Tony Strazisar for the time, effort and interest he has spent on this project. NASA Lewis also provided me with financial support during the majority of my graduate studies.

My thanks also goes out to all my fellow office mates who have helped me in various capacities during my research. I would especially like to thank: Dr. Philip Andrew, Dr. Kumud Ajmani, John Alday, Todd Ninnemann and Mary Beth Morris. Phil was a constant source of technical help and information. He has the rare quality of unselfishly giving his own time even when he is busy himself. John and Todd were both instrumental in getting me started with my research (no pun intended). Todd passed on his experience in building and testing high-frequency instrumentation. John educated me on the experimental procedures employed during the application of high-response instrumentation. John and Todd also provided answers to hundreds of questions for which I am truly grateful.

Table of Contents

List of Illustrations

List of Tables

Nomenclature

a	calibration constant, local speed of sound
A	cross-sectional area
C	degrees celsius
d	hot wire diameter
k	coefficient of thermal conductivity
K	degrees Kelvin
l	hot wire length
L	compressor or throttle duct length
m	calibration constant
P	pressure
Pa	pascals
r	ratio of static to total temperature
R	ideal gas constant for air, electrical resistance
s	seconds
T	temperature

U	mean blade speed
V	anemometer bridge voltage, plenum volume

GREEK LETTERS

γ	ratio of specific heats for air
η	isentropic efficiency
μ	absolute viscosity
π	pi (3.141593)
τ	time constant
ω	helmholtz resonator frequency

SUBSCRIPTS

1	refers to properties at rotor inlet
2	refers to properties at rotor exit
c	refers to the wire plane channel, refers to compressor
p	refers to plenum
s	refers to property of series resistor in anemometer circuitry
T	refers to a total or stagnation property
t	refers to throttle
w	refers to hot wire property
x	refers to axial direction

SUPERSCRIPTS

*	refers to property at aspirating probe throat
-	refers to non-dimensional variable

ACRONYMS AND ABBREVIATIONS

AC	refers to fluctuating quantity
atm	atmospheric pressure
BASIC	computer language
DC	refers to mean quantity
FFT	Fast Fourier Transform
GPIB	General Purpose Interface Board
IBM PC	International Business Machines Personal Computer
IFFT	Inverse Fast Fourier Transform
LVDT	Linear Variable Displacement Transducer
MIT	Massachusetts Institute of Technology
mil	one one-thousandths of an inch
NASA	National Aeronautics and Space Administration
rpm	Revolutions Per Minute
VPI	Virginia Polytechnic Institute and State University

1.0 Introduction

Since the birth of turbomachinery propulsion, one of the principal efforts of researchers has been to better understand the unstable operating range of axial-flow compressor systems. A better understanding of the unstable operating range provides information necessary for recovery, as well as information needed to extend the stable operating range. The study of compressor instability involves the integration of mathematical and analytical models with experimental techniques and measurements. The development of these models and experimental techniques is an iterative and continually evolving process.

This thesis presents the results of some exploratory type measurements taken during the transient unstable operation of a transonic core-compressor rotor. The word transient is used because the measurements were taken immediately after the rotor was 'tripped' into unstable operation by slowly closing the downstream throttle valve. The measurements were made with a single circumferential, high response, dual hot-wire aspirating probe, mounted 'piggyback' with a Kulite pressure transducer [1]. The rotor tested, commonly referred to as Rotor 37, was the first stage of a NASA Lewis, low

aspect-ratio, transonic, eight-stage, core-compressor design [2]. The rotor-only configuration was tested without the presence of the downstream stator. The experiment was conducted at the NASA Lewis Research Center's high-speed, single-stage, core-compressor research rig [3]. The data presented is quite unique in that this was the first time high response measurements of stagnation pressure, stagnation temperature, and hence efficiency have been taken in a harsh transonic environment during unstable operation. The probe was used to obtain data at different spanwise locations at the rotor exit and at two different operating speeds (100% and 90% design speed). This thesis presents and discusses the results obtained from the observations made from these measurements.

The unclassified literature contains very few measurements and very little information about transonic compressor rotors operating in the unstable range. Almost all measurements published are taken from low-speed machines; however, Garnier et al. [4] do present some high-speed machine data taken with high response pressure transducers. Thus, one of the goals of this research was to obtain some rather rare in-stall measurements of a transonic core-compressor rotor.

A few words are in order concerning the areas of application of the experimental measurements and observations presented in this thesis. The study of the behavior and general flow properties of the non-axisymmetric flow field present during unstable compressor system operation, has been of increasing importance and concern in recent years [5]. The motivation for this increased interest in post-stall compressor system behavior lies in the applications of stall recovery and stable operating range extension

(stall inception).

The observations presented in this thesis do not focus on the inception of stall, but instead concentrate on the post-stall behavior of the compressor. It is hoped that the information presented here can improve our understanding of the study of post-stall operation and recovery for a transonic rotor. If the engine enters a 'stagnation' stall condition, the only possible form of recovery may be to shut the engine down and restart. Therefore, it is clearly important to gain the ability to predict post-stall compression system behavior, as a basis for rational design of stagnation-resistant compressor systems [5]. Thus, as more is learned about the properties of post-stall compressor system operation, the more these variables can be incorporated into the process of designing compression systems that resist the danger of falling into non-recoverable stall.

Post-stall compression system operation is predicted by application and continued development of analytical mathematical models that simulate the fundamental physics of the system and its response. Moore [5,6] and Greitzer [5] have developed a model that predicts general post-stall transient behavior in axial compressor systems. Through the use of this model, much can be learned about the nature and governing behavior of the compression system after the onset of stall. This information can then be incorporated back into the engine design process to help design engines that resist 'stagnation' stall.

However, before any modeling efforts are considered successful, they must first be proven valid by comparison with experimental results. Thus, it is also of interest to research experimental and instrumentation techniques that can be used to measure the instantaneous post-stall transients present during the unstable operation of a compressor.

These experimental results can then be used for model modification and validation. No attempts have been made to use the present data to validate some of the existing models in the literature. This is reserved for future efforts. However, for completeness, a brief description of the efforts made to use the data to match Greitzer's one-dimensional, lumped-parameter model [7] is included.

The objective of this research work was to experimentally measure and subsequently document the flow physics of post-stall, transonic core-compressor operation. General observations and discussions concerning the unstable operation of the stage mentioned will be presented. Observations from the measurements revealed that the surge and rotating stall were coupled more by total pressure interactions than by temperature or efficiency interactions. The surge/stall cycle variations that occurred as the instability progressed are presented and discussed. The spanwise data showed basically the same phenomena occurring at all spans surveyed, the significance of this is discussed. Comparisons are made between the data taken at different operating speeds, this revealed the importance of wheel speed on the form of the unstable flow that was present. These and other observations presented in this thesis will provide general flow physics observations for future model development and alteration.

The following chapter outlines a brief literature review of the study of rotating stall and surge. The differences between the mechanism for rotating stall in a low-speed machine and a high-speed machine are discussed. Also presented is a summary of the instrumentation techniques that have been used to measure post-stall compressor operation. Chapter 3 discusses in detail the experiment, including: the rotor and test

facility, the probe and instrumentation set up, the data acquisition procedure, and a summary of the data presented. Chapter 4 presents data reduction and presentation concerns along with a full discussion of the observations taken from the measurements. Chapter 4 also presents the attempt made to fit the data to Greitzer's one-dimensional, lumped-parameter model [7]. Finally, chapter 5 summarizes the conclusions and discusses potential areas of future research. Appendix A presents traces of the raw data for total pressure ratio. Appendix B presents some unique contour plots of the spanwise transient stall behavior of the rotor.

2.0 Literature Review

This chapter gives a brief summary of some relevant background information pertaining to the study of compressor instability research. Two types of compressor instability flow phenomena (surge and rotating stall) are reviewed, and their relevance to engine operation discussed. The mechanism for rotating stall in a low-speed machine is reviewed, as well as the limitations of this theory when extended to high-speed machinery. Thus, a hypothetical mechanism for rotating stall propagation in a transonic machine is also discussed. Also presented is a brief summary of some of the past research efforts to measure transient unstable compressor operation with the use of high response instrumentation. Both sections are included for the facilitation of comparison with the results and observations presented in this thesis.

2.1 Types of Compressor Instability Flow Phenomena

As the mass flow rate through an axial compressor system is reduced from the

design value, the steady, attached, axisymmetric flow pattern that exists becomes unstable [7]. The basic flow patterns that could possibly result from this instability can be described as two separate flow phenomena. These are known as blade rotating stall (stall) and transient system mass flow surging (surge) [7]. They are two very different, but by no means unrelated phenomena. This is one of the main results discovered from the measurements presented in this thesis. The following presents a discussion of the phenomena of rotating stall and surge. Note that the discussion of the mechanism for rotating stall initially given here is limited to low-speed machinery. A hypothetical mechanism for rotating stall in a high-speed machine will be given subsequently.

The phenomena of rotating stall was first discovered by the group developing the centrifugal air compressors for the Whittle turbojet engine in 1938 [8]. Rotating stall involves a continuous stalling and un-stalling pattern of the compressor blades so that the stall 'cells' or 'zones' rotate around the circumference of the rotor. Emmons, et al. [9] was the first to give a qualitative explanation for the physical mechanisms that cause rotating stall cell propagation. Emmons' theory of rotating stall in an incompressible (low-speed) turbomachine environment is summarized by Greitzer [10] as follows.

Figure 1a shows a row of low-speed axial compressor blades operating at a high angle of attack. Suppose that there is some local inlet flow non-uniformity such that a high enough angle of attack is produced on blade B which causes separation. This separates the flow from the suction side of the blade and causes a region of flow blockage between blades B and C. This blockage causes the incoming flow to divert away from blade B and towards blades C and A, as the streamlines indicate. This results in an

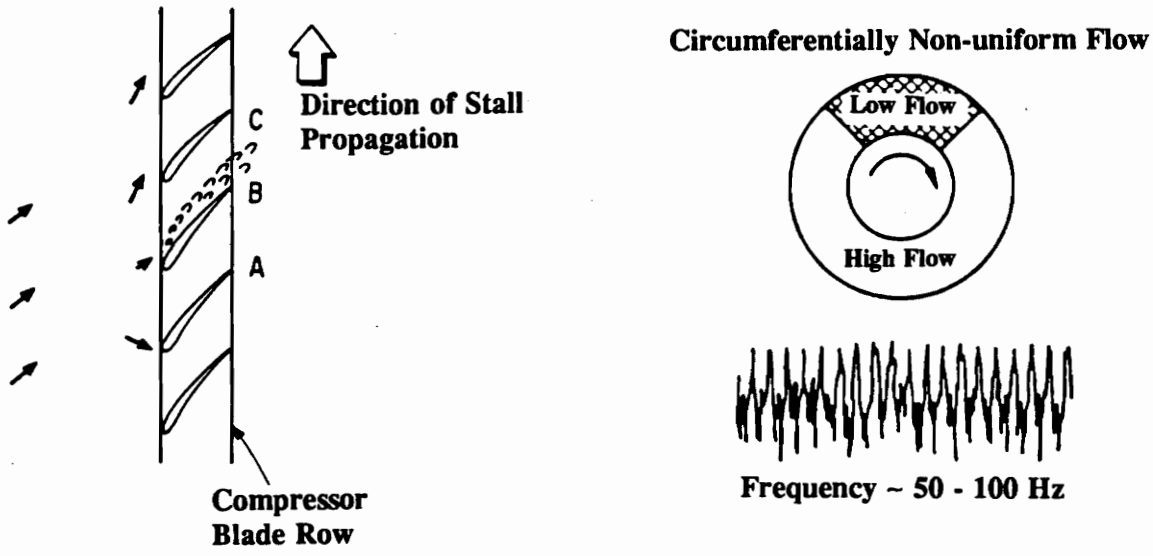

1a. Rotating Stall - Low Speed Machine

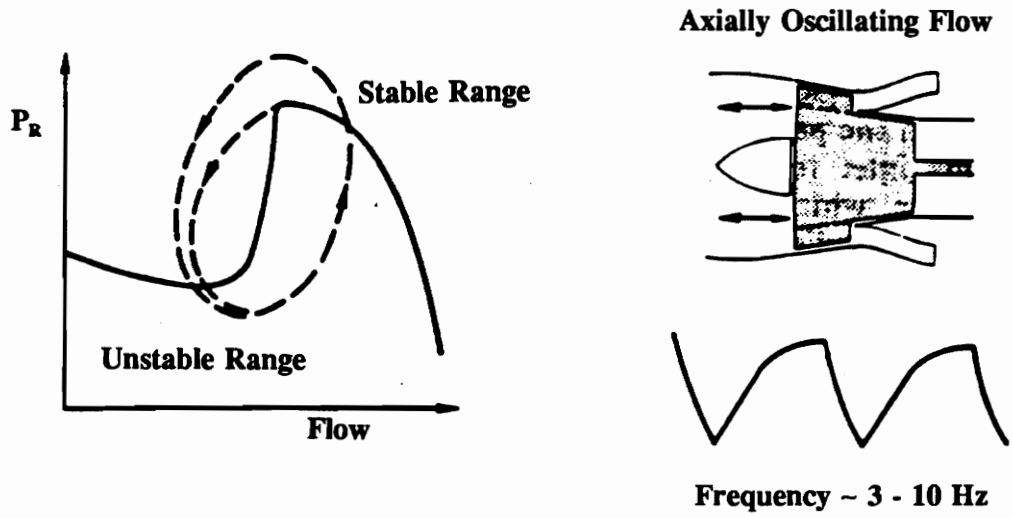

1b. Surge

Figure 1. Types of Compressor Instability Phenomena - Low Speed Machines (after Greitzer [7]).

increased angle of attack on blade C and a reduced angle of attack on blade A. Therefore, blade C is on the verge of separation while the flow across blade A is likely reattach. The stall will then propagate along the blade row in the direction shown, and under sufficient conditions may grow to occupy as much as half the compressor circumference [10]. Note that the large swing in the inlet flow angle of attack (see figure 1a) is made possible because of the ability of incompressible flow environments to propagate information upstream of a disturbance. This is a crucial requirement for Emmons' low-speed rotating stall propagation theory.

The following summarizes some general findings about rotating stall. One to several stall cells may simultaneously exist on a rotor [11], and they typically rotate at a constant speed (once fully developed) of approximately twenty to seventy percent of the wheel speed (in the absolute reference frame) [10]. The circumferential extent of a fully developed stall cell may vary from only a few blades to a substantial portion of the compressor annulus [8]. The stall cells may also appear only at the tip, or the hub of the blading, or may extend across the entire blade span [10]. Fully spanwise rotating stall is typical for high hub-tip ratio (low-speed) machines. These rotating stall cells consist of regions of highly reduced net through flow that contain local reverse flow and recirculation zones. However, the annulus averaged mass flow is relatively constant once the rotating stall becomes fully developed [10].

Emmons' theory for the mechanism of rotating stall propagation is based on the flow field properties of low-speed turbomachinery. The incompressible environment present in low-speed machines allows a relatively large swing in the inlet flow angle of

attack because of the ability of the flow to propagate disturbance information upstream. A relatively incompressible turbomachine environment alerts the oncoming flow (before the blades) of the downstream blockage, separation, and diversions that are present (at the blades) during rotating stall. It is critical to Emmons' low-speed rotating stall model for this information to be conveyed upstream to divert the oncoming streamlines and thus enable the stall to propagate.

The rotor investigated in this thesis has an inlet relative mach number of 1.2 at the blade hub (at 100% speed). The rotor contains a shock that stretches across the entire blade span. Thus, no information downstream of the shock wave can be propagated upstream of the rotor (except through the casing and hub boundary layers). Thus, in a fully spanwise transonic rotor, the oncoming flow does not see any possible disturbances in the rotor passages (even though the absolute inlet mach number is subsonic) [12]. Thus, the variation in the inlet angle of attack for transonic rotors is typically only about ±2° [12]. Without the ability of downstream information to be conveyed upstream, Emmons theory of rotating stall propagation does not hold in high-speed environments [12]. Furthermore, the open literature contains no theories for the mechanism of rotating stall propagation in a transonic rotor [12, 13].

The following presents a hypothetical mechanism for rotating stall propagation in a transonic rotor. The additional complexity believed to be fundamental in transonic rotor rotating stall is the shock wave structure. It is the shock wave that ultimately leads to the breakdown of Emmons' low-speed rotating stall theory. It is also the shock wave that is believed to provide the mechanism for (separation) rotating stall in transonic rotors. Figure 2 shows a schematic of the normal (stable) operation shock structure and the shock

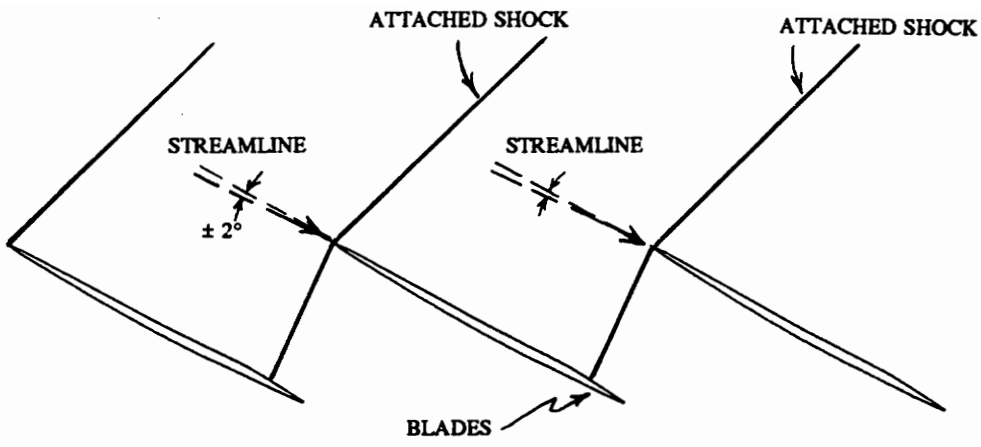

SHOCK STRUCTURE - NORMAL OPERATION

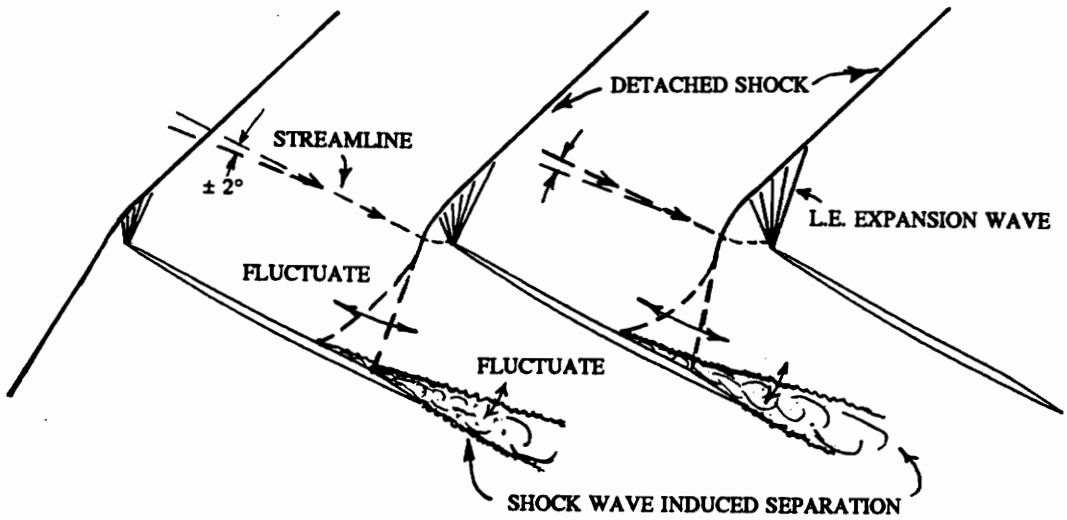

SHOCK STRUCTURE - ROTATING STALL

Figure 2. Hypothetical Mechanism for Rotating Stall in a Transonic Rotor (after Bölcs [12]).

structure present during rotating stall [12]. Normal operation shows an attached and relatively steady shock wave with the oncoming streamlines varying by approximately ±2°. However, during rotating stall the shock waves detach from the blades and fluctuate significantly, causing separation of the suction surface boundary layer and thus creating the separation necessary for the existence of rotating stall cells. It is worth noting that the oncoming streamlines still only fluctuate by ±2° during rotating stall because no information is propagated upstream of the rotor. The exact nature of the fluctuating shock structure could be caused by a surge cycle, a rotating 'pre-stall' wave, or a 'starting' and 'unstarting' type behavior in the intra-blade passages. The exact mechanism driving the shock structure is unknown at this time. However the importance remains that there is a more complex, shock structure/boundary layer type interaction that is the controlling mechanism for rotating stall cells in transonic rotors.

Prolonged engine operation in pure rotating stall is intolerable for several reasons. The extremely low efficiencies that occur during rotating stall can result in excessive temperatures that can effect both compressor, turbine and combustor life span [10]. Rotating stall also subjects the blades to rather large unsteady oscillating loads that tend to cause blade metal fatigue or even catastrophic failure [10]. Also, it may be impossible to return to an unstalled operating condition simply by opening the throttle because of system hysteresis effects. In this case, the only way to recover is by reducing the rotational speed of the compressor and subsequently cause a large decrease in pressure ratio [10]. Clearly, rotating stall is a condition that cannot be tolerated during normal engine operation.

Axial-flow compressor surge is a fundamentally different kind of flow phenomena than rotating stall. Surge is basically the same phenomena for both low-speed and high-speed machines because surge involves the entire compressor system and not the localized flow around the blades (as with rotating stall). As illustrated in figure 1b, surge is a varying amplitude oscillation of the total annulus averaged flow and pressure through the entire compressor and its system [10]. Surge has also been described as a Helmholtz, organ-pipe resonance of the mass flow and pressure rise throughout the compressor pumping system [9]. This simple theory has laid the foundation for many of the surge models that have been developed. Huppert and Benser [14] describe surge as a limit cycle type of oscillation on the compressor operating map, which is also illustrated in figure 1b. As can be seen from the figure, the compressor operates on the stable steady-state operating conditions for half of the surge cycle, and on the unstable operating conditions for the other half of the cycle [14]. Thus, the conditions are better for returning to steady operating conditions during surge than during pure rotating stall, because surge operates on the stable part of the operating curve during part of its cycle.

The frequency of these mass flow oscillations depends upon the geometry and characteristics of the inlet ducting, the compressor, the plenum being pressurized, the exit ducting, and the throttle settings [5,7]. This frequency is typically an order of magnitude smaller than the frequency associated with rotating stall (for a given low-speed machine) [10].

There are two possible types of surge that are basically different extremes of the same phenomena. Deep surge is used to describe mass flow oscillations of large enough

magnitude to cause actual reverse flow throughout the compressor system. Classic surge is used to describe the normal mass flow oscillations present without the criteria of reverse flow. The exact type of surge that a system will experience is still being researched; however, the variables of plenum volume, blade speed, compressor duct area and length have been shown by Greitzer [10] to influence the surge mode. Again, both deep and classical surge can occur for both low-speed and high-speed machinery because surge involves the entire compressor pumping system.

A surge cycle can be described by the following process. Consider a compressor delivering a very high plenum pressure with a relatively low mass flow rate. If the mass flow rate (i.e. impedance to plenum reverse flow) is continually decreased then eventually the highly pressurized plenum will relieve itself by draining its potential energy upstream. When sufficient potential energy is drained from the plenum, it no longer needs to relieve itself. At this point, the surge cycle is half completed. The second half of the surge cycle is basically normal operation involving plenum re-pressurization. When this pressure again becomes too large, the entire cycle will repeat.

Surge can cause large inlet over-pressures that can result in severe structural damage to aircraft engines. Also, surge tends to interrupt the normally steady and relatively efficient combustion process. Clearly surge cannot be tolerated in aircraft engine systems during normal operation.

Surge and rotating stall are two separate flow phenomena. Pure rotating stall is steady in the proper frame of reference, but not axisymmetric [5]. Pure surge, on the other hand, is axisymmetric, but unsteady [5]. If it is assumed that a transient instability

is initiated by a general disturbance that is both unsteady and axisymmetric, we would expect surge-like and rotating-stall-like features to be coupled as the unstable flow progresses [5]. Indeed, several researchers have measured the simultaneous existence of stall and surge phenomena in an unstable compressor operation. The typically reported form of coupling is for rotating stall to be present only over the first half of the surge cycle and then disappear over the second half of the surge cycle. This form of coupling has been observed by many researchers [7], [8], [9], [10], [14], only to mention a few. Although surge and stall are fundamentally different, they are not unrelated and they are not independent phenomena.

2.2 High frequency instrumentation used to study compressor instability phenomena

The rapidly changing flow phenomena present during transient unstable compressor operation requires the use of high response instrumentation to capture any useful measurements. Iura and Rannie [11] have reported that pressure or velocity measurements with low response instrumentation give no indication of the phenomena of rotating stall. This section presents a brief review of the types of instrumentation that have been used to measure compressor instability.

The hot-wire anemometer and the high response pressure transducer have been used as the primary types of instrumentation to measure rotating stall and surge. In fact, it is difficult to find any experimental studies that have not used at least one of these instruments. These instruments allow the measurement of instantaneous flow velocities

and pressures in either the absolute or rotating reference frames, depending upon the application.

Prior to 1965, the hot-wire anemometer was by far the most popular tool for measuring stall and surge phenomena. During this time, the anemometer was used as a qualitative sensing instrument as well as a quantitative measuring device. Emmons [9,15], Huppert [14], Iura [11], Pearson [16], Rockett [15,17], and many others, all used hot-wire anemometer theory in various forms to investigate compressor instability phenomena. It is beyond the scope of this thesis to summarize each individual application; however, a summary of their general findings was presented in section 2.1.

Emmons [9] was probably the first to discover the need to place more than one hot-wire about the compressor circumference in order to evaluate the direction of stall cell rotation, the number of stall cells, and the growth of a developing stall cell. Huppert [14] and Iura [11] were the first to perform spanwise surveys necessary to evaluate the radial extent of the stall cells.

High response pressure measurements of compressor instability have been made as far back as 1946 [18]; however, they are not as common as hot-wire measurements. Approximately half of the researchers mentioned used high response pressure transducers in addition to hot-wire anemometry. One of the problems with high response instrumentation is the vast amount of data that can be obtained. Prior to 1965, the interpretation of fast response measurements entailed the tiresome study of endless paper traces, of course this entire operation can now be handled by a computer operating and digitizing in real time [19].

Today, the hot-wire is still a valuable compressor instability research tool. More recent experimental work by Day [19,20,21,22], Greitzer [7,4], McDougall [23], Cumpsty [19,23], and many others still involves the use of hot-wires to measure compressor instability phenomena. However, as the state of the art in compressor design is extended, the flow field environment becomes transonic and hence so harsh that hot-wires can simply not survive for any extended period of time. The high-speed, transonic compressor environment is the limiting factor for the use of hot-wires.

Modern high response pressure transducers are one alternative for measuring compressor instability in transonic environments. Recent advances in transducer size, durability, and thermal drift properties, make them very well suited for such environments. A series of experiments by Garnier, Epstein and Greitzer [4] was performed in which the low-speed compressor was successfully instrumented with hot-wires; however, for the high-speed compressor it was necessary to use high response screen protected pressure transducers.

Fundamental research is still being carried out on low-speed machines with hot-wire anemometry as the principle form of instrumentation. This research is continually revealing new information about compressor stability; however, these theories must eventually be verified and/or modified for high-speed machinery. This requires the further application of existing high frequency instrumentation to the study of compressor instability. This thesis presents the results obtained from an experiment involving the measurement of a high-speed transonic compressor during unstable operation with a high response pressure, temperature, and efficiency probe.

3.0 The Experiment

This chapter presents a discussion of the transonic rotor and test facility, the high response instrumentation, the data acquisition system and experimental procedure, and a brief summary of the transient stall data presented in the results chapter. Each topic is covered in a separate section, and the discussions are kept brief. The goal here is to provide information needed to facilitate a better understanding of the measurements presented in the following chapter on the results.

3.1 The Rotor and Test Facility

The rotor instrumented (Rotor 37) was the first stage of an eight-stage, axial-flow, transonic core-compressor having good efficiency, high pressure ratio (about 20:1), and sufficient stall margin. Rotor 37 was initially designed and tested by NASA Lewis as one of four possible choices for the inlet stage of the eight-stage core-compressor. The loading-per-stage and the design speed were both considerably higher than the state-of-the-art in core-compressor designs (as of 1980) [24]. A discussion of the design criteria

and restraints for the eight-stage core-compressor is presented by Hauser et al. in reference [25].

Figure 3 shows a photograph of the leading edge of Rotor 37, courtesy of the NASA Lewis Research Center [26]. A detailed discussion of the aerodynamic design and performance of Rotor 37 can be found in references [24] and [2], respectively. However, a brief summary of some of the more important operating parameters of Rotor 37 are presented in table 1 (reference [2]). Of particular interest are the high pressure and temperature ratios, the extremely high wheel speed, the low-aspect ratio, and the fully spanwise transonic flow. Figure 4 shows the overall performance map of Rotor 37 without the stator present (reference [24]). A complete description of the blade geometry and manufacturing coordinates for Rotor 37 is presented in references [2] and [24], respectively.

For the transient stall data presented in this thesis, Rotor 37 was tested as rotor only, no stator was present, nor were any of the following seven stages. Rotor 37 was tested at the NASA Lewis, single-stage, high-speed compressor test facility, shown in figure 5. Also, a close-up meridional view of the test section with Rotor 37 in place is shown in figure 6. Both instrumentation stations, 30% and 130% axial chord, are indicated on figure 6. Figure 7 shows a photograph of Rotor 37 in place in the high-speed test facility [26]. For orientation purposes, the ruler shown in figure 7 is located upstream of the rotor. The test facility is described in detail in reference [3], and will only be briefly described here as summarized in reference [24].

Atmospheric air enters the test facility (figure 5) through an inlet on the roof of

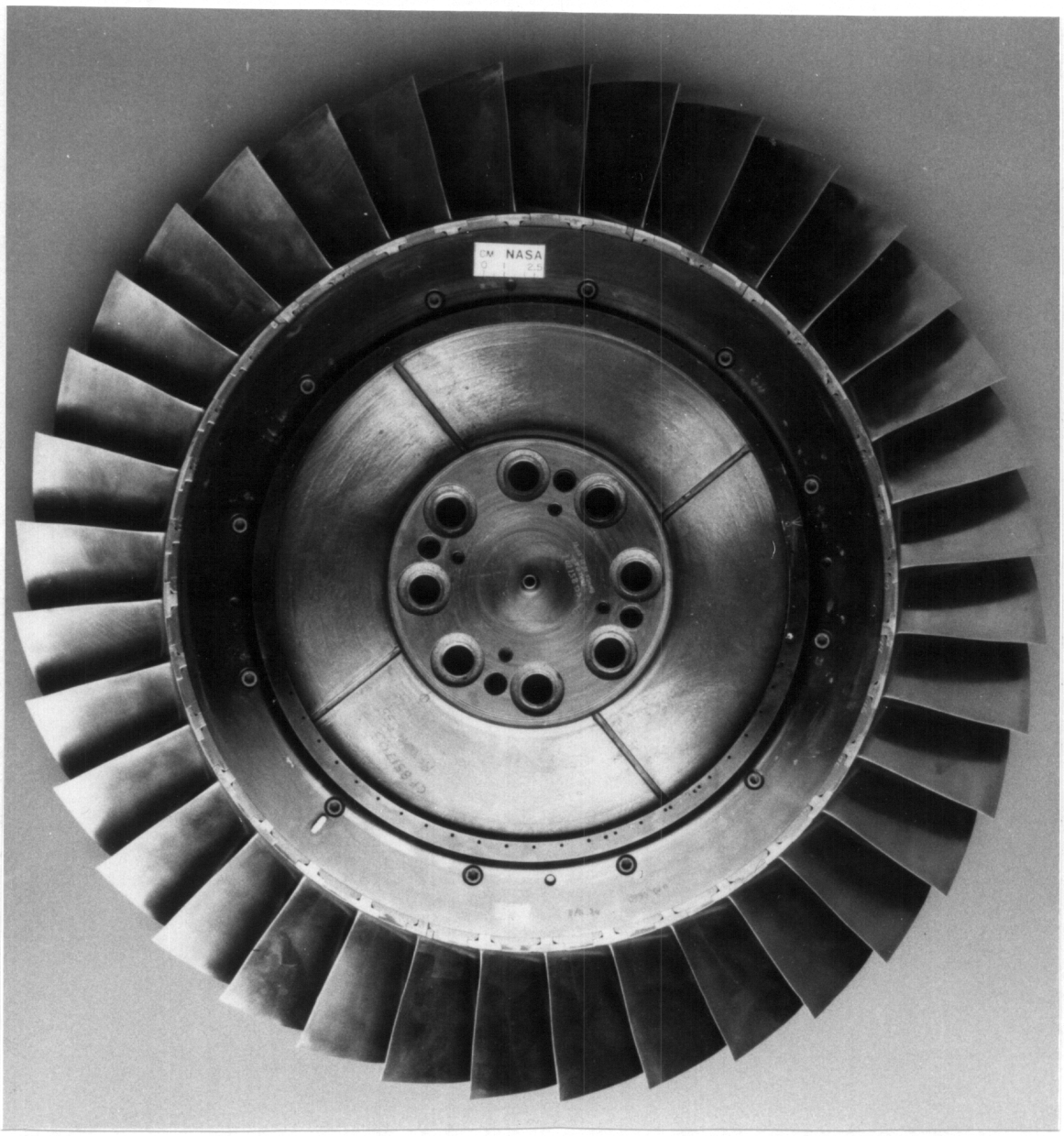

Figure 3. Rotor 37, Leading Edge View (after Suder [26]).

Table 1. Operating and Design Parameters for Rotor 37.

PARAMETERS	100% SPEED; NEAR STALL	90% SPEED; NEAR STALL
WHEEL SPEED	17200 rpm	15500 rpm
CORRECTED MASS FLOW	19.6 kg/s	17.3 kg/s
TOTAL PRESSURE RATIO: ROTOR/STATOR STAGE	2.196/0.953 2.093	1.909/0.968 1.847
TOTAL TEMP. RATIO: ROTOR/STATOR STAGE	1.296/1.000 1.296	1.236/1.000 1.236
ADIABATIC EFFICIENCY ROTOR/STAGE	85.2 / 79.3 %	86.0 / 81.2 %
INLET RELATIVE MACH NUMBER AT BLADE TIP	1.5	1.3
INLET RELATIVE MACH NUMBER AT ROOT	1.2	1.0
BLADE SPEED AT TIP	445 m/s	400 m/s
BLADE SPEED AT HUB	335 m/s	300 m/s
BLADE PASSING FREQUENCY	10.5 KHz	9.45 KHz
# OF BLADES ROTOR/STATOR	36 / 46	36 / 46
TIP SOLIDITY ROTOR / STATOR	1.3 / 1.3	1.3 / 1.3
ASPECT RATIO ROTOR / STATOR	1.19 / 1.26	1.19 / 1.26
MEAN ROTOR RADIUS OUTSIDE/INSIDE	0.250 / 0.183 m	0.250 / 0.183 m

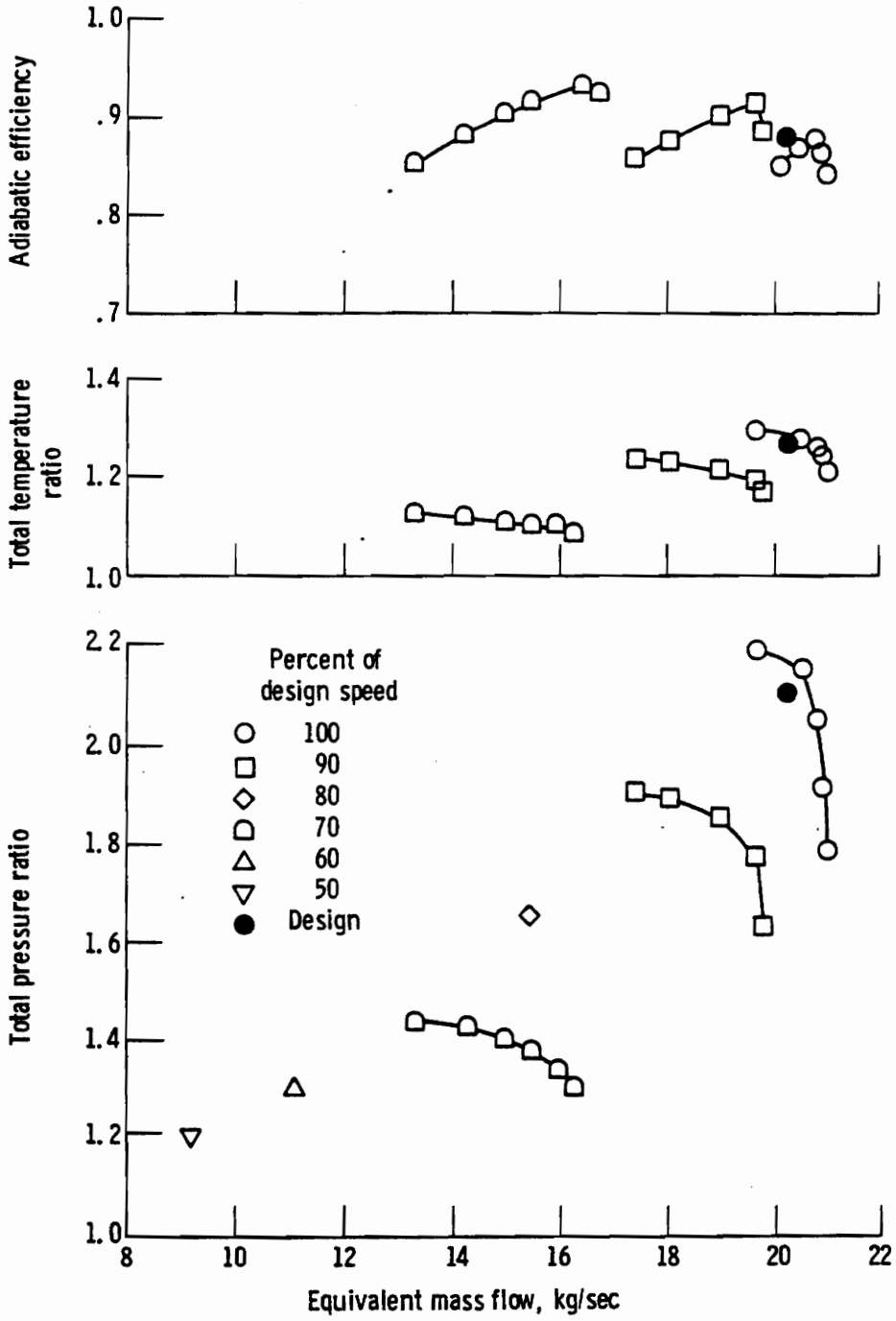

Figure 4. Overall Characteristics of Rotor 37, without Stator (after Moore and Reid [24]).

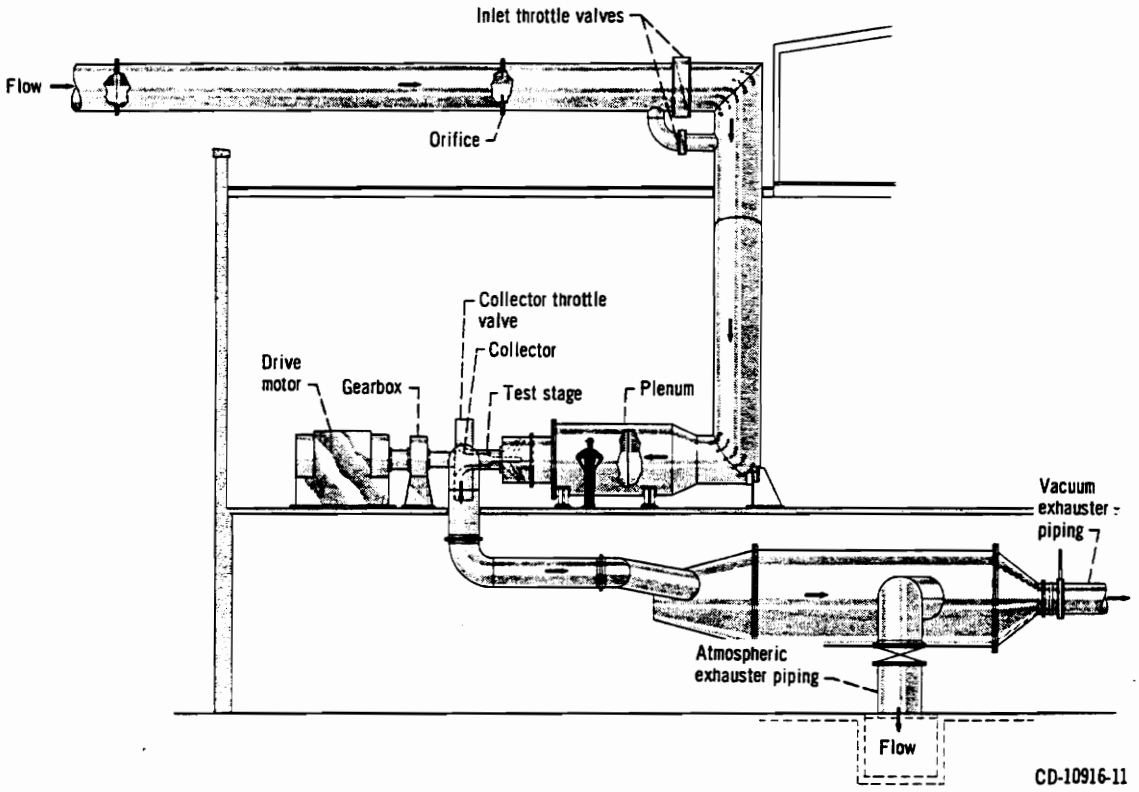

Figure 5. NASA Lewis High Speed Compressor Stage Test Facility (after Urasek [3]).

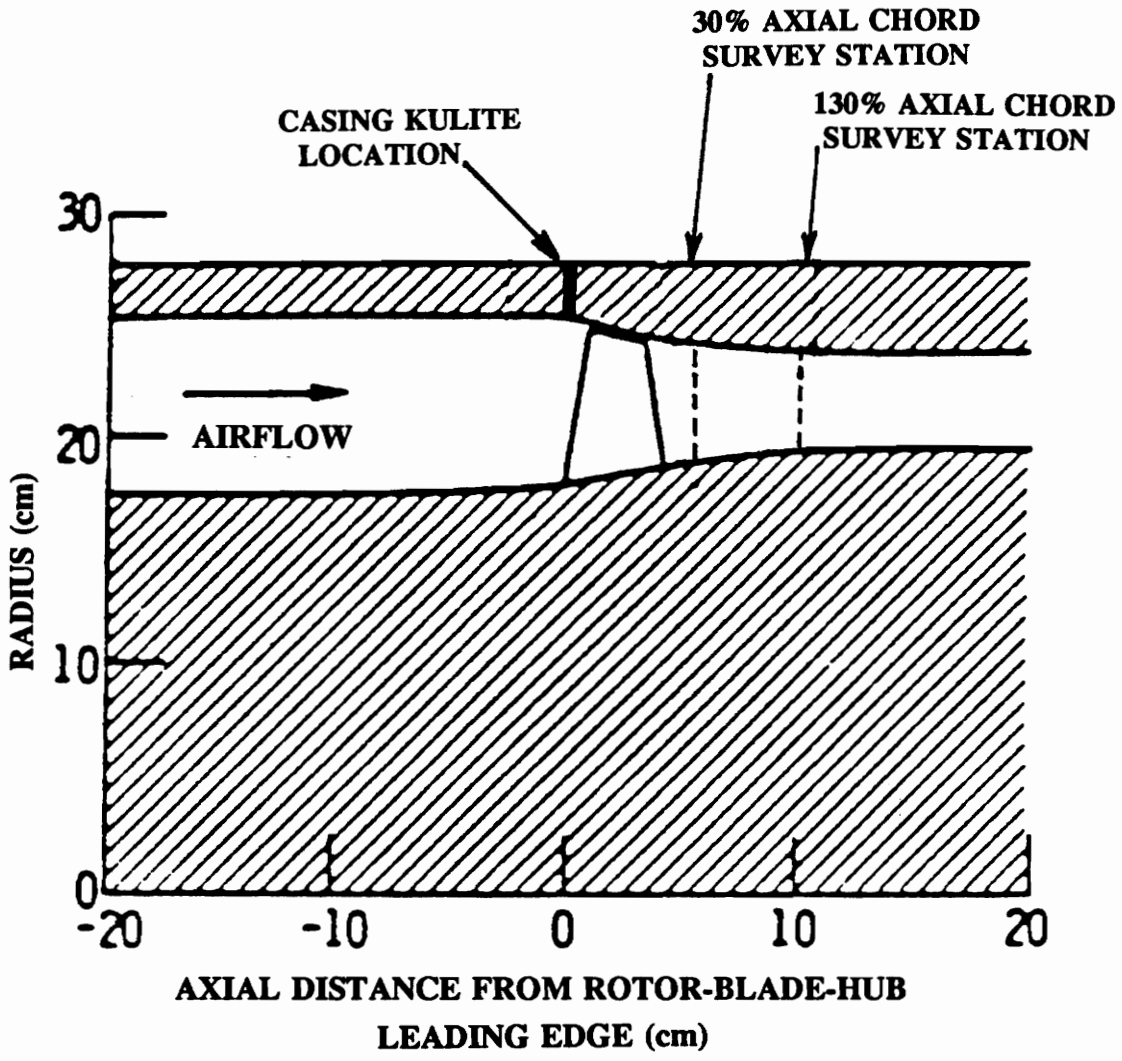

Figure 6. Meridional View of Compressor Test Section and Rotor 37 (after Morris [32]).

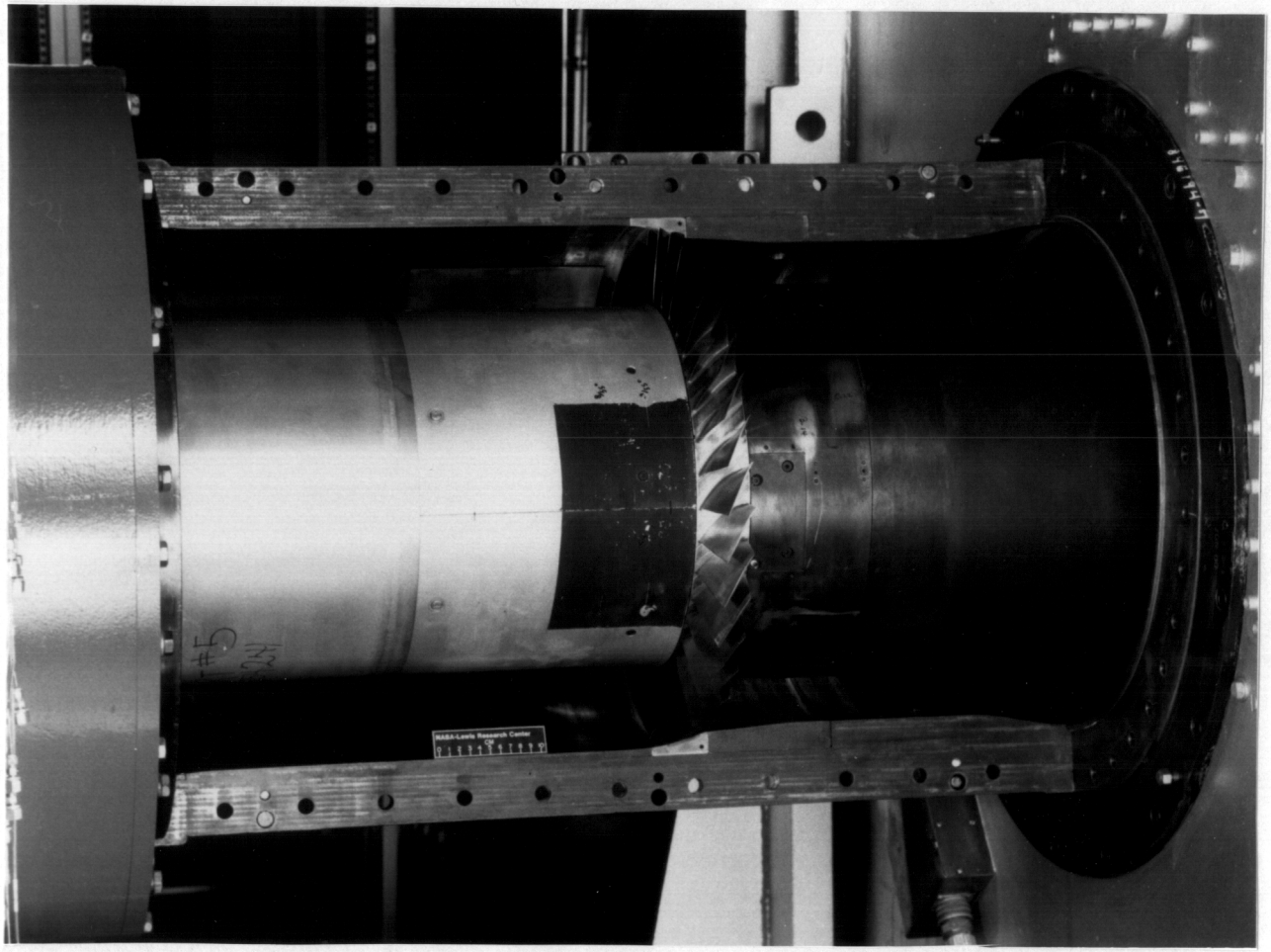

Figure 7. Rotor 37 in High-Speed Compressor Test Facility (after Suder [26]) (orientation - flow from left to right).

the building. The air then flows through the flow measuring orifice and passes through straighteners into the plenum upstream of the test section. The air then passes through the compressor stage test section and goes to the atmospheric exhaust system by means of the downstream collector throttle valve. This facility has a throttle both upstream and downstream of the compressor test section. However, for the measurements presented in this thesis, the upstream throttle was left wide open, and only the downstream throttle was varied. A more detailed schematic of the compressor duct, downstream plenum and throttle duct is presented in section 4.6 during the presentation of the attempts to fit the data to Greitzer's one-dimensional, lumped-parameter model.

3.2 The Aspirating Probe

The following section contains a summary of the theory of operation and governing equations for the probe. Also briefly discussed are the calibration system and procedure and the probe actuator system.

The high frequency response dual hot-wire aspirating probe measures time resolved total pressure and temperature and is well suited for use in an unsteady high speed gas environment. The probe was developed during the early 80's at MIT by Ng and Epstein [27]. For an in-depth discussion of the probes operation and applications refer to either Ng and Epstein [1], or Ng [27,28]. The probe is unique because of its ability to make high response simultaneous measurements of pressure and temperature in a high-speed compressible environment.

Figure 8 shows a detailed schematic of the aspirating probe. The probe consists of two platinum coated, co-planar, constant temperature hot-wires with differing diameters operating in separate anemometer circuits and at different overheat ratios. The probe continually aspirates by connection to a vacuum. The vacuum pressure is low enough to cause continuous choking of the flow through the choked orifice; hence, the flow past the wires is always at a constant mach number. Thus, assuming a uniform gas environment, the mass flux across the wires is only a function of free stream total temperature and pressure.

By applying the following: an energy balance between the anemometer bridge voltage and the heat dissipated to the fluid, the continuity equation for one-dimensional flow, assuming negligible heat loss at the wire ends, and assuming a relationship between the Reynolds number and the heat transfer coefficient, the governing equation of each wire can be derived, as shown below in equation 3.1.

$$V^2 = \frac{(R_s + R_w)^2}{R_w} \pi l k a \left[\frac{d}{\mu} \frac{P_T}{\sqrt{T_T}} \frac{A^*}{A_c} \sqrt{\frac{\gamma}{R}} \left(\frac{2}{\gamma+1} \right)^{\frac{\gamma+1}{2(\gamma-1)}} \right]^m (T_w - rT_T) \qquad [3.1]$$

It is emphasized that this governing equation holds for each hot wire. The variables stand for the following: V is the anemometer bridge voltage that is produced from each hot wire during operation. R_s is the resistance of the anemometer Wheatstone bridge that is in series with a wire. R_w and T_w represent the operating resistance and

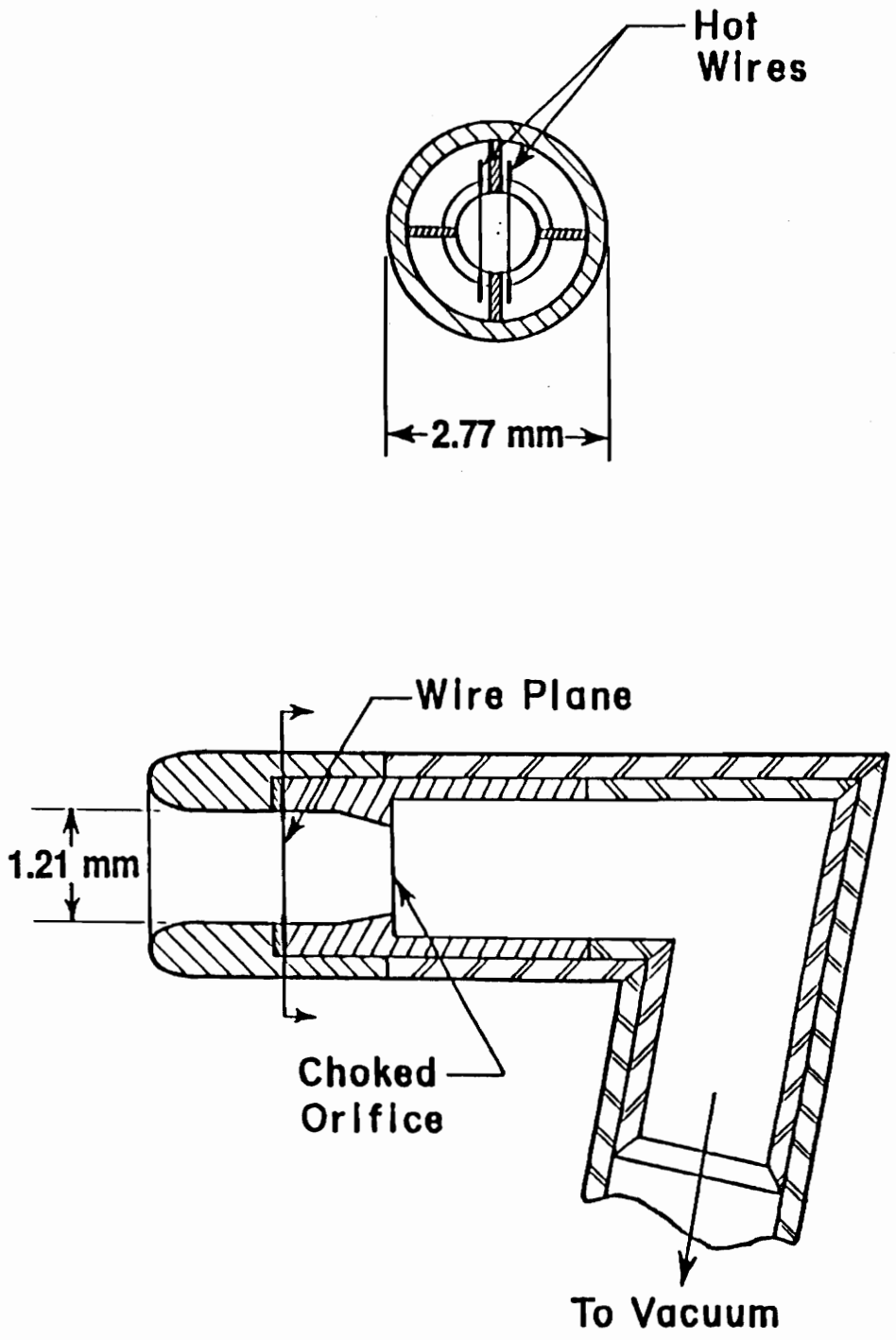

Figure 8. Detail of the Dual Hot-Wire Aspirating Probe (after Ng & Epstein [1]).

temperature of a wire, respectively. The quantities ℓ, d, A^* and A_c refer to the effective wire length, wire diameter, area of the choked orifice and area of the orifice at the wire plane, respectively. The quantities k and μ stand for the thermal conductivity and absolute viscosity of the fluid. The quantities γ and R represent the ratio of specific heats and the gas constant for air, respectively. The quantities P_T, T_T and r are the total pressure, total temperature and ratio of static to total temperature, respectively, of the flow field being measured. The values a and m are the calibration constants determined for each wire during the calibration of the probe.

Inspection of equation 3.1 reveals that once the probe dimensions, hot-wire parameters (i.e. diameters, resistances and operating temperatures of both hot wires) and properties of the fluid to be measured are set, the only unknown variables left in the two equations are V_{w1}, V_{w2}, T_T, P_T, a and m. The probe calibration constants are determined by placing the probe in a calibration tank fitted with pressure and temperature transducers. Thus, as the conditions in the tank are varied, the tank temperature, tank pressure, and the anemometer bridge voltages from each wire are all recorded. The only unknowns remaining are a and m, which can both be backed out from the two governing equations of the wires. Once a and m are determined, the only unknowns are V_{w1}, V_{w2}, T_T and P_T. Thus, if the voltages from the two wires are recorded during the experiment, the two equations can be simultaneously solved for total pressure and total temperature. This static calibration procedure has been proven to be adequate by Ng et al. [1,27,28,29,30], and is the accepted practice for the aspirating probe. No attempt has been made to perform a dynamic calibration.

The established calibration procedure has been to vary the tank pressure over the range expected in the experiment, while the tank temperature is kept around the mean of the values expected in the experiment. All previous applications of the probe involved the measurement of temperatures and pressures very close to atmospheric values. However, the mean total temperature of the flow exiting Rotor 37 is around 100 °C. This required the construction of a calibration tank that could elevate the temperature as well as the pressure. This was accomplished by placing drum heaters and insulation around the calibration tank. Two Omega standard blanket type drum heaters were used that produced a total of 1400 watts of thermal energy. It was necessary to allow the tank approximately 45 minutes to heat up and obtain a uniform steady temperature, before the calibration was performed. For the Rotor 37 experiment, calibrations were made at mean tank temperatures of 100 and a 125 °C, while the tank pressure was varied from one to two atm.

The wire diameters were 0.20 and 0.35 mil, and were operated with over-heat ratios of 1.8 and 2.0, respectively. Higher over-heat values result in higher wire operating temperatures and this speeds up the wire aging process. These over-heat values are quite high, but are required and recommended for use in higher temperature environments, such as Rotor 37. Otherwise, there is very little difference between the wire operating temperature and the free stream total temperature which results in unacceptably low sensitivities.

The aspirating probe is always constructed with a high response Kulite pressure transducer mounted 'piggyback' [1]. Figure 9 shows a schematic of the aspirating probe

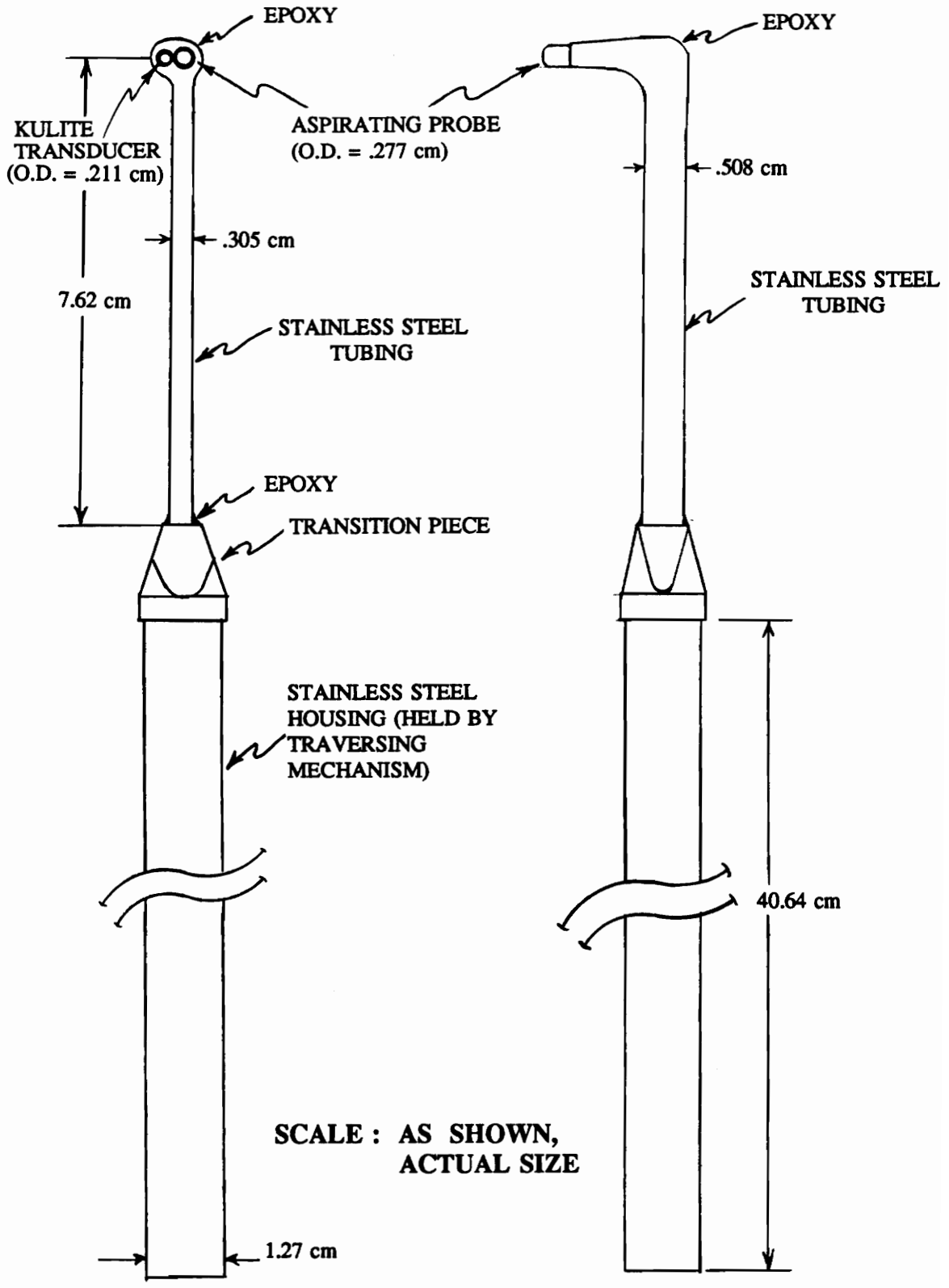

Figure 9. Schematic of Aspirating Probe Mounted 'Piggyback' with Kulite Transducer.

and Kulite transducer mounted 'piggyback' as used in the experiment. A side-by-side mounting technique was chosen because of the expected significant spanwise variation in the flow properties. The Kulite transducer adds a redundant (total pressure) to the set of governing equations to be solved. It has been shown several times that more accurate results can be obtained by taking the known pressure from the Kulite and then determining the temperature with the use of one of the hot-wires [1,27,28,29,30]. Thus, all measurements presented in this thesis were obtained by using the known Kulite transducer total pressure and the voltage from hot-wire #1. Figure 10 shows a plot of the sensitivities of this configuration. As can be seen, once the Kulite pressure is determined, the total temperature can be determined from (equation 3.2) the plot shown. The first consideration here is that an unacceptable loss in spatial resolution would result. One possible solution would be to apply a time shift to the Kulite data to account for the spacing between the two transducers. This analysis was carried out by the author [30] and it was shown to have negligible effect if the time lag was or was not used. Thus, all measurements presented in this thesis do not incorporate a time lag.

The values of total temperature and total pressure can be combined to calculate isentropic efficiency, as shown below in equation 3.2.

$$\eta = \frac{\left(\frac{P_{T2}}{P_{T1}}\right)^{\frac{\gamma-1}{\gamma}} - 1}{\left(\frac{T_{T2}}{T_{T1}}\right) - 1} \qquad [3.2]$$

The variables stand for the following: η stands for isentropic efficiency. γ represents the ratio of specific heats of air. P_{T1} and T_{T1} represent the total pressure and total temperature

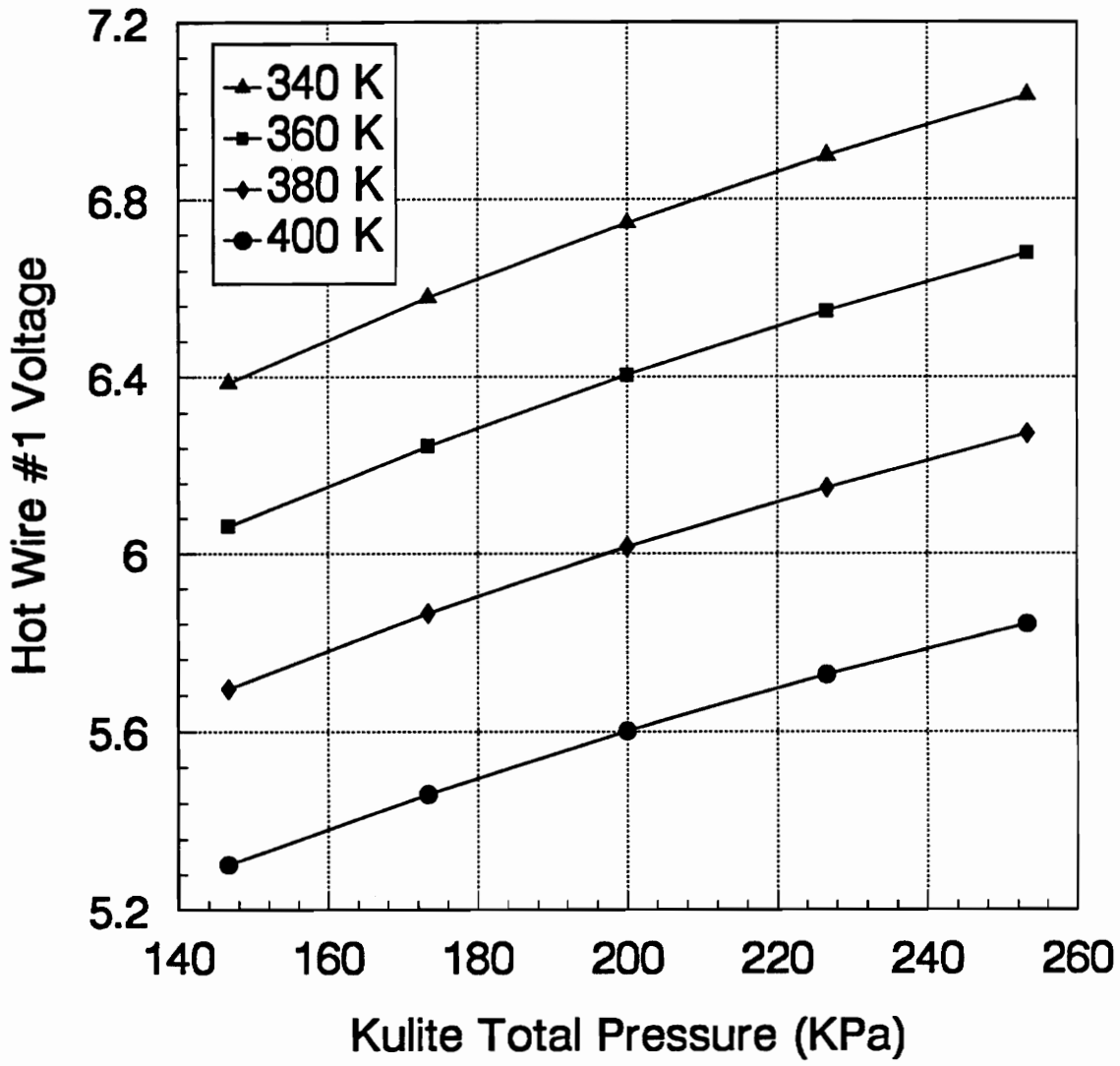

Figure 10. Calibration Sensitivities for Kulite/Hot Wire #1 Reduction.

in the upstream plenum, and are assumed constant over the time that data was taken. P_{T2} and T_{T2} represent the total pressure and total temperature measured by the probe downstream of Rotor 37. The efficiency measurements presented in the results section are calculated according to these specifications.

3.3 Experimental Procedure and Data Acquisition System

This section briefly outlines the experimental set-up and hardware necessary to operate the probe. Also discussed is the data acquisition equipment, set-up, and procedure used to capture the transient instability data at its inception.

The probe was actuated across the span of the blades by the use of a specially designed traversing mechanism. The mechanism had a linear variable displacement transducer (LVDT) attached to monitor the probe position. The LVDT signal could be digitized for later probe position determination purposes, or could be immediately used to determine if the probe was properly recessed to the 'home' resting position. The probe head orientation was aligned with the mean flow angle of the flow exiting the rotor in the absolute reference frame.

The traversing mechanism mounted directly to an inserted plug on the Rotor 37 test rig casing. The plug contained a recessed area for the probe head to rest while it was not taking data. This effort was taken to prolong the life of the hot-wires. Two downstream locations were constructed for instrumentation, they were located at 30% and

130% axial chord lengths downstream of the trailing edge (figure 6). The mechanism was driven by a stepper motor that was controlled by a portable personal computer (PC). BASIC programs were used to send commands out the PC's printer port that subsequently controlled the position of the probe. The programs were written generically so that the user could simply enter the desired per cent span(s) for the probe to traverse.

Extending from the traversing mechanism were the following: input power and output signal of the LVDT, the stepper motor power and control lines, the two hot-wire signals (active arms of the two anemometer's wheatstone bridge configuration), the Kulite signal, and the aspirating line for the probe. The LVDT's output signal was ran to the control room for digitization and monitoring. The LVDT's input power was supplied by a standard DC power supply. This power supply along with other monitoring electronics (DC voltmeters and oscilloscopes) were kept in the rig test facility for on-site evaluation. The output voltages from the two anemometers were sent through a signal conditioning circuit that applied a DC voltage offset. This was necessary to get the best resolution possible from the digitization process.

The Kulite signal was sent through an amplifier to raise the signal to an acceptable level so it could be sent to the control room where the data acquisition system was located. The Kulite signal also had a DC offset applied to maximize the resolution of the digitization process. The Kulite was a gage-type and was specially ordered to be thermally compensated for the high operating temperatures of the rig. Thus, it was initially required to operate the rig to bring the Kulite up to the mean temperature of the flow. Once the Kulite was heated up, it could then be balanced to zero voltage at

atmospheric pressure, as its gage operation requires. This process was necessary before each day of rig running and resulted in an almost negligible drift of the Kulite signal.

The probe aspirating line was connected to a vacuum tank that was used to remove unsteady effects from the vacuum pump. The aspirating line contained a solenoid valve that could be remotely turned off in an effort to prolong hot-wire life. The anemometers could also be turned off via remote control from the control room when they were not in use. This was also an effort exercised to prolong hot-wire life. In summary, when the probe was not in use it was recessed in the probe cavity with the hot-wires and the aspirating line both cut off.

None of the signals were sent through anti-aliasing filters because of the extremely high sampling rate used to digitize the data (500 KHz). Filters of this high cut off frequency (250 KHz) are difficult to obtain and are very expensive. There was really no energy in the flow field at frequencies this high so the absence of filters was not considered a problem [31].

The Kulite signal, both hot-wire signals, and a once-per-revolution signal from the rotor were the signals of interest during the taking of the data. These analogue signals were all digitized and subsequently stored using a LeCroy 8013A data acquisition system. The system was fitted with two multi-channel 6810 Waveform Recorders and two 6310 expanded memory (512 Kbyte) modules. The machine had a total of 2 Mbytes of memory per-run and had 12 bit analogue-to-digital resolution for any given voltage range. The blade passing frequency of Rotor 37 was 10.5 KHz at 100% of design speed. Thus, a sampling rate of 500 KHz resulted in approximately 48 data points per blade passing.

With four channels being used at these sampling rates approximately 300 revolutions of data were acquired during each run. After each run, the data was down-loaded from the LeCroy to a 300 Mbyte hard drive on an IBM 286 PC via a 8901A GPIB data communication interface. The data was then down-loaded to floppy disks for storage and back-up purposes.

The procedure used to capture the transient stall data at its inception can be summarized by the following. The rig was taken to the near stall operating condition and allowed time to settle. With the probe aspirating line open and the wires turned on, the user then entered the desired per cent span to traverse the probe. It is very important to aspirate the probe before it is immersed into the flow. Once the probe was at the desired location, the rig operator slowly closed the downstream throttle. Eventually the rig would go into unstable operation, at which time a Kulite pressure transducer mounted on the rig casing (just upstream of the rotor, see figure 6) would experience large fluctuations. The output from this transducer was input into the data acquisition systems' trigger window. When the rig stalled the Kulite would exceed the set window trigger levels and activate the data acquisition system to digitize the oncoming signals. The data acquisition system was placed in 50 % continuous over-writing memory mode. Thus, when the trigger came, the data acquisition system would freeze the data already present in the first half of its memory, and then fill the second half of memory with the oncoming signals of unstable operation. Using this mode of acquisition, approximately 150 revolutions of pre-stall data and 150 revolutions of post-stall data was obtained. Once the data was taken, the user could bring the probe back to the 'home' resting position. The aspirating line and hot-

wire anemometers would then be subsequently cut off.

It is very important to mention that the data presented in this thesis is not the operation of Rotor 37 in fully developed unstable operation. The time required to reach fully developed unstable operation is too long to allow the rotor to operate in this mode. The unstable operation measurements presented here are transient in nature, i.e. they were obtained immediately after the rig stalled. It is unknown if the data obtained was a function of the movement of the downstream throttle position or if other system parameters were more important. Regardless of the cause of the transient unstable operation traces that were obtained, this thesis makes observations from the trends and behavior patterns that were captured. Future work could involve the digitization of the downstream throttle position for possible correlations with some of the patterns found in the unstable operation traces.

Another important note to mention is that severe mechanical vibrations were present during and even before the surging of the compressor test rig. The magnetic pickup in the once-per-revolution signal picked up the machine's vibrations as revolutions. The result was complete noise on the once-per-revolution signal, to the degree that it was useless. Future unstable operation research on Rotor 37 and this test rig would benefit by correcting this problem.

Table 2 presents a summary of the transient stall data presented in the results chapter. Data was taken at two downstream locations, 30% and 130% axial chord from the rotor trailing edge. Only the 130% downstream data is presented in this thesis.

Table 2. Summary of Transient Stall Data Presented.

RUN No.	DOWNSTREAM LOCATION (% Axial Chord)	PER CENT SPEED	PER CENT SPAN
38	130	100	90
40	130	100	80
43	130	100	60
44	130	100	30
47	130	100	90
48	130	100	95
59	130	90	90

Run 59 is 90 % speed data, all other runs are 100% speed data.

4.0 Results and Discussion

This chapter presents and discusses the results of the measurements taken during the previously described experiment. Each of the following topics are covered in individual sections. The averaging technique employed to present and analyze the vast quantities of acquired data is discussed, along with several other instrumentation concerns. General observations of the transient instability flow field characteristics are presented along with the typical form of a surge/stall cycle that is found immediately after the inception of stall. Also, the different types of surge/stall cycle variations that were present as the unstable operation progressed are documented and discussed. Evidence of coupling between the two phenomena of surge and stall is presented and some preliminary attempts at quantification are made. Also, the significant differences between the characteristics of the 100% and 90% speed transient stall data is documented and discussed. Finally, the attempt made to use the data to verify Greitzer's one-dimensional, lumped-parameter model [7] is discussed and reasons for poor agreement are given.

4.1 Data Presentation

As mentioned in Chapter 2, one of the biggest obstacles of high response transient stall measurements is the subsequent storage, reduction and presentation of the data. Today, the storage and reduction requirements can be easily met with a large hard disk drive (200 MBytes or more) and a relatively fast PC (386 motherboard or faster). However, the presentation of the data in hard copy format is still a challenge. There were approximately 250,000 data points digitized for each transducer during each run. Clearly, the presentation of a quarter million data points on one plot is unfeasible. On the other hand, presenting only 'blocks' or 'chunks' of the raw data at a time tends to confuse and distort the actual meanings and trends in the measurements (see Appendix A).

A method of processing the data was required that could retain the basic transient stall patterns, shapes and characteristics, yet would significantly reduce the total number of data points required to represent these trends. The resulting data sets could then be easily presented and compared for relative flow field content.

The technique employed to process the data involved a moving block average. This involved, for example, averaging all of the first fifty points and calling this point one, then averaging the next fifty points and calling this point two, and etc. An important consideration was the size of the moving block and its effective ability to retain the general characteristics of the transient flow field. In summary, Moore [5] states that transient stall flow patterns generally have length scales on the same order of the compressor diameter. Thus, the transient stall patterns will change on a time scale that

is typically very much longer than the unsteady response of a single blade passage. Based on this comment and on a general trial and error evaluation of different block sizes, it was determined that approximately two and one-half blades (125 data points) was a sufficiently small block size. This block size retained the general transient stall compressor characteristics and facilitated relatively easy hard copy production. Furthermore, since the general unsteady characteristics were retained, relatively easy comparisons could be made between the data sets (i.e. different spans or speeds).

Appendix A presents traces of the raw data superimposed on the block averaged data for an entire surge cycle. Analysis of these plots reveals the importance and convenience of the averaging technique used to present and subsequently compare the data. These plots show that the general shape of the unsteady transient compressor behavior was retained. The averaging process basically removed the individual blade passage wakes from the data. All the data presented in this thesis (unless otherwise noted) has been averaged using this moving block technique.

There were two possible modes of data reduction. The first mode calculated temperature and efficiency (discussed in Chapter 3.3) from the raw data and then performed the block averaging process. The other option was to perform the block averaging process first and then use these average traces to calculate temperature and efficiency. There was almost no difference between the final traces regardless of the mode used. Thus, to facilitate speed of computation, most of the data presented in this thesis was averaged first and then reduced. This basically goes back to the spatial resolution problem that was settled in Chapter 3.3 (reference [30]).

A few additional words are in order concerning the data presented in this thesis. Temperatures were calculated by using the known Kulite pressure and one of the hot-wire voltages as discussed in Chapter 3.3. Hot wire 1 (0.20 mil. diameter) was used to reduce all the data presented in this thesis. Also, all measurements of pressure and temperature are presented as ratios. These were obtained by dividing the reduced data by the respective upstream plenum total pressure and temperature. Isentropic efficiencies are presented as percentages according to Equation 3.2. Also, the natural abscissa for the data acquired was time; however, the data is presented with the abscissa represented by rotor wheel revolutions in the absolute reference frame. This conversion was performed by using the average wheel speed obtained from the (useable content) once-per-revolution signal. This conversion gives the reader a little better relative feel for the time scales of interest. In summary, pure time represented by seconds is somewhat arbitrary; however, rotor revolutions makes a better relative time scale for presenting data of this nature.

It is important to remember that all the measurements presented in this thesis were taken from the absolute frame of reference. This is particularly important for the rotating stall phenomena present in the data. Rotating stall rotates with respect to the wheel; thus, to determine the circumferential extent of a stall cell it is necessary to express the data with respect to the rotating wheel reference frame. It may initially appear in some of the plots that rotating stall is present over more than an entire revolution; however, this is misleading. To make statements about the circumferential extent of a stall cell the data must first be represented with respect to the rotating wheel frame of reference.

Another very important issue is the accuracy of the measurements presented in this

thesis. It is a well known fact that the resolution of the aspirating/Kulite probe is better than its absolute accuracy (references [1,26,29,30]). In other words, the probe is very adept at responding to transient fluctuations in the flow field, but is not so accurate at determining the absolute DC values of which these fluctuations are superimposed. This is typical for many hot-wire instrumentation applications. The main reason for this is hot-wire aging and day-to-day drift, of which the operator has no control.

The adopted practice (references [26,29,30]) has been to match the DC value of the aspirating/Kulite probe data with the DC value determined from steady-state instrumentation. The result is the correct absolute DC levels along with the superimposed transient fluctuations of the unsteady operation. Before the transient stall data was taken, a near stall steady-state operating condition was surveyed spanwise by both NASA's steady-state instrumentation and VPI's aspirating/Kulite probe. The steady-state instrumentation directly give a DC result and the aspirating/Kulite probe gave a DC result by time averaging all the data obtained. The results of these two data sets were compared to determine the DC offset required and the subsequent DC accuracy once the offset was applied. A complete discussion of this process was given by Morris [32]. However, a summary of the conclusions is given in the following: the steady-state pressure and DC Kulite pressure measurements agree to within ± 0.6%, the steady-state total temperature and DC high response total temperature measurements agree to within ± 0.7%. The DC value of the transient stall data was offset using this same procedure. It is worth noting that this discussion was mentioned mostly for the sake of completeness. All the results and subsequent observations presented focus on the varying transient unsteady content of

the measurements. The absolute DC levels of the transient stall data are really of minor concern.

An additional concern of the measurements presented is the angular sensitivity of the probe. Ng and Epstein [1] determined the aspirating probes angular acceptance to be approximately ± 15° from the mean flow angle. As shown in figure 8, the aspirating probe has a fat lipped inlet that facilitates this 30° total swing in angular acceptance. On the other hand, the Kulite is mounted in a sharply chamfered stainless steel channel, and is thus more sensitive to angular flow fluctuations. As mentioned previously, the probe axis was aligned with the mean flow angle of the flow exiting the rotor in the absolute reference frame. This is satisfactory for steady-state operating condition surveys. However, during surge and rotating stall cycles the flow exiting the rotor experiences angular fluctuations much greater than 15°. Furthermore, as mentioned in Chapter 2, and as can be seen in figure 1a and figure 2, rotating stall cells typically involve flow recirculation and mixing. The influence of this on the data is not known at this point.

To minimize the consequences of this problem several measures were taken. The block averaging of the data brought out the general quasi-steady transient characteristics. This averaging process removed the blade passage wakes from the axisymmetric flow part of the transient cycle and also removed the rather ambiguous fluctuations present in the rotating stall cells. Consequently, relative comparisons were then made with these averaged or 'smoothed' transient characteristics. This reduces the effect of potential extreme differences in transient operation flow angularity based on per-cent-span or wheel speed. Thus, the data from different spans and the data from different operating speeds

can be relatively compared for general transient instability flow content.

In general, the author was careful about trying to infer too much from this stationary angled probe. It is also readily admitted that more detailed analysis of the AC content of the transient data could be investigated. However, as a first start, this thesis only makes relative comparisons and observations from the 'smoothed' transient unstable characteristics.

One final issue of concern that was also briefly mentioned in section 3.3 is the exact type of unstable operation measurements that are presented here. The measurements presented were obtained immediately after the machine was 'tripped' into rotating stall by slowly closing the downstream throttle valve. Rotor 37 was not in fully developed unstable operation during the measurements that are presented. The time required to get Rotor 37 to stable unsteady operation is much longer than the acceptable time for the rotor to be operating in the unstable range. Thus, the measurements taken represent the initial transient unstable operation of Rotor 37, i.e. immediately after the machine stalls, but prior to stable unsteady operation. It is unknown what effect the movement of the downstream throttle valve had on the form of the unstable operation measurements that are presented. Future research in this area would involve the digitizing of the downstream throttle position during the unstable operation measurements. This would allow any possible correlations between the throttle valve position and the unstable operation features to be determined. This thesis does not focus on the exact cause of the features observed during unstable operation. This focus of this thesis is to document the observations made from the transient unstable measurements.

4.2 General Observations

This section discusses several general observations made from the transient instability measurements of Rotor 37. Figure 11 shows plots of block averaged total pressure ratio, total temperature ratio, and isentropic efficiency of Rotor 37 during unstable operation. This data was taken from run 40 (see table 2), 100% speed, 80% span, at 130% axial chord of the rotor trailing edge. However, the observations presented are typical of all other spans surveyed. The data is plotted with the abscissa represented by rotor revolutions in the absolute reference frame. Approximately 150 revolutions of data were obtained before the rig stalled; however, figure 11 plots only the last twenty-five revolutions prior to stall. After the inception of stall, 150 revolutions of data was captured of the subsequent transient unstable operation. This is clearly evident by the large fluctuations that begin at revolution 150.

Figure 12 shows a close up (revs. 140-190, just after inception of instability) of the same traces presented in figure 11. Both types of unstable phenomena discussed in section 2.1 were present during the unstable operation of Rotor 37. Surge is evident by the low frequency (approximately 20 rotor revolutions/cycle) continuous sinusoidal wave. Rotating stall is evident by the higher frequency (approximately 1.5 rotor revolutions/cycle) sharp down spikes that are superimposed on the aforementioned surge cycles. The rotating stall cells are somewhat shallow at their inception; however, they quickly grow to fully developed size in approximately nine rotor revolutions. Furthermore, the rotating stall cells are only present over the first half of the surge cycle.

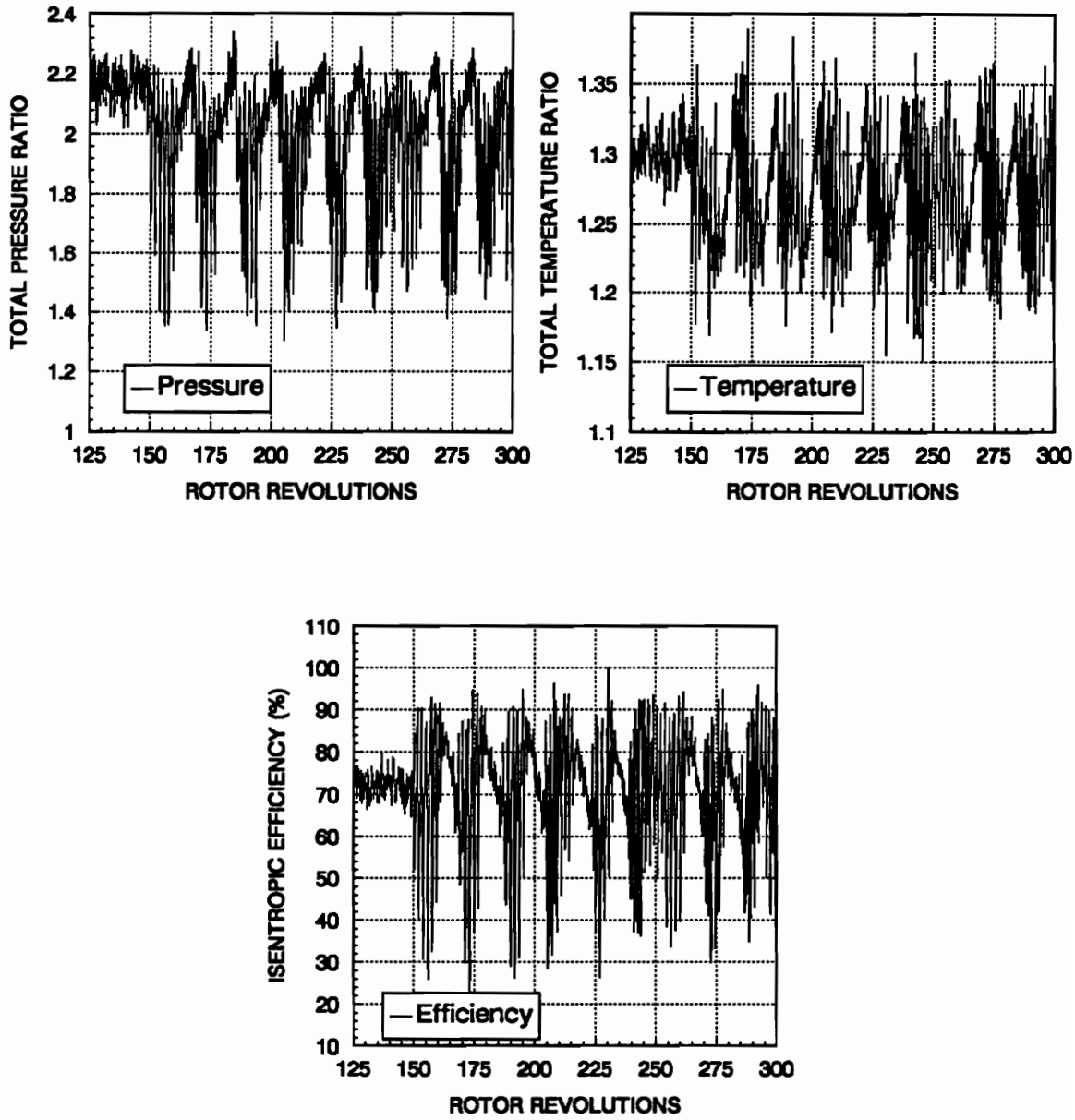

Figure 11. Rotor 37, 100% Speed, 80% Span, Transient Stall Data.

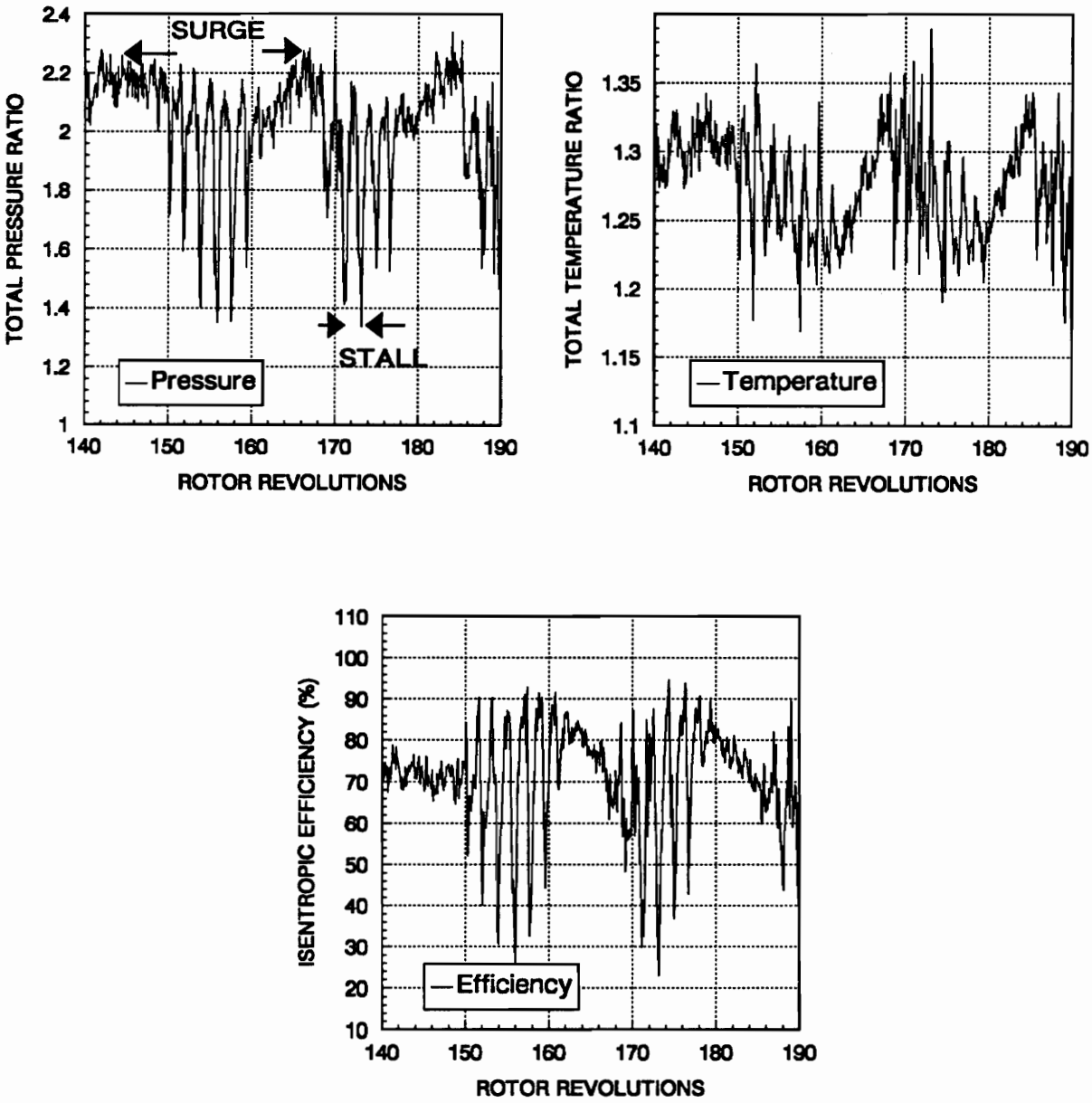

Figure 12. Rotor 37, 100% Speed, 80% Span, Transient Stall Data, Close up of Revs. 140-190.

The stall goes away during the second half of the surge cycle. This behavior is typical and is well documented in the literature; however, this was not the only type of surge/stall cycle interaction observed in the data. More will be discussed concerning this issue in the following section.

Fourier Transforms (FFT's) were performed on the average data sets to reveal the prominent frequencies of the unstable characteristics. More detailed results of these FFT's will be given in the following sections; however, a few general results are given here. The FFT's revealed prominent frequencies at approximately 16 Hz and 155 Hz. These correspond to the phenomena of surge and rotating stall, respectively. The frequency of the wheel at 100% speed is approximately 286 Hz. Rotating stall in this case is 54% of the wheel speed, which is typical of the expected values reported in section 2.1 from low-speed machines. Furthermore, the surge frequency is approximately an order of magnitude smaller than the rotating stall frequency. This is also typical of the values found in the published literature on low-speed machines. Thus, the basic flow phenomena present have been identified and are shown to generally agree with the values expected in the open literature (for low-speed machines).

Figure 11 also reveals the operating condition swings associated with the two unstable phenomena. A surge cycle takes the compressor through total pressure ratio, total temperature ratio, and isentropic efficiency swings of approximately .20, .10, and 25%, respectively. The fully developed rotating stall cells take the compressor map through similar swings of .60, .075, and 40% η. It is worth noting that the swings mentioned above are taken from the block averaged traces. Appendix A shows that blade

wakes and other fluctuations are superimposed on these smoothed or quasi-steady characteristics. However, the interest here is only in the quasi-steady transient characteristics. These swings were typical for all the other spans surveyed; however, further comparison was impossible since each spanwise data point was taken during separate runs. Thus, it was impossible to distinguish between a spanwise position that surged strongly or an overall deeper surge of the machine.

The form of surging here appears to be 'classical' surge. The waveform of the surge content was very near sinusoidal. This is typical for 'classic' surge; 'deep' surge (reverse flow) involves distorted exponential decay type waveforms due to the longer times associated with plenum draining and subsequent re-pressurization [7]. Also, the lower limit of the surge cycle does not come very close to the upstream plenum total pressure. If reverse flow occurred, this value would drop very close to or below the upstream plenum total pressure. Thus, this high-speed machine does exhibit many of the same unstable characteristics that have been observed in low-speed machinery.

As mentioned in Chapter 2, a single circumferential probe is undesirable for the instrumentation and subsequent interpretation of rotating stall measurements. Thus, the following statements involve some intuition and some educated assumptions based on the literature search performed. Further experimentation of this nature should involve the use of another circumferentially placed probe.

The form of the stalling appears to be a fully spanwise single rotating stall cell with a rather large circumferential extent (42% or 150° of the compressor annulus). The large circumferential extent is evident from the data (once transformed to the rotating

wheel frame of reference), and it is typical for only one cell to be present when this occurs. Furthermore, the data presented in figures 11 and 12 was taken from 80% span; however, the data taken from all other spans revealed very similar behavior. Figure 13 shows traces of transient stall total pressure ratio taken from various spans. Very little relative difference can be found between the spanwise traces at the first sign of stall. Thus, Rotor 37 also appears to exhibit instantaneous stall across the entire span of the blades. Appendix B shows some interesting contour plots made from the traces of figure 13 that further supports this result. This is contrary to the progressive type stalling that typically originates at the tip or hub and subsequently spreads spanwise as the stall fully develops. This instantaneous fully spanwise stalling is also typical of single-cell large circumferential extent rotating stall (for low-speed machines) [12]. Also, typically low-speed compressors of a high hub-tip ratio exhibit this instantaneous fully spanwise stalling [12]. This data reveals that this high-speed, high hub-tip ratio compressor exhibits this same characteristic. The cause of this is attributed to the relatively short blade spans of high hub-tip ratio machines. This allows conditions necessary for stall inception to simultaneously occur across the entire span of the blades. Instantaneous fully spanwise stalling also supports the hypothesis of section 2.1 that the Rotor 37 shock structure is paramount in causing the rotating stall cells. Since the blade is fully supersonic in the rotor relative reference frame there is a shock structure across the entire blade span. Thus, if shock structure fluctuations are indeed the mechanism for rotating stall cells, it makes sense that this rotor experience instantaneous full span stall simply because the stall mechanism stretches across the entire blade. Full span stall also indicates a sharp

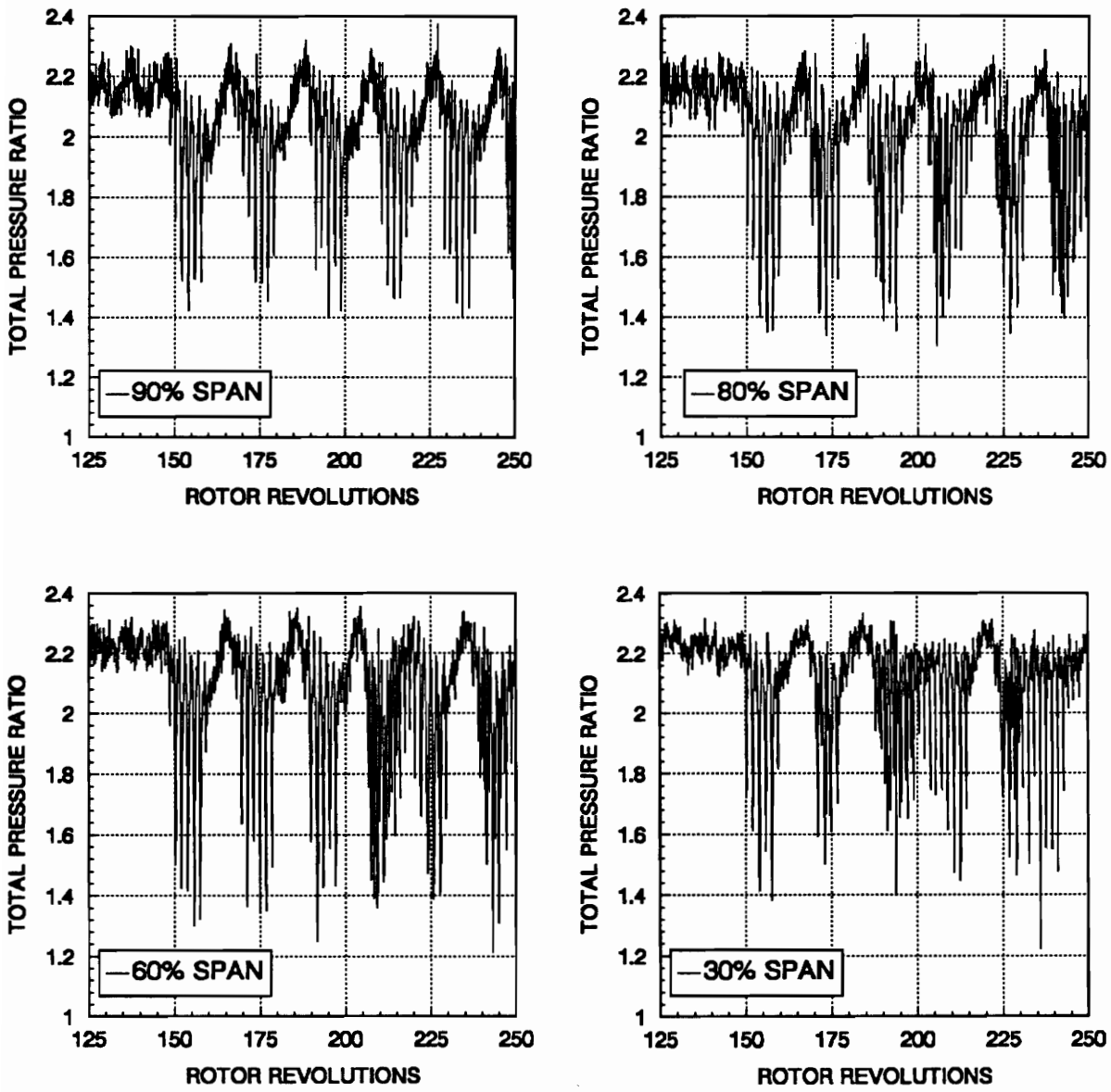

Figure 13. Rotor 37, Spanwise Transient Stall Data, Total Pressure Ratio.

discontinuity between the steady-state and stalled steady-state compressor characteristics [10,14]. However, it is worth mentioning that this rotor would probably exhibit different unstable characteristics if it were tested in the full eight stage compressor configuration.

Figure 14 shows an estimation of the growth of the stall cell as it travels around the rotor. If the frequency of the wheel speed in the absolute reference was 286 Hz, and the frequency of the rotating stall in the absolute reference was 158 Hz, then the frequency of the rotating stall relative to the wheel is simply the difference between these two frequencies (286 Hz - 158 Hz = 128 Hz). This value was used to represent the rotating stall in the rotating wheel reference frame. The circumferential extent of the stall cell on the wheel was then determined. Figure 14 shows that stall was fully developed after nine revolutions and occupied approximately 42% (150°) of the compressor annulus. Figure 14 also makes a comparison with a three-stage low-speed compressor investigated by Greitzer [7]. The rotating stall in Rotor 37 seems to develop somewhat more linear than the three-stage rig. Also, the initial slopes of the two curves differ in that the rotating stall in the three-stage compressor develops faster than Rotor 37. However, after approximately five revolutions the rotating stall develops at the same rate. Whether this effect was due to the high speed nature of Rotor 37 or due to the stacked stage influence of the three-stage compressor is not known. It is worth mentioning that the validity of these statements is based on the previous assumption that only one stall cell was present when Rotor 37 stalled. Multiple circumferential probes would be required to validate this claim.

The assumption that only one stall cell was present when Rotor 37 initially stalled

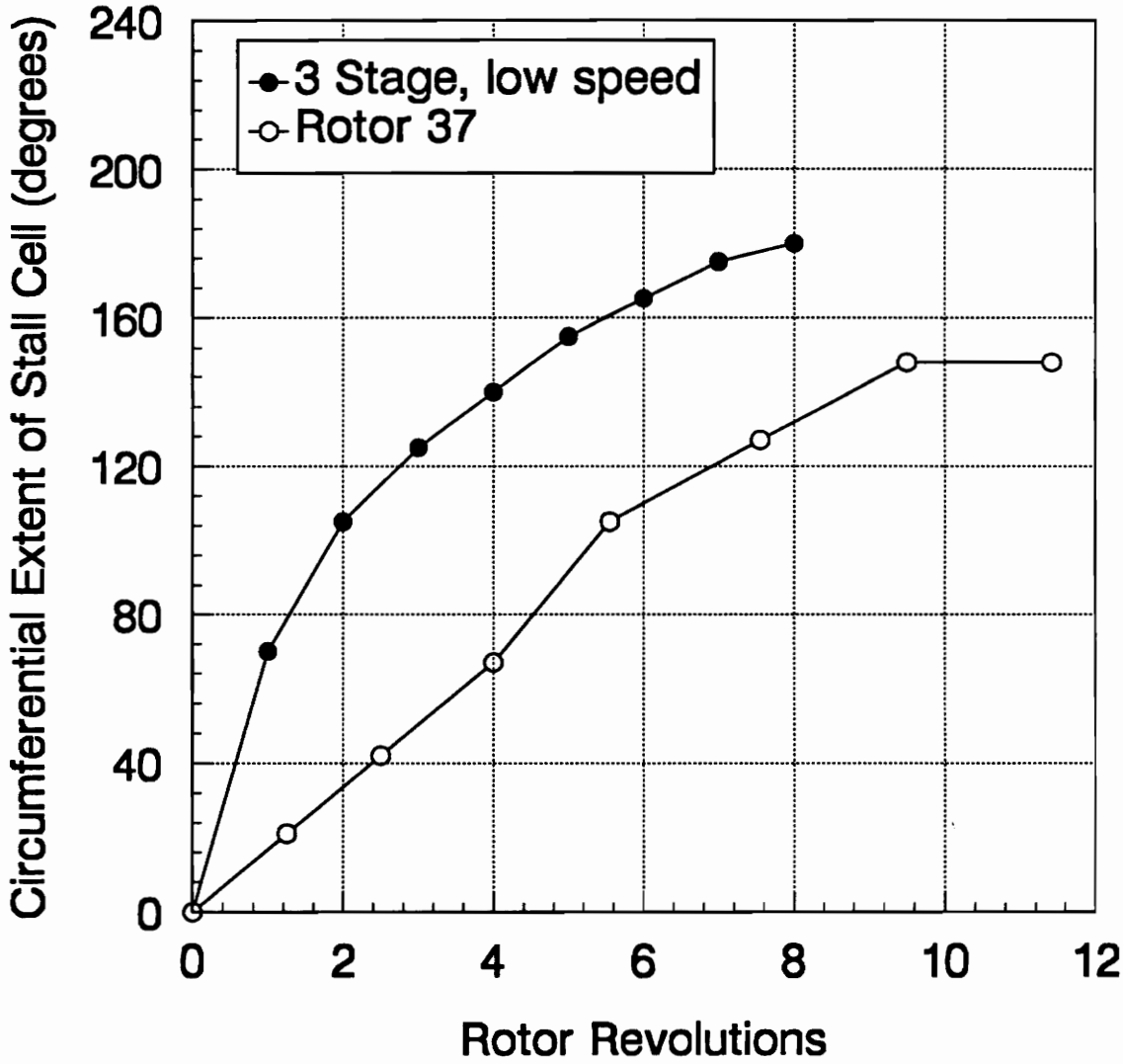

Figure 14. Rotor 37, Stall Cell Growth.

is based on several facts. When a rather large circumferential extent stall cell is present it is typical for only one stall cell to be present (in low-speed machines). Furthermore, when the data is translated to the rotating wheel frame of reference, it is clear that it would be very difficult for two cells of this large extent to be present on the rotor at the same time. Also, the growth rate of the large-extent stall cell is typical of that found in other (low-speed) machines. Also, analysis of the stall cells growth in figure 12 reveals a steady growth in magnitude until the cell is fully developed. If multiple cells had been present neither of these previous two arguments would hold. In summary, it is very likely that the assumption of only one cell being present is correct; however, to validate this claim without uncertainty, would require multiple circumferential instrumentation.

This section has presented some general observations present in the data acquired. The following sections present some more specific results about the behavior of Rotor 37 during unstable operation.

4.3 Surge/Stall Cycle Variations

Figure 15 shows the typical form of the surge cycles found immediately after the inception of unstable operation. These initial surge cycles contain the large circumferential extent single rotating stall cells that were discussed in the previous section. Furthermore, figure 13 shows that this type of large stall cell surge cycle always occurs right after the inception of instability (for all spans tested). Figure 15 illustrates

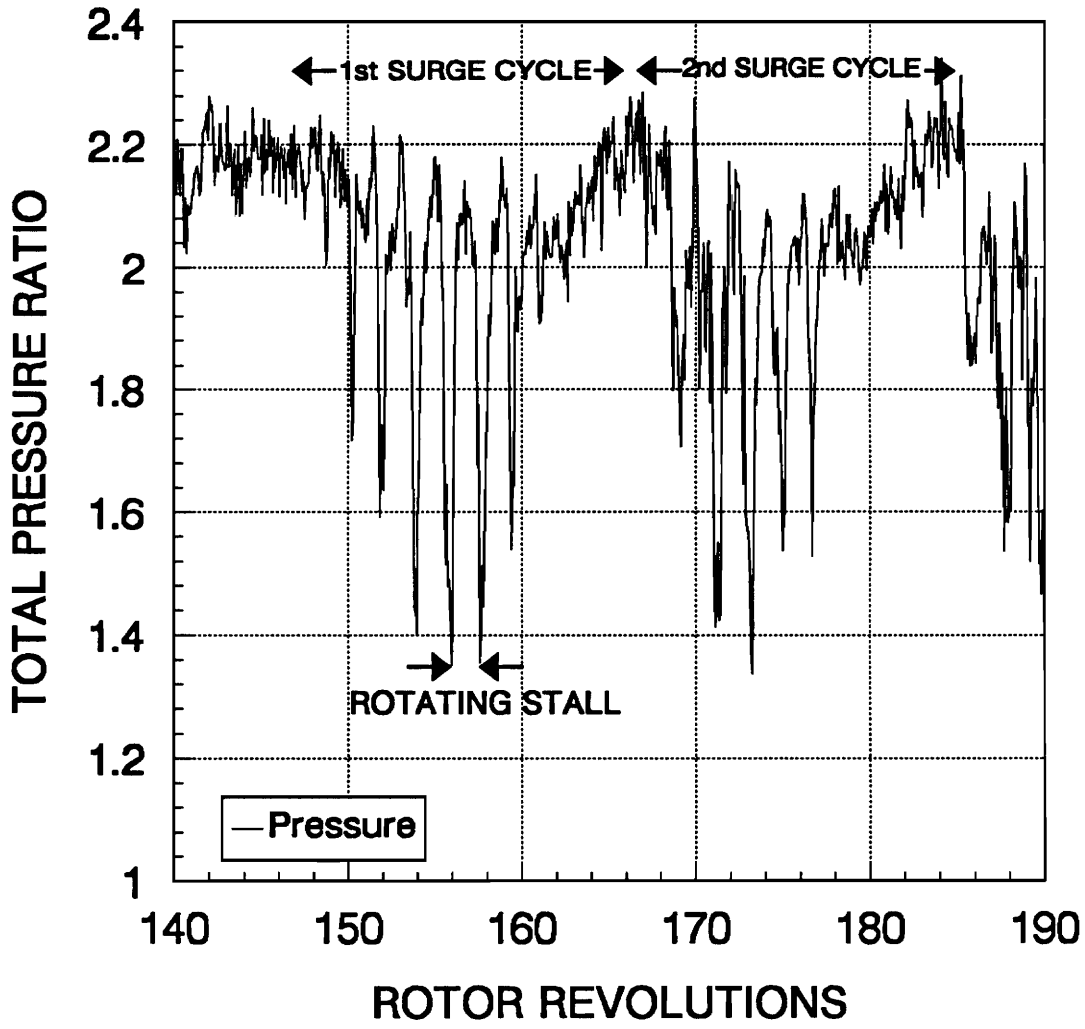

Figure 15. Rotor 37, Typical Form of Surge Cycle.

that large-scale rotating stall developed over the first half of the first surge cycle. At the end of the first half of the first surge cycle the annulus averaged total pressure was at a minimum. At this point, the adverse pressure gradient across the rotor was also minimized. This also means that the impedance to forward flow through the rotor is minimized. At this point, the compressor was able to clear itself out and remove the large-scale single rotating stall cell. The rotor then operated with attached axi-symmetric flow over the second half of the first surge cycle. Subsequently, the pressure ratio for the given mass flow became too high for stable operation and the entire process repeated. Thus, the rotor operated on the stalled characteristics over the first half of the cycle and over the stable characteristics for the second half of the cycle. As mentioned previously, this behavior is typical for axial compressor machines and is widely reported in the literature for low-speed machinery.

Figure 16 presents a close up of the familiar 80% span total pressure ratio trace. Several specific cases of interest are indicated on figure 16 and are represented by the following: case one (revs. 145-185, also shown in fig. 15), case two (revs. 180-220), case three (revs. 215-255), and case four (revs. 235-275). Also, figures 17 and 18 contain close-ups of these four cases for total pressure ratio and isentropic efficiency, respectively. All the cases represent the same number of rotor revolutions (40 revs./two surge cycles) to facilitate comparisons. Furthermore, the cases basically represent different blocks in the forward sequence of time with some slight overlaps. The following discusses the significance of these various cases.

The four various cases are presented to describe the development of the unstable

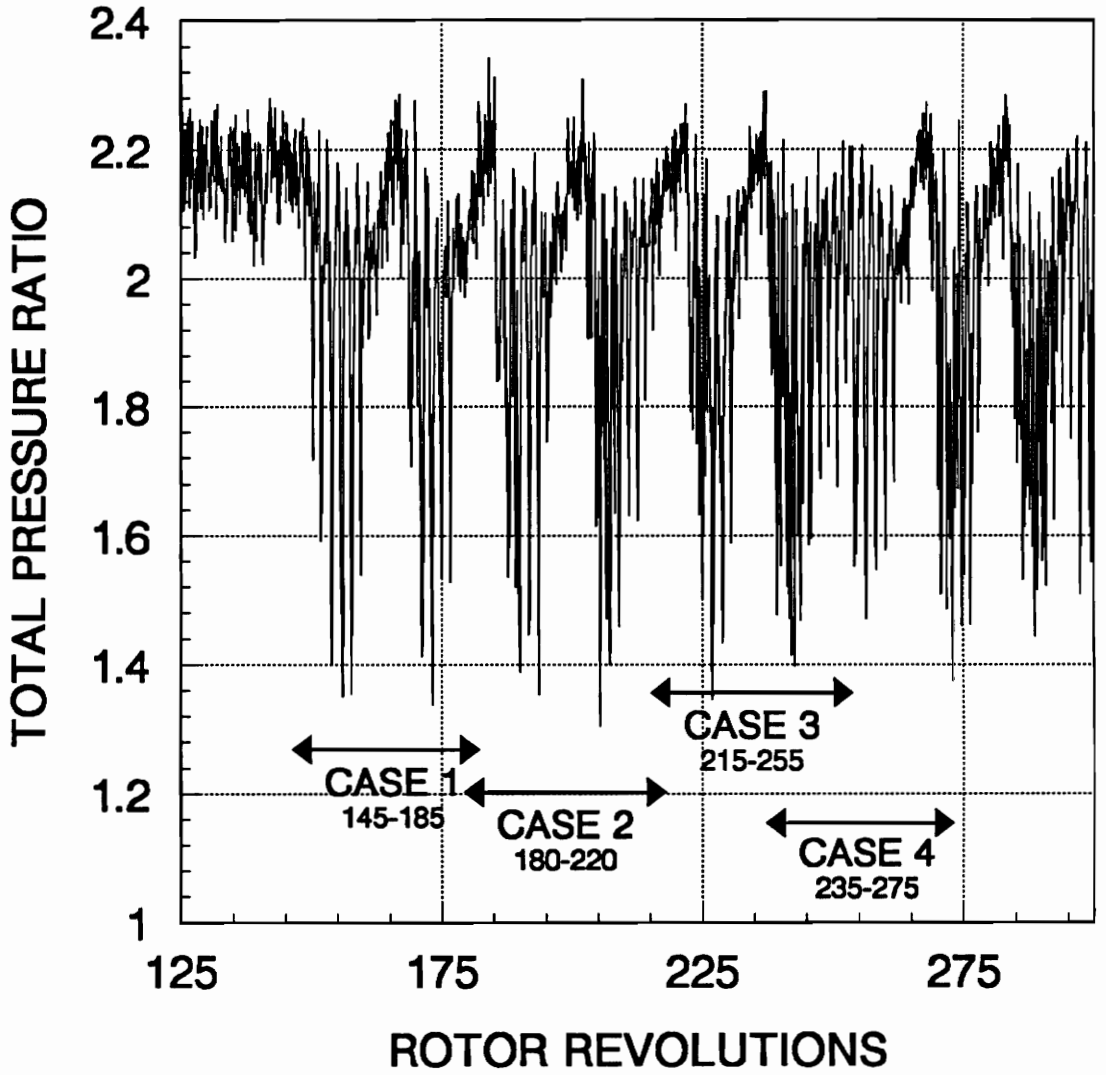

Figure 16. Rotor 37, Transient Stall Data, Total Pressure Ratio, Various Surge/Stall Cycles.

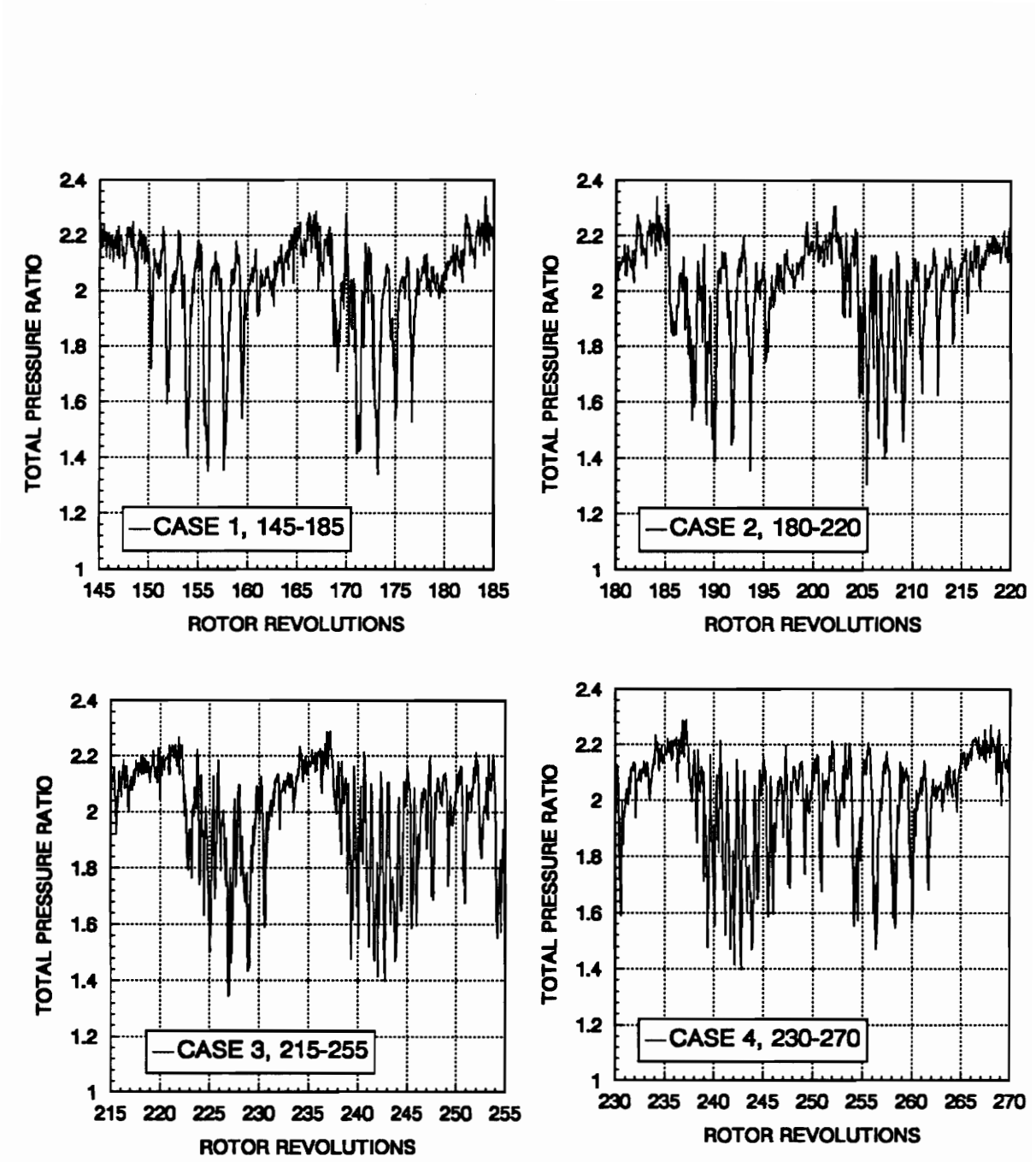

Figure 17. Close Up of Four Cases of Surge/Stall Cycle Variations, Total Pressure Ratio.

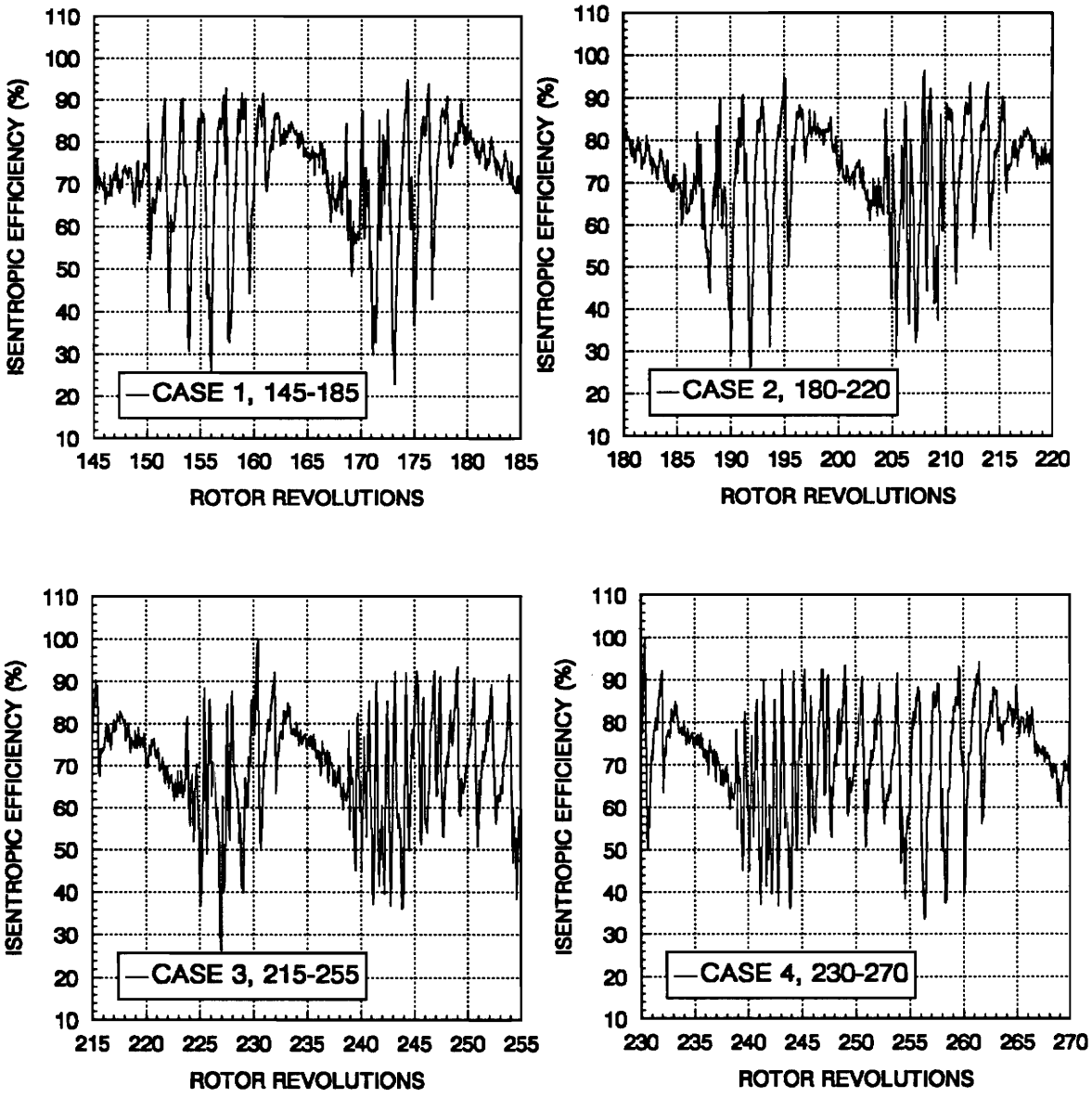

Figure 18. Close Up of Four Cases of Surge/Stall Cycle Variations, Isentropic Efficiency.

operation subsequent to inception. Case one (revs. 145-185) represents the typical large-scale single-cell rotating stall/surge cycles discussed above (figure 15) in which the large-scale stall is present only over the first half of the surge cycles. Both the surge cycles shown in case one exhibit this type of behavior. Furthermore, the rotor always begins unstable operation with at least one surge cycle of this type (see figure 13). The rotor and its system does not have a difficult time in flushing out the large-scale single-cell rotating stall. Cycles of this type always take the compressor in and out of the stable and unstable operating regions.

Moving forward in time to case two (revs. 180-220), we see that the first surge cycle shown is the typical type discussed above. As usual, this cycle flushes out the rotating stall; however, the second surge cycle contains a different type of rotating stall. This rotating stall is characterized by multiple-cells of smaller-extent. This is evident by the closer spacing between the down spikes of the stall cells. However, near the end of the first half of this cycle (rev. 210), the multiple-cell small-scale stall converts to the familiar single-cell large-scale stall. The compressor subsequently flushes out this large-scale stall and again operates on the stable operating range. No attempt is made to predict the growth of the small-scale stall because this information cannot be extrapolated from the data of a single probe.

The first surge cycle in case (revs. 215-255) three behaves very similar to the second surge cycle in case two. Again, stall initially appears as multiple-cells of small-extent, but then turns to a single-cell of large-extent. Subsequently, the compressor flushes out the stall. Case four (revs. 230-270) represents an important distinction in

cycle operation. The first surge cycle in case four contains very strong and developed multiple-cells of small-extent. The big distinction is that the compressor cannot completely flush out rotating stall of this nature. Rotating stall exists through the entire surge cycle and into the second surge cycle. The only 'flushing out' involved is the transition from multiple-cells of small-extent to a single-cell of large-extent that occurs (rev. 247) at the same place the surge usually clears out. The importance here is that it is easier for the compressor and pumping system to flush out a single large-extent-cell than to flush out multiple small-extent-cells.

With only one stall-cell of large-extent present on the rotor, the system operates in both the stable and unstable operation regimes. Thus, the chances of recovery are good because the rotor operates in the stable region during part of the surge cycle. When fully developed small-extent multiple-cell rotating stall is present the system operates over an entire surge cycle in the unstable operating range only. Thus, the chances of recovery are very poor because the rotor never operates in the stable operating region. In this case, the rotor is on its way to forming fully developed rotating stall that results in a stagnation stall condition. If there was some artificial way to control the form of rotating stall present (single-cell of large-extent or multiple-cells of small-extent), the compressor would be much more likely to be able to recover from a potential stagnation stall condition.

Analysis of cases one through four reveal a gradual decrease in the period of the surge cycles as the transient progresses. Case one barely contains two surge cycles in the twenty revolutions shown. However, case four contains significantly more than two surge

cycles for the twenty revolutions shown. This indicates that the period of the surge cycle is a function of the mode of rotating stall that develops. Thus, if the period of the surge cycle could be artificially altered, the mode of rotating stall could be influenced and the chances for recovery from a potential stagnation stall condition increased.

Figure 19 shows the familiar 80% span trace with the surge content superimposed. The ordinate is presented in Psia. to give the reader a better physical feel for the amplitudes of the swings of the unstable phenomena. The surge content was obtained by first performing an FFT over the data trace, filtering out the higher rotating stall frequencies present in the trace, and subsequently performing an inverse fourier transform (IFFT). The result left only the surge content waveform. Of particular interest is the waveform of the surge content present over the case four type surge cycle (revs. 230 - 270). The surge cycle present during case four is severely retarded in comparison to the surge cycle amplitude found in the other cases. This proves that the compressor undergoes a smaller limit cycle oscillation during case four than case one. Such a small limit cycle oscillation that it never reaches into the stable operating region.

A strong surge cycle has the capability to flush out rotating stall while a retarded or weak surge cycle cannot flush out rotating stall. Whether the retarded surge cycle is a result of the multiple stall cells, or whether the multiple stall cells are a result of the retarded surge cycle is unknown. More importantly, these findings indicate that rotating stall and surge are coupled phenomena. How the two phenomena are coupled lies in the future research and analysis of possible coupling mechanisms.

It is also important to note that the phenomena discussed was seen at all spans

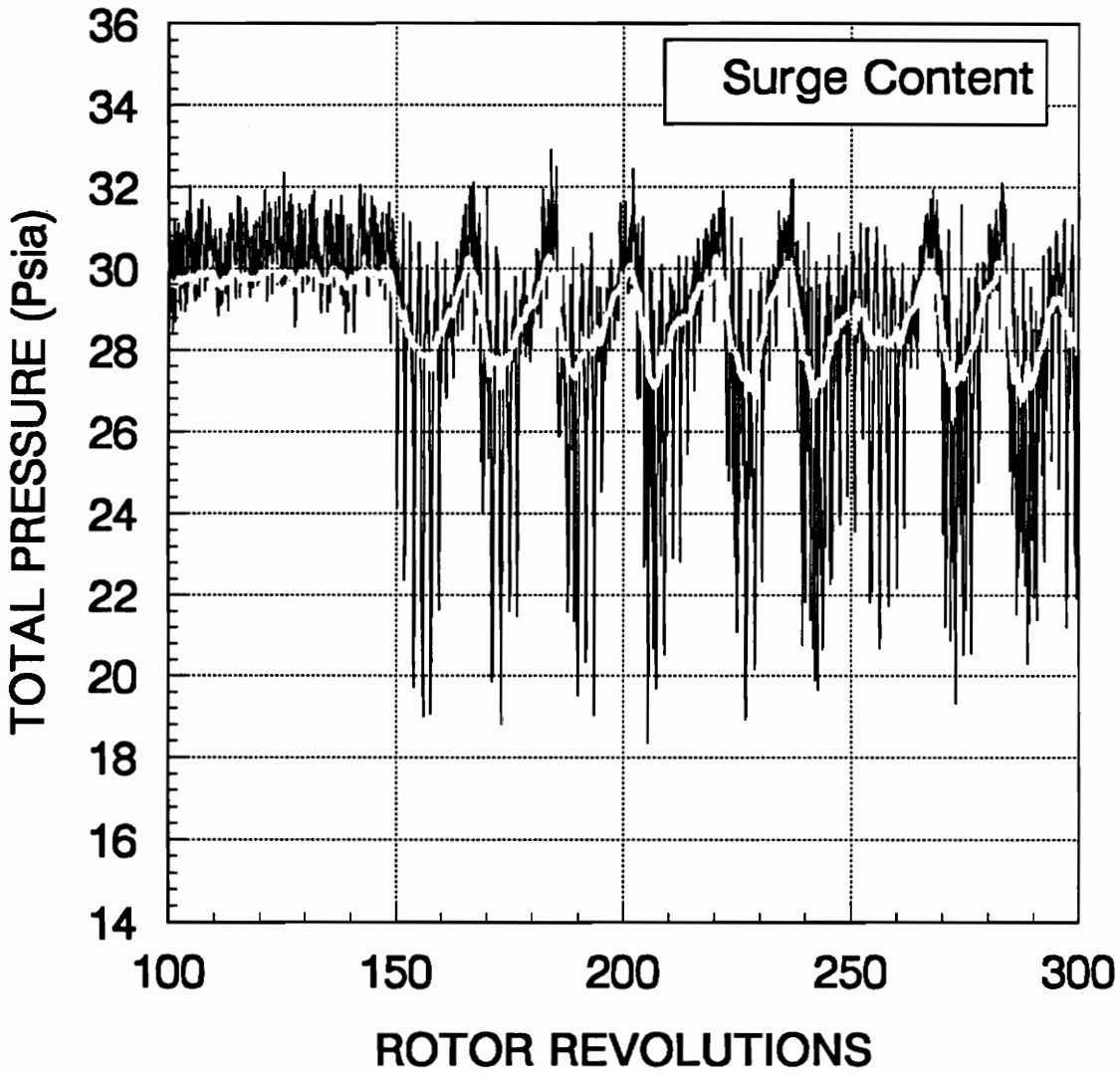

Figure 19. Surge Cycle Content Superimposed on the Block Averaged Data, 80% Span, Run 40.

instrumented. Also, the compressor system went in and out of the various four modes of unstable operation during a single transient cycle. Again, it is unknown what effect the position of the downstream throttle had on the mode of rotating stall that was present. Future research could search for a possible correlation between the throttle position and the transition from single-cell large-extent stall to multiple-cell small-extent rotating stall. Regardless of the influence of the throttle position the observations discussed above stand on their own. Furthermore, to the knowledge of the author, no such measurements of this type in a transonic rotor have ever been published in the open literature.

4.4 Surge/Stall Coupling

The retarded surge cycle coinciding with the small-extent multiple rotating stall cells (figure 19) indicated that there was some form of coupling present between the two phenomena. This section presents some attempts at quantifying this apparent coupling. FFT's were performed on the block averaged characteristics to reveal the prominent frequencies during unstable operation. Figure 20 presents FFT's of total pressure at four different spanwise locations. Figures 21 and 22 present similar plots of total temperature and isentropic efficiency, respectively. The FFT's are represented by amplitude versus frequency in the absolute reference frame.

Analysis of the spanwise FFT's indicate that the amplitudes of the rotating stall and surge frequencies seem to vary in a coupled fashion. For example, figure 20 shows

that at 60% span, the amplitude of the surge frequency is greater than at any other span. Similarly, the amplitude of the rotating stall content is also greater than at any other span. The converse is true for the 30% span data. The point is that the relative amplitudes of the two phenomena vary in a coupled fashion. It is worth mentioning that the slight variations in amplitudes at different spans could be either a function of span or a function of how deep the machine surged. Since the depth of the surging was dependent upon how fast and how far the rig operator closed the downstream throttle valve, no distinction could be made.

A preliminary attempt at quantifying the coupling was made by taking the ratio of the maximum amplitudes of the surge and rotating stall frequencies. However, this ignored all other prominent nearby frequencies except the one that corresponded to the maximum. Thus, another method of quantification was made that took the ratio of the area averages of the entire prominent frequency bandwidth of each phenomena. The surge frequency amplitudes were integrated from 5 to 25 Hz. Similarly, the rotating stall frequency amplitudes were integrated from 130 to 180 Hz. The result was the ratio of the total surge energy content to the total rotating stall energy content. This ratio was computed for total pressure, total temperature, and isentropic efficiency at several spans. Table 3 contains a summary of these calculations as well as the equation used for comparison. Also shown are the mean frequencies of surge and stall for the runs listed.

The ratios are not constant, as would be expected for perfect quantification of the coupling. However, the pressure and efficiency ratios agree fairly well. The pressure ratios agree to within 9% of the mean, while the efficiency ratios agree to within 24% of

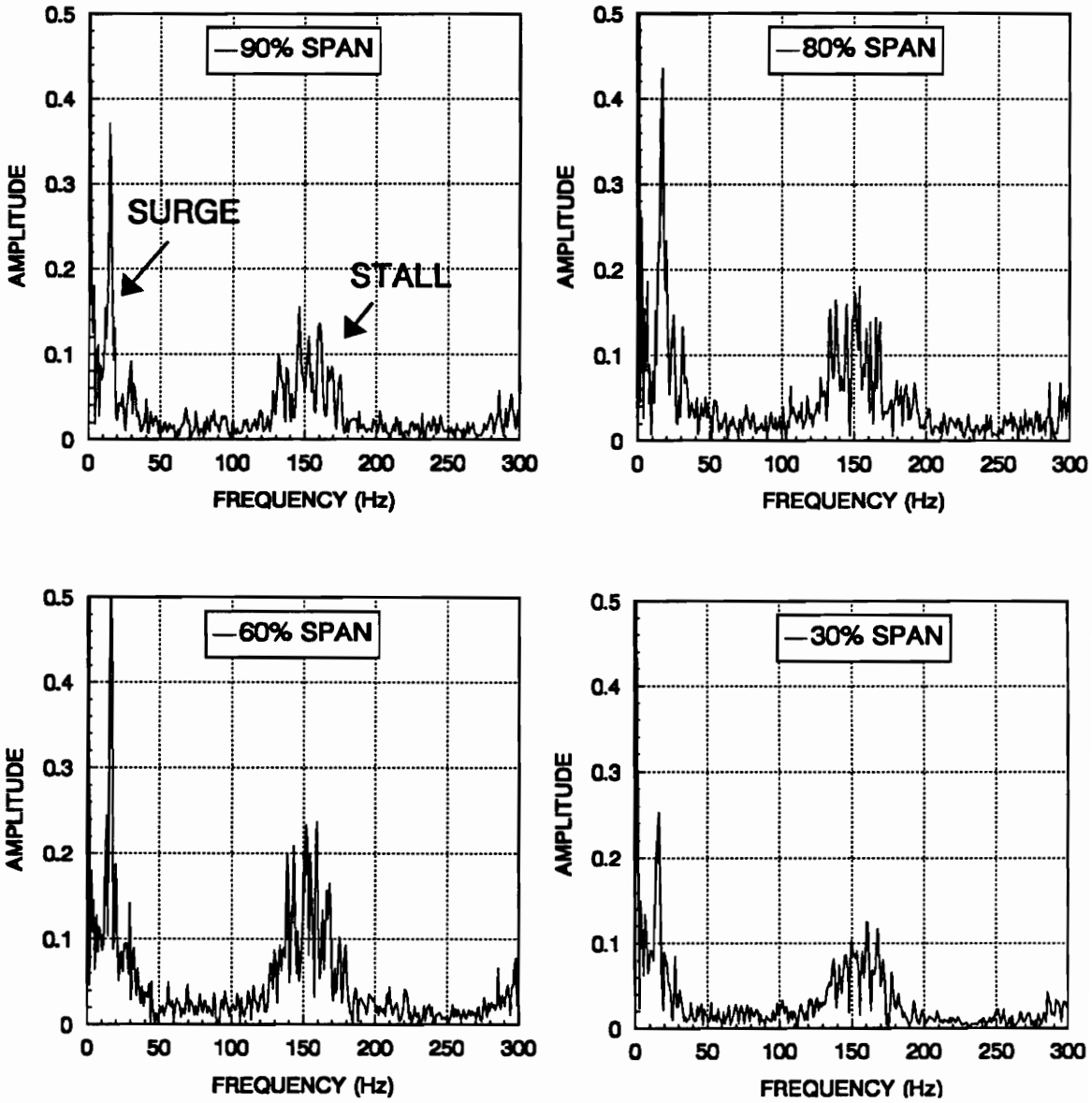

Figure 20. Spanwise Comparison of FFT's, Total Pressure.

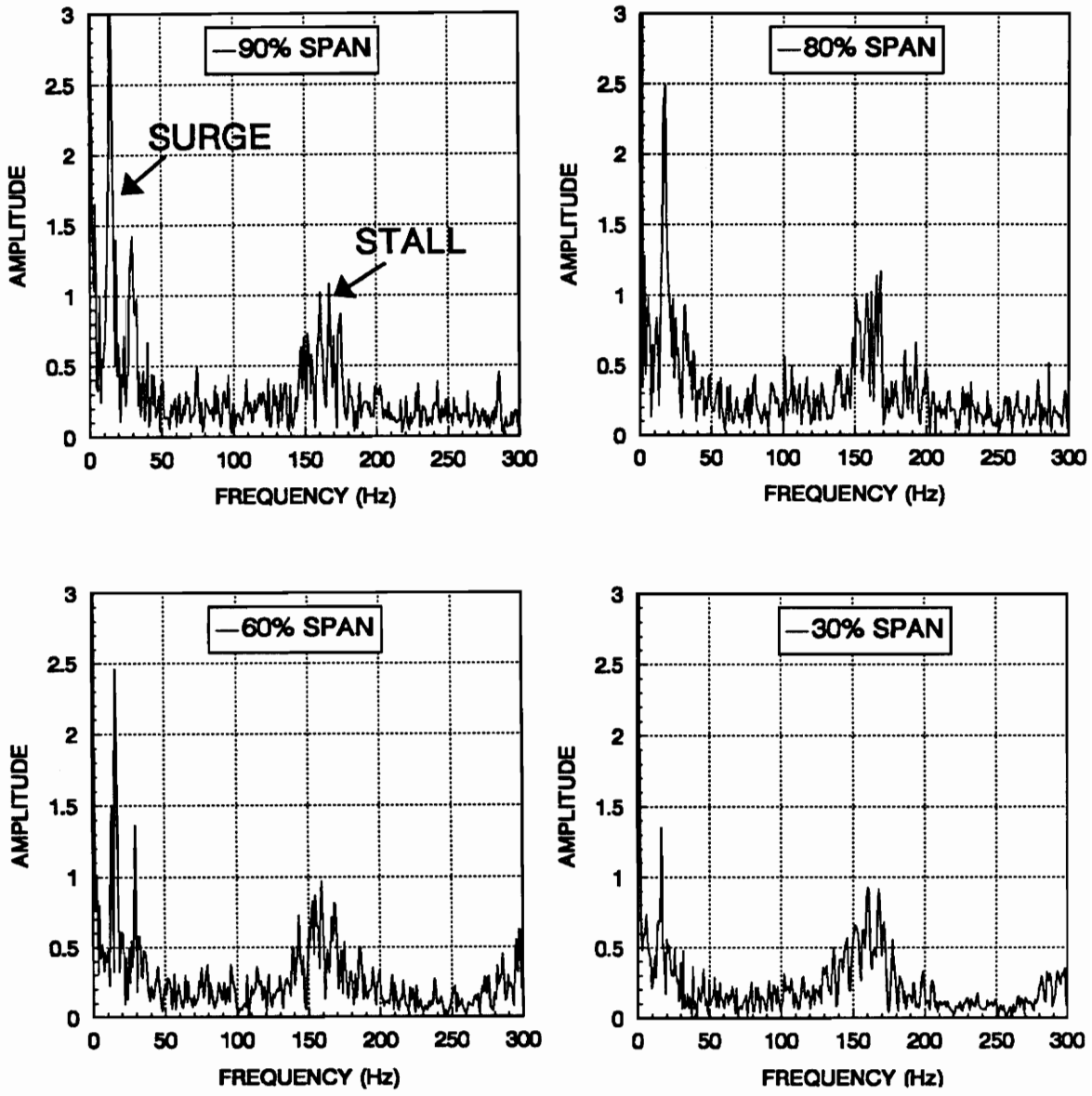

Figure 21. Spanwise Comparison of FFT's, Total Temperature.

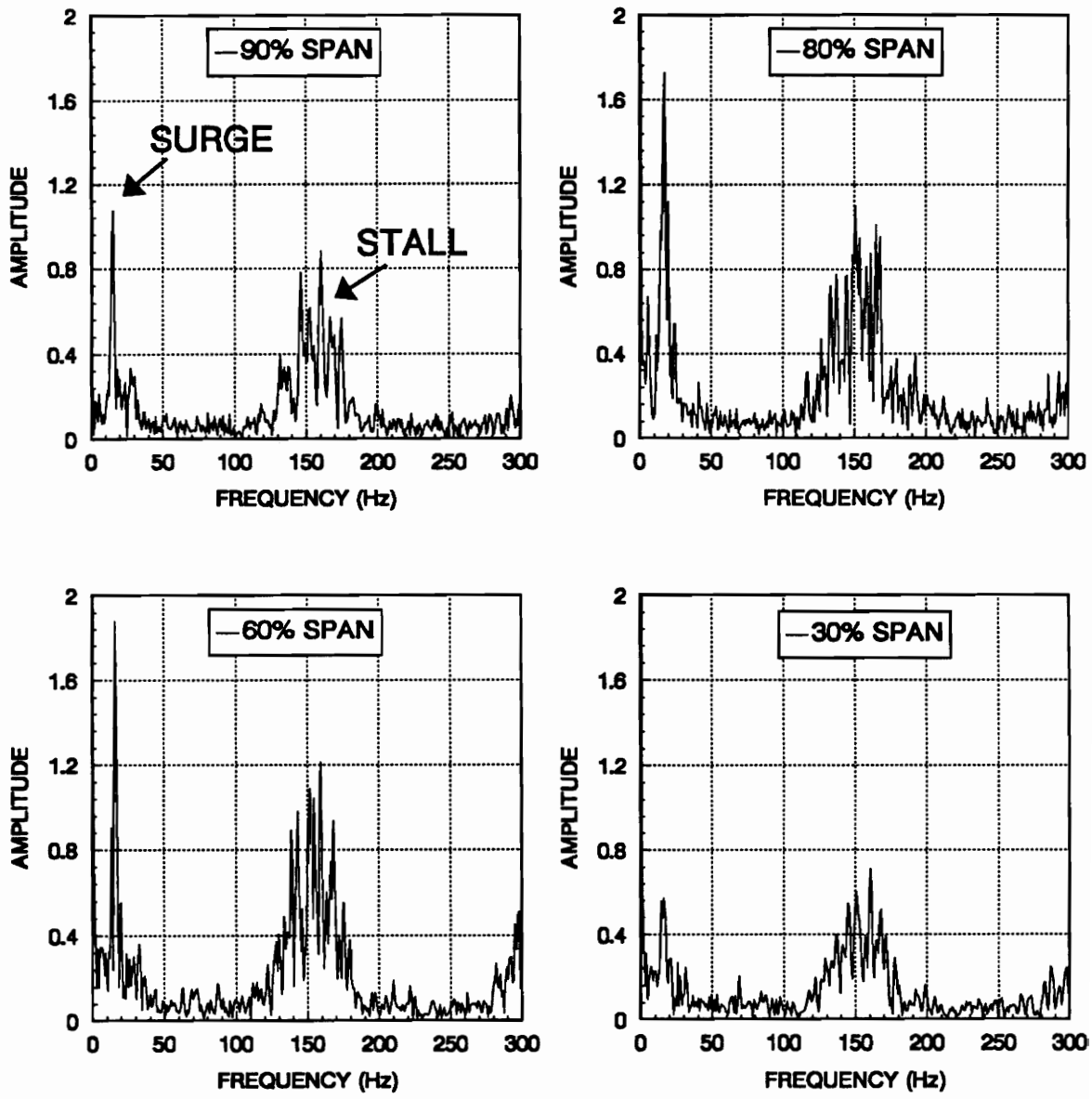

Figure 22. Spanwise Comparison of FFT's, Isentropic Efficiency.

the mean. The temperature ratios vary widely for the runs presented. This indicates that surge and stall are coupled more by a pressure type interaction than by any efficiency or temperature interactions. This is precisely the form of coupling that has been incorporated into the existing stall/surge models found in the open literature.

The mean surge frequency varied from 15 to 17 Hz. While the rotating stall frequency varied from 150 to 160 Hz. Thus, there was no general trend noticed between the mean surge and mean stall frequencies as shown in Table 3. For example, the rig surged at a mean of 17 Hz and stalled at a mean of 158 Hz during run 40; however, run 48 shows that the rig also surged at a mean of 17 Hz while the rotating stall occurred at a mean of 150 Hz. This could be an effect of the throttle valve not going through exactly the same traverse each time unstable operation data was obtained. Note earlier that individual surge cycle periods were shown to be smaller for cycles that contained small-extent multiple-cell rotating stall. These findings still hold because we were looking at the frequencies of individual cycles, not the mean frequency of the entire unstable operation. The surge and rotating stall were coupled but they also exhibited some degree of independence. More exact analysis could be performed by performing FFT's on individual surge cycles; however, the absence of a once-per-revolution signal makes the breaking up of the surge cycles difficult to perform without introducing a phase shift into the data sets. This would effect the very thing that was trying to be measured. Also, another circumferentially located probe would give better data for this type of comparison since the data would be captured during the same transient. In conclusion, the coupling between the two phenomena is related more by total pressure interaction than

Table 3. Summary of Surge/Stall Coupling Quantification

RUN (#)	SPAN (%)	RATIO OF TOTAL ENERGIES: Pressure/Temperature/Efficiency	SURGE (Hz)	STALL (Hz)
38	90	.685 / .914 / .328	15	155
40	80	.689 / .714 / .454	17	158
43	60	.600 / .603 / .344	16	159
45	30	.666 / .438 / .308	16	160
48	95	.655 / .837 / .391	17	150

$$\text{RATIO OF TOTAL ENERGIES} = \frac{\Sigma \text{ Surge Amplitudes (5-25 Hz)}}{\Sigma \text{ Stall Amplitudes (130-180 Hz)}}$$

by total temperature or efficiency effects. However, since the data being compared (at different runs) was obtained during different transients, it is difficult to make any concrete conclusions.

4.5 Comparison of 100% and 90% Speed Data

Figure 23 shows a comparison of instability data taken at 100% speed (80% span) and 90% speed (90% span). This was the only data taken at off-design speed; however, several interesting observations are apparent from the comparison presented. The FFT's indicate an almost reversal of the energies associated with surge and rotating stall. The 100% speed data is dominated by surge; however, the 90% speed data is dominated by rotating stall. This is quite a drastic change in the systems transient characteristics for only a 10% decrease in wheel speed.

Figure 24 shows a close up of the 90% speed data. The transient operation initially underwent a surge cycle in which the rotating stall developed and then went away. Subsequently, the surge content of the trace decayed very similar to that of an underdamped system. By revolution 250, the surge was almost completely dissipated and the rotor was operating in almost pure rotating stall. Thus, it seems that surge was instrumental in initiating the instability; however, rotating stall was the final result.

The mean frequencies of the surge and rotating stall were 15 Hz and 146 Hz, respectively. These are similar to the values found at 100% speed. However, the

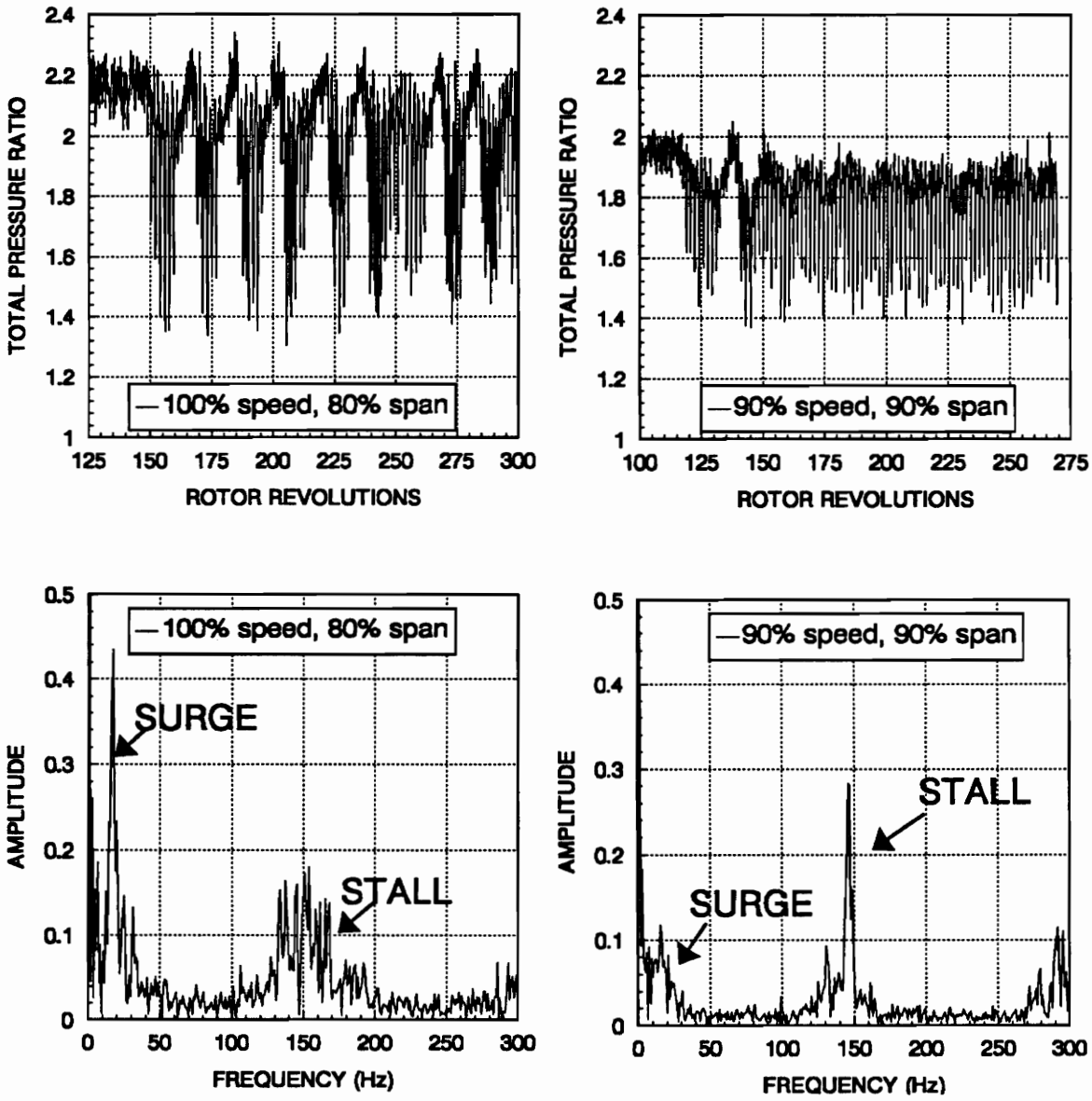

Figure 23. Comparison of 100% and 90% Speed Data.

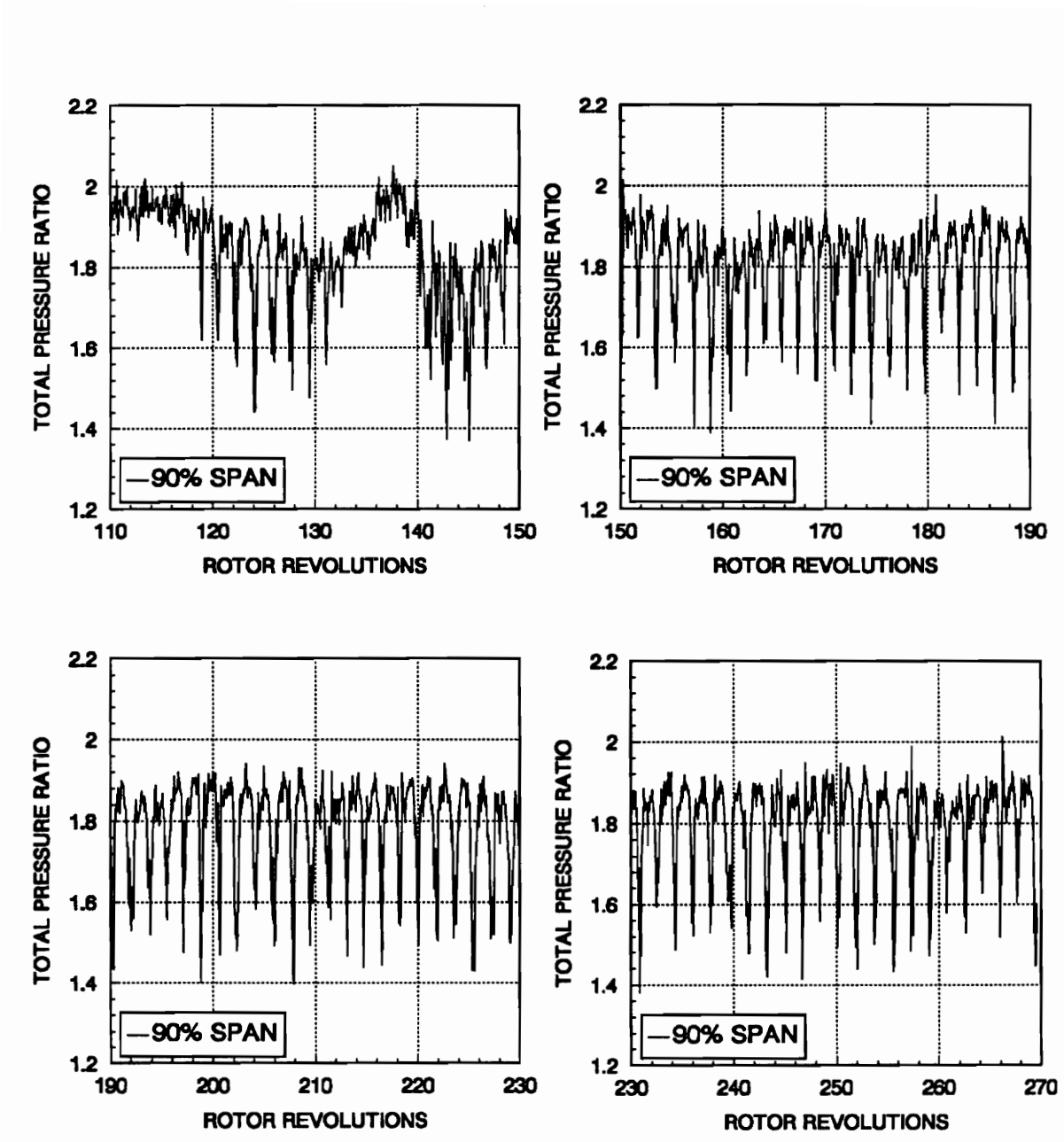

Figure 24. Close Up of 90% Speed Data.

bandwidth of the rotating stall prominent frequencies are much wider for 100% speed than for 90% speed. The 90% speed stall frequency displays a very sharp narrow spike. This indicates that rotating stall at 100% speed varies considerably in frequency content as discussed in section 4.4. This is not surprising since the stall develops and decays several times in the trace presented. Rotating stall at 90% speed has a more repeatable pattern much like that found in pure rotating stall. The 90% speed rotating stall occupied from 22% (80°) to 35% (125°) of the compressor annulus. This was obtained by first representing the data in the rotating wheel reference frame. The number of rotating stall cells cannot be determined from the information available.

These conclusions support similar findings on low-speed machines that high operating speeds are likely to exhibit surge while lower operating speeds are likely to feature rotating stall [7,14]. This trend is shown to be consistent with this particular transonic rotor and the system tested. Wheel speed is a strong function of the mode of unstable operation for this low aspect-ratio transonic rotor.

4.6 Comparison to Greitzer's Model

The following section presents a discussion of the attempts made to match the data taken with Greitzer's non-linear, one-dimensional, lumped-parameter stability model. A complete derivation of the model is presented in reference [7]. The model was developed with the following important assumptions: a low inlet relative mach number, a small

pressure rise compared to the ambient, a containment of all the kinetic energy to the rotor and compressor ducting (helmholtz resonator system), a containment of all the potential energy to the downstream plenum (helmholtz resonator system), an ideal system with a large plenum volume compared to the volume of the compressor ducting and throttle ducting, and incompressibility in the compressor and throttle ducts. Also, the model's system of governing equations incorporates a time lag that simulates the fact that the system's unstable operating characteristics do not act the same transiently as they do in the steady-state. In other words, there is a definite time lag between the onset of instability in a compressor and the establishment of the fully developed rotating stall pattern [7]. Despite all these assumptions, the model was tried anyway because it was the simplest model available and this facilitated a good starting point. The use of the data for more complicated model validation is reserved for future work.

Greitzer's model simulates a slight perturbation off the steady-state characteristics and predicts the subsequent transient unstable operation. Outputs from the model include the quasi-steady transient response of the total pressure and mass flow of the compressor system. Quasi-steady meaning that the model does not predict rotating stall, only the transient operation of the mean flow quantities (i.e. sinusoidal type surge oscillations or the exponential decay type response for developing pure rotating stall).

Inputs to the model included system geometry parameters, stable steady-state characteristics, and unstable steady-state characteristics. The stable steady-state characteristics of Rotor 37 were obtained during the experiment and were also well documented from past researchers [23,24] (see figure 4). The unstable steady-state

characteristics were not obtained during the experiment. Furthermore, these characteristics cannot be obtained because prolonged rig operation of Rotor 37 at 100% speed involves the risk of melting the blades or destroying the rig [33]. Thus, the approach was to simply make educated guesses at the general level and trends of the unstable steady-state characteristics until an acceptable solution was obtained.

The level of the unstable characteristics was the controlling factor in the amplitude of the surge cycles output form the model. Also, the trends of the unstable characteristics were the controlling factor in the waveform of the surge cycles (i.e. sin wave, saw-tooth wave, clipped sin wave, etc.). The amplitude of the surge cycles found in Rotor 37 are apparent from figure 15. The surge cycles swing from a pressure ratio of 2.24 to a pressure ratio of 1.9, a total swing of 0.34. The sinusoidal type waveform of the surge cycles is also apparent from figure 15. Thus, the unstable steady-state characteristics must be chosen to deliver surge cycle swings from 2.24 to 1.9 pressure ratios with a sinusoidal type waveform. These requirements were met by a trial and error method.

Figures 25 and 26 illustrate the use of different unstable steady-state operating characteristics and their ability to match the amplitude and waveform of the surge cycle required. The figures include plots of pressure ratio and non-dimensional mass flow rate versus non-dimensional time (top two plots), and pressure ratio versus non-dimensional mass flow rate (bottom plot). Figure 25 represents an unstable steady-state curve that is too 'deep', i.e. the surge cycle amplitude swings from 2.24 to 1.65 pressure ratios. However, the waveform of pressure trace is approximately sinusoidal as required. The excessive amplitude of the surge cycle was corrected by shifting the unstable

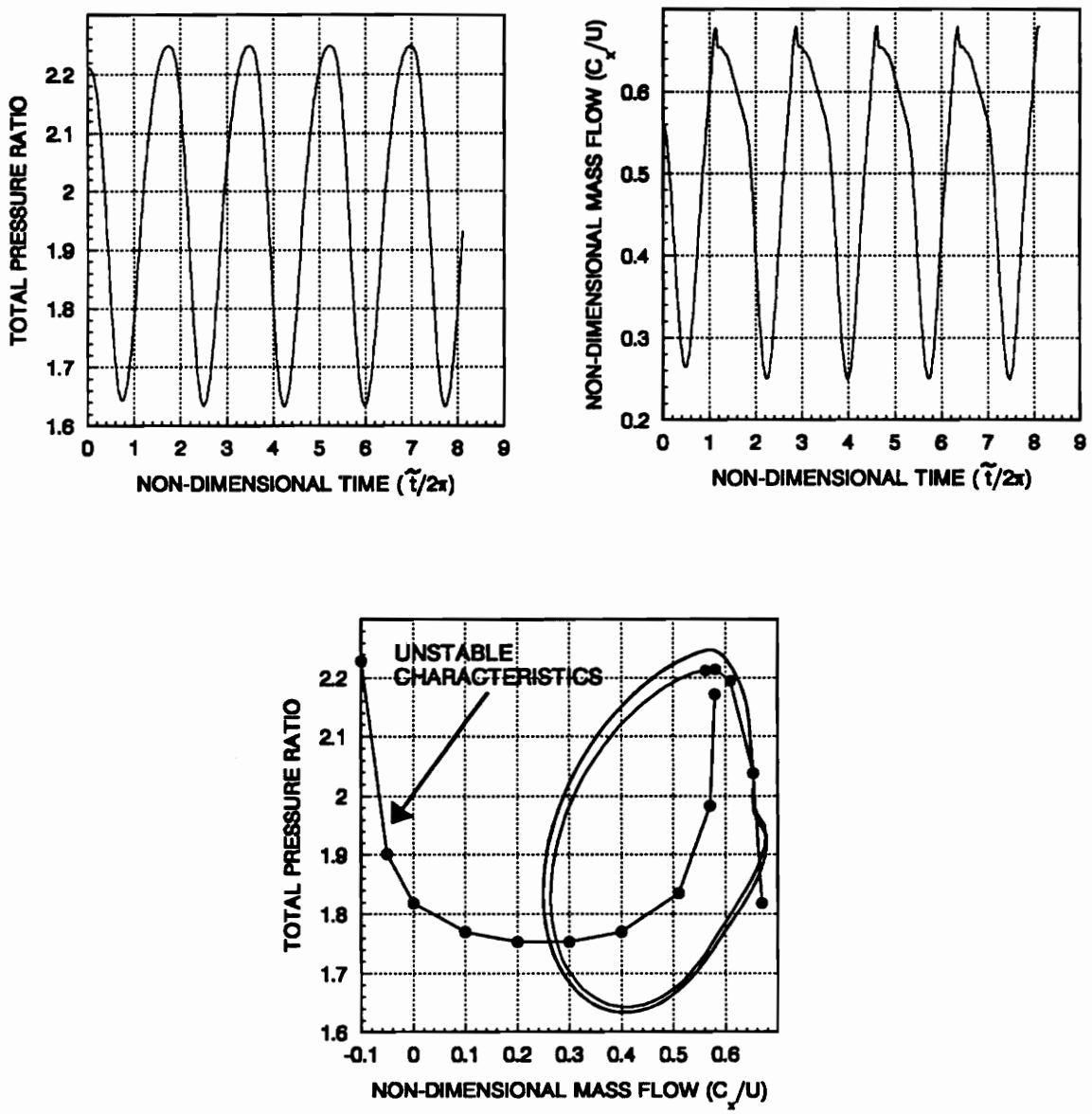

Figure 25. Solution of Greitzer's Model with Incorrect Unstable Characteristics.

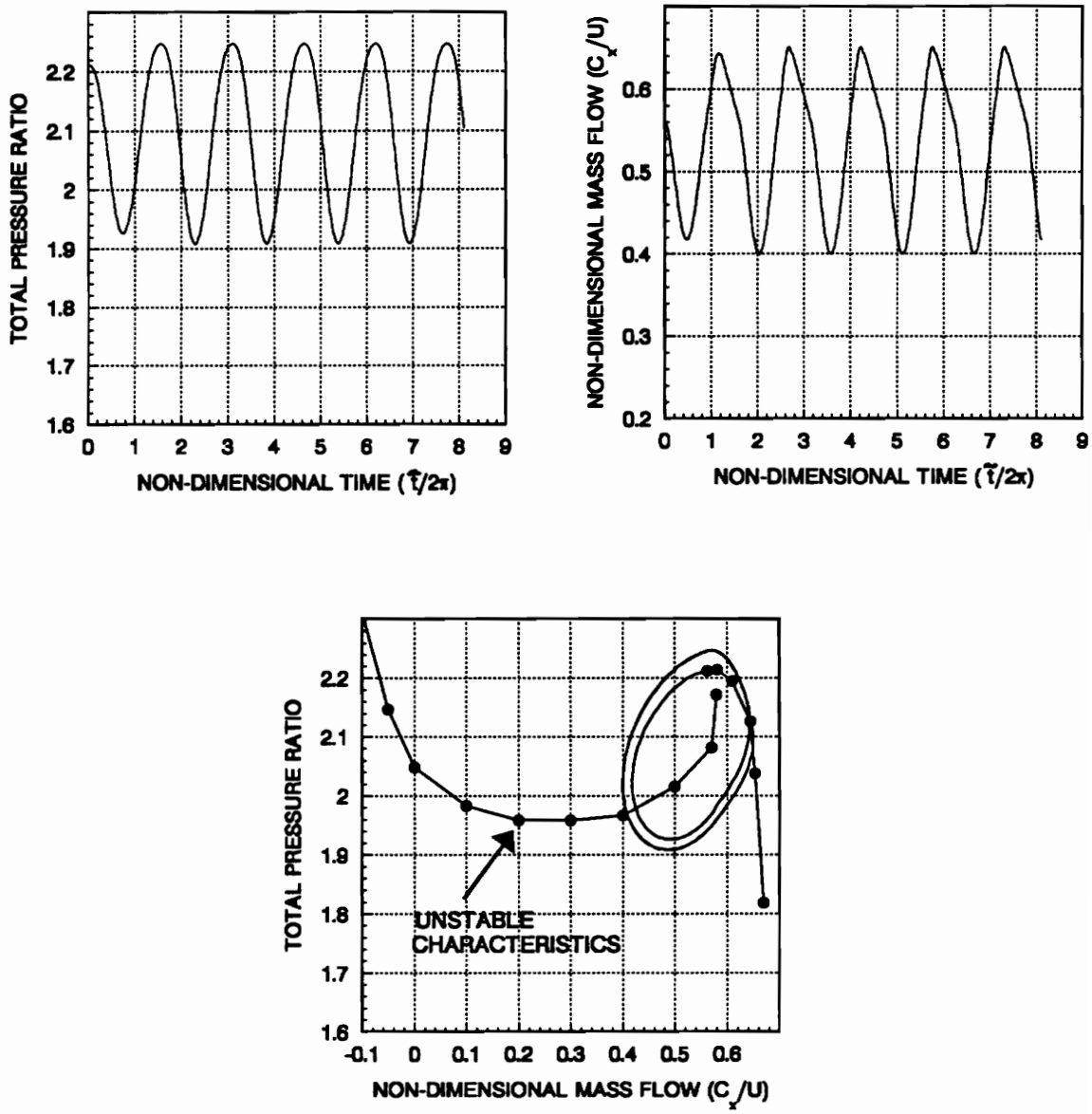

Figure 26. Solution of Greitzer's Model with Acceptable Unstable Characteristics.

characteristics of figure 25 upward. Figure 26 shows the solution obtained when the unstable characteristics are set at the proper level to give the correct surge cycle swings. Figure 26 shows a surge cycle swing from 2.24 to 1.9 pressure ratios with a sinusoidal type waveform as required from the experimental data. The unstable characteristics presented in figure 26 give a very close simulation to the amplitude and waveform of the surge cycles found in the experimental data. Thus, the unstable characteristics shown in figure 26 were employed in the following computations using Greitzer's model.

The geometry of the compressor pumping system is also one of the most important inputs into Greitzer's stability model. The compressor system geometry was determined as accurately as possible by inspection of existing shop drawings, listed references, and personal inspection of the test rig. Two possible configurations of the system geometry were possible because of uncertainties involved in the flow path of the downstream collector valve. The uncertainty lies in whether or not the diverging annulus downstream of the rotor contained a step change (decrease) in diameter. The result of this step change contributes to a larger effective downstream plenum.

Figures 27 and 28 show cross sectional views of both possible system geometries. The figures show the location of the compressor duct length, the throttle duct length, and the volume that was modeled as the plenum volume. Also apparent in the figures is the cross sectional area of the compressor rotor. The distinguishing feature between the two geometries is the size of the plenum volume. It is uncertain if this step change in the diverging annulus was completely sealed during the experiment. If it was not sealed, this additional volume would be considered part of the compressor pumping system. Thus,

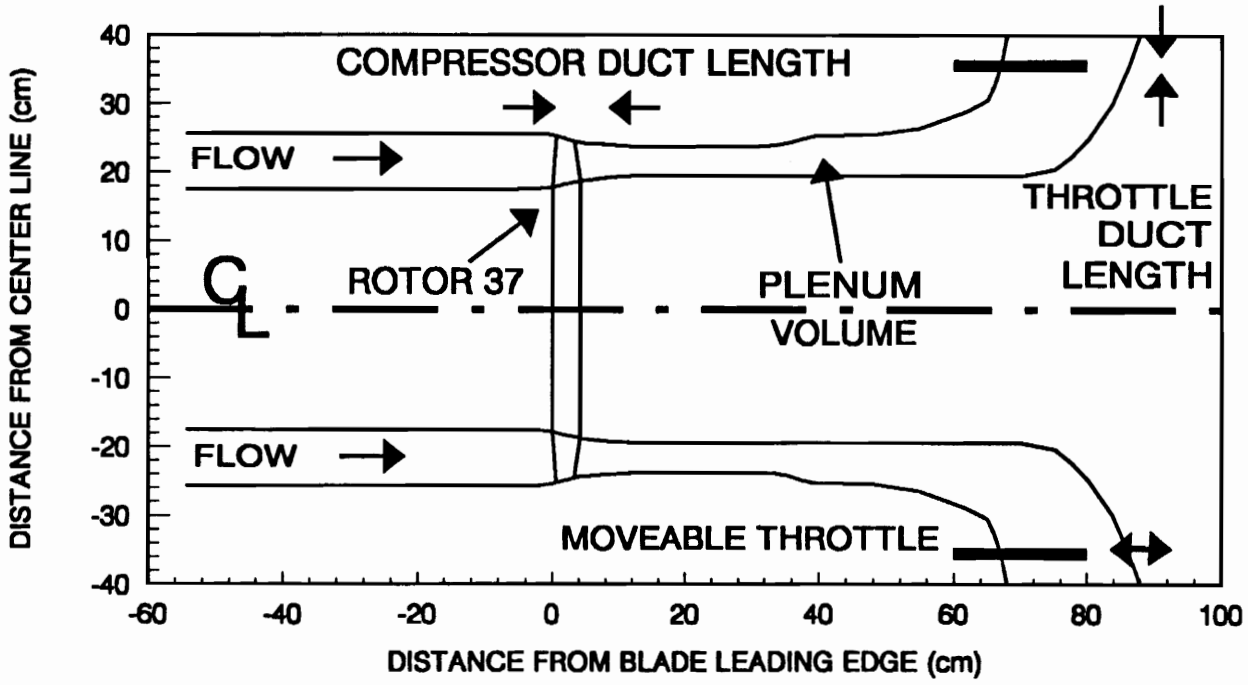

Figure 27. Detail of Compressor System Geometry used in Greitzer's Stability Model - Small Plenum Volume.

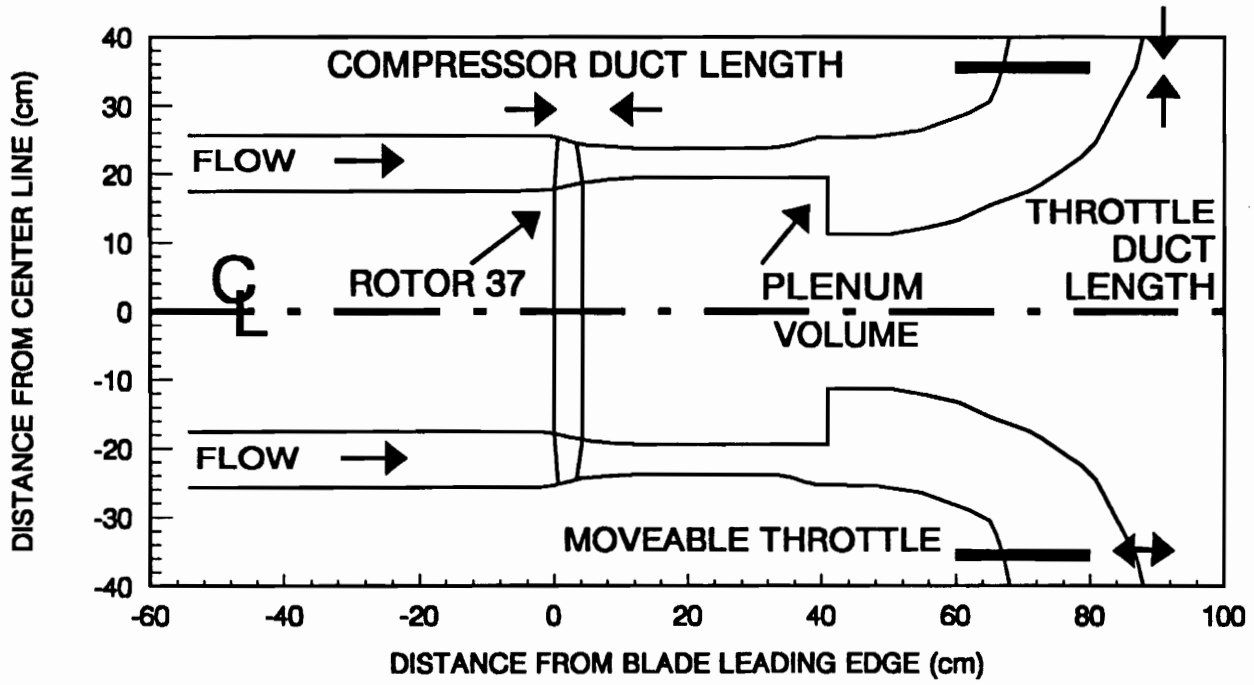

Figure 28. Detail of Compressor System Geometry used in Greitzer's Stability Model - Larger Plenum Volume.

the procedure employed was to solve both system geometries during the efforts to model the systems unstable operation. The results from both geometries are presented in the following discussions.

Table 4 presents the results from Greitzer's model for several different cases that were applied to the geometry presented in figure 27. The different cases represent trade-off's between compressor duct length and the downstream plenum volume (i.e. the longer the assumed compressor duct length, the smaller the downstream plenum volume). This was necessary because of the unclear dividing line between the compressor duct length and the plenum volume (apparent from figures 27 and 28). This uncertainty was not present in the experimental system constructed by Greitzer to meet the assumptions made in the development his model. The geometry of the Rotor 37 test rig was very different from the system geometry used by greitzer to validate his model [7]. Greitzer's mechanical model met all the assumptions previously discussed, the most important being the helmholtz resonator theories. The system geometry present for Rotor 37 does not really have a separated downstream plenum as greitzer's model has. Also, there is really no throttle duct as Greitzer's model has. Thus, the various cases presented in Table 4 represent attempts to find the 'best' geometric combination possible to match the system geometry modeled by the governing equations.

The variables in table 4 stand for the following: A_c is the cross sectional area of the compressor annulus at the rotor, L_c is the compressor duct length, A_t is the throttle discharge area, L_t is the length of the throttle duct, V_p is the volume of the downstream plenum, B is Greitzer's non-dimensional stability parameter, ω is the helmholtz resonator

frequency of the system, $\mathfrak{t}$ is the non-dimensionalized time constant, and $f_{predicted}$ is the frequency of the surge cycles predicted by the model. The values of B, ω and $\mathfrak{t}$ are defined below.

$$B = \frac{U}{2a}\sqrt{\frac{V_p}{L_c A_c}} \qquad [4.1]$$

$$\omega = a\sqrt{\frac{A_c}{V_p L_c}} \qquad [4.2]$$

$$\mathfrak{t} = (\frac{\pi R}{L_c})(\frac{N}{B}) \qquad [4.3]$$

The additional variables stand for the following: U is the mean blade speed, a is the local speed of sound, R is the mean rotor radius, and N is the number of stall cell revolutions required to obtain fully developed rotating stall. The value of N was kept at 2 for the calculations presented in table 4 (reference [7]). G, which is a non-dimensional geometric parameter, defined by equation [4.4], was shown to have little effect on the output of the model. Greitzer also documented a weak effect of G while developing his model [7].

$$G = \frac{L_t A_c}{L_c A_t} \qquad [4.4]$$

Thus, the value of G was kept at .133 (value obtained for case 1 in tables 4 and 5) for all the following calculations presented.

Figure 29 shows the typical solution obtained from Greitzer's model using the cases presented in table 4. Figure 29 is for case 10, with B = .737. The figure shows

Table 4. Greitzer's Model Attempts for Geometry without Extra Plenum Volume.

CASE #	A_c (m^2)	L_c (m)	A_t (m^2)	L_t (m)	V_p (m^3)	B	ω	$\tilde{\tau}$	$f_{pred.}$ (Hz)
1	.10	.05	.15	.01	.095	2.53	1560	11.42	233
2	.10	.09	.15	.01	.092	1.86	1180	8.63	171
3	.10	.13	.15	.01	.090	1.52	893	7.31	122
4	.10	.17	.15	.01	.087	1.31	768	6.49	106
5	.10	.21	.15	.01	.084	1.16	680	5.93	96
6	.10	.25	.15	.01	.081	1.05	614	5.53	83
7	.10	.29	.15	.01	.079	.955	560	5.22	80
8	.10	.33	.15	.01	.076	.880	516	4.98	78
9	.10	.37	.15	.01	.073	.816	479	4.79	73
10	.10	.41	.15	.01	.066	.737	433	4.78	66
11	.10	.46	.15	.01	.059	.658	386	4.77	61
12	.10	.51	.15	.01	.052	.587	344	4.83	54

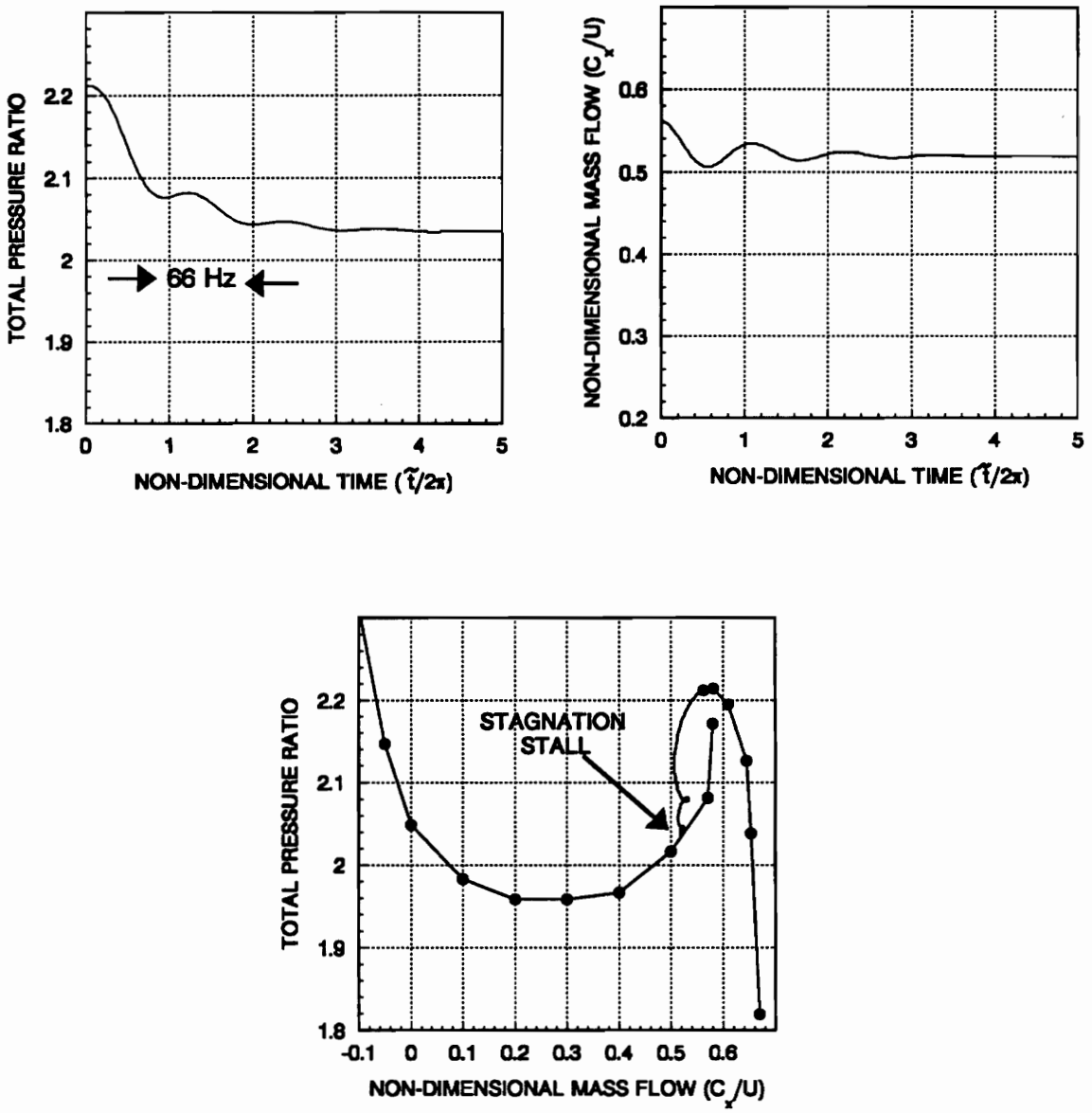

Figure 29. Greitzer's Model Typical Solution for the Cases shown in Table 4.

that the model predicts a stagnation rotating stall type operation. This solution is typical for all the cases presented in table 4. Clearly, this is far from the surge type operation prediction that is desired. The $f_{predicted}$ values shown in table 4 are the frequencies of the first oscillations, as shown in figure 29. Thus, the model must first be adjusted to predict surge type operation, rather than rotating stall. However, the results from the geometry shown in figure 28 will be presented first.

Table 5 presents the same parameters applied to the system geometry with the added plenum volume (figure 28). Figure 30 shows the typical solutions obtained from the cases presented in table 5. Figure 30 is for case 12, with B = .714. Again, figure 30 is typical for all the cases shown in table 5. As before, the prediction is a stagnation rotating stall type condition. Thus, all the cases shown in tables 4 and 5 predict a stagnation rotating stall condition as shown in figures 29 and 30. Since this is clearly different from the surge operation that should be predicted, some deficiencies in applying Greitzer's model to this system must exist. The most likely being the fact that the ideal system (geometry) used to develop the model is not the same as the experimental system (geometry).

Note that the observations presented in section 4.5 showed that at 100% speed the rig surged, but at 90% speed the rig went into rotating stall. According to Greitzer's model, this indicates that this compressor system is very close to the critical B parameter of .70 that is the dividing line between surge or rotating stall operation. Thus, according to Greitzer's theory, the B parameter for the Rotor 37 compressor system is very close to .70. This was the reasoning behind presenting cases 10 (B = .737) and 12 (B = .714)

Table 5. Greitzer's Model Attempts for Geometry with Extra Plenum Volume.

CASE #	A_c (m^2)	L_c (m)	A_t (m^2)	L_t (m)	V_p (m^3)	B	ω	$\tilde{\tau}$	$f_{pred.}$ (Hz)
1	.10	.05	.15	.01	.119	2.82	1396	10.24	205
2	.10	.09	.15	.01	.116	2.08	1053	7.72	148
3	.10	.13	.15	.01	.113	1.71	886	6.50	125
4	.10	.17	.15	.01	.111	1.48	784	5.76	112
5	.10	.21	.15	.01	.108	1.31	714	5.24	98
6	.10	.25	.15	.01	.105	1.19	663	4.87	95
7	.10	.29	.15	.01	.102	1.09	623	4.58	89
8	.10	.33	.15	.01	.099	1.01	593	4.35	85
9	.10	.37	.15	.01	.097	.938	568	4.16	79
10	.10	.41	.15	.01	.090	.858	558	4.11	77
11	.10	.45	.15	.01	.083	.787	556	4.08	74
12	.10	.50	.15	.01	.076	.714	551	4.05	72

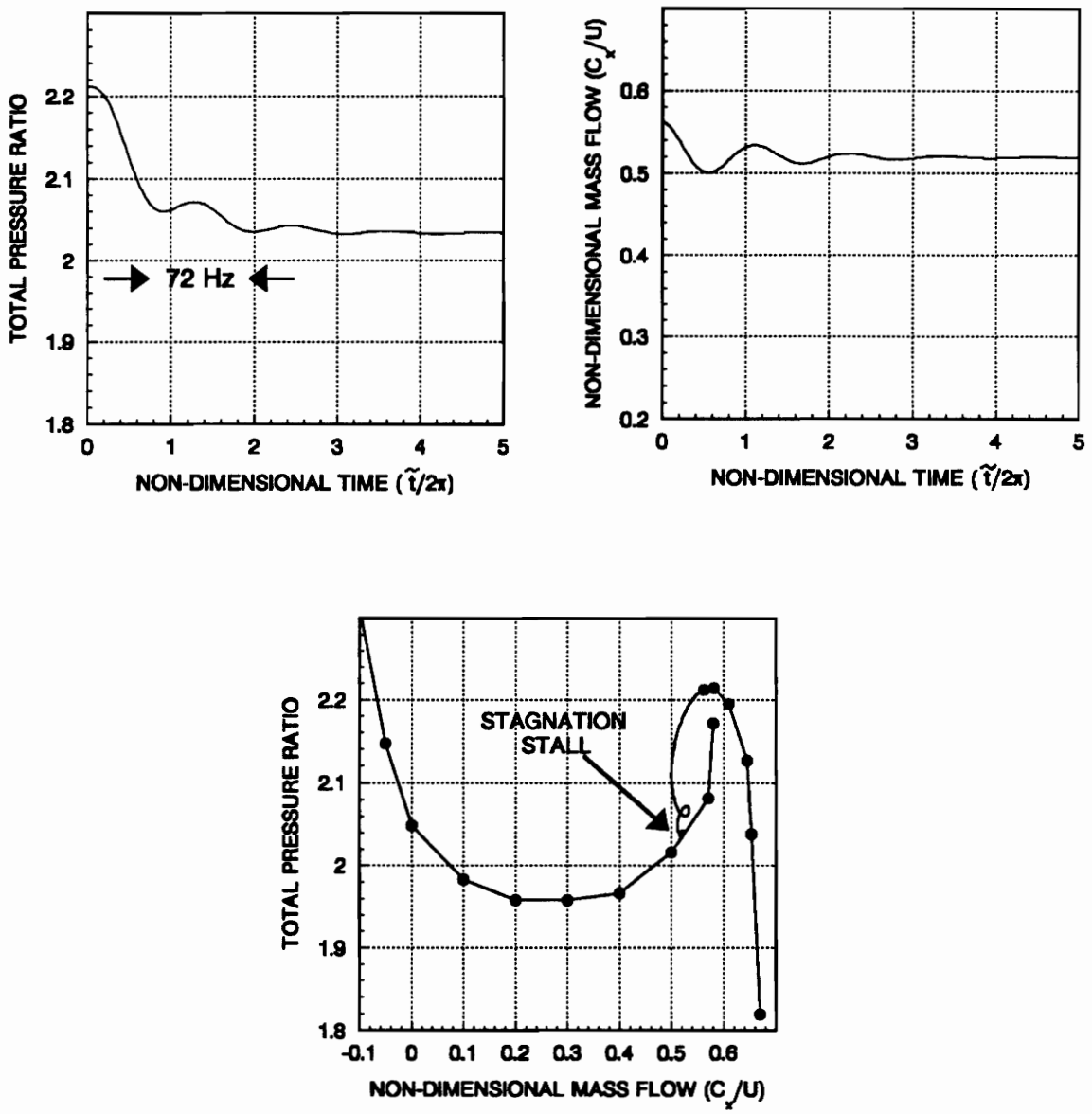

Figure 30. Greitzer's Model Typical Solution for the Cases shown in Table 5.

for figures 29 and 30, respectively. These two cases should ideally be the correct configurations for the matching of the experimental system.

The solutions of all the cases shown in tables 4 and 5 predicts a stagnation stall condition (figures 29 and 30), not a surge type operation. It is hypothesized that Greitzer's model was not able to predict the correct mode of operation (surge or rotating stall) because the ideal system used in the model derivation was not the same system present during the experiment. Greitzer used an ideal system (assumptions outlined above) in the development of his model and in the subsequent experimental rig that was used to verify the model. This ideal system was simply not present in the rotor 37 test rig. There was really no separate plenum present downstream of the Rotor 37 compressor duct. Also, there was really no separate throttle duct present either. The kinetic (compressor duct) and potential (plenum) energies were by no means separate in the system tested, thus the system would not behave the same way that Greitzer's model predicts. Greitzer went to great lengths to insure that his model system and his experimental system were compatible. In this case, the wrong governing equations are being used to model the experimental system. This illustrates the importance of having an identical model and experimental system, as Greitzer did.

Attempts to closer match the predicted surge frequencies of the model, with the measured surge frequency of 16 Hz, were performed by varying the non-dimensional time constant, $\tilde{\tau}$. The non-dimensional time constant was chosen because it could potentially compensate for the differences between the experimental system and the ideal model system. This was believed because experience in running Greitzer's model showed that

adjusting $\tilde{\tau}$ also significantly changed the predicted surge frequency. Thus, $\tilde{\tau}$ was varied in attempts to better match the experimental surge frequency. No actual improvements in the modeling of the existing system are obtained by varying $\tilde{\tau}$; however, it was varied as a last possible effort to improve the model's prediction. Note that $f_{predicted}$ is only a function of the solution of the governing equations of the model.

Table 6 shows the effect that different values of $\tilde{\tau}$ has on the values predicted for the surge frequencies ($f_{predicted}$). Table 6 plots several of the cases presented previously in table 5 (extra plenum volume geometry). The columns indicate different values of $\tilde{\tau}$ and the subsequent values of $f_{predicted}$ that were obtained. The second and third columns again gave solutions predicting rotating stall as observed previously in figures 29 and 30. However, if $\tilde{\tau}$ is continually decreased, surge operation will eventually be predicted by the model. Columns four through seven give solutions predicting surge operation. Thus, only columns four through seven give results even close to the correct values. Also note that if $\tilde{\tau}$ is decreased too much the predicted surge frequency begins to increase. The closest the model could come to the experimental frequency of 16 Hz was 50 Hz. This was obtained for case 11, with B = .787 and $\tilde{\tau}$ = 1.8. Figure 31 shows a plot of this best prediction that was obtained from Greitzer's model. The surge amplitudes are slightly off, but they can be corrected by adjusting the unstable steady-state characteristics as previously discussed. The best prediction possible from Greitzer's model (by adjusting $\tilde{\tau}$) was off by more than a factor of three. Again, the inability of Greitzer's model to predict the correct surge frequency is attributed to the inconsistencies noted between the experimental system and system used to develop the model.

Table 6. Variations of Table 5 by Using Different Values of $\tilde{\tau}$ to Better Match $f$experimental = 16 Hz.

CASE #	$f_{pred}/\tilde{\tau}$ Hz/-	$f_{pred}/\tilde{\tau}$ Hz/-	$f_{pred}/\tilde{\tau}$ Hz/-	$f_{pred}/\tilde{\tau}$ Hz/-	$f_{pred}/\tilde{\tau}$ Hz/-	$f_{pred}/\tilde{\tau}$ Hz/-
1	205/10.2	200/9.0	91/7.5	91/5.1	85/2.6	84/1.0
3	123/6.5	119/5.5	67/4.5	69/3.5	69/2.5	69/1.5
5	98/5.2	96/4.12	58/3.5	60/3.1	62/2.1	63/1.0
8	85/4.4	83/2.8	51/2.5	54/2.2	58/1.1	59/.54
9	81/4.2	79/2.5	51/2.3	51/2.1	57/1.2	59/.56
11	77/4.1	73/1.85	50/1.8	56/1.5	60/1.1	61/.54

ROTATING STALL $\Longleftrightarrow$ SURGE

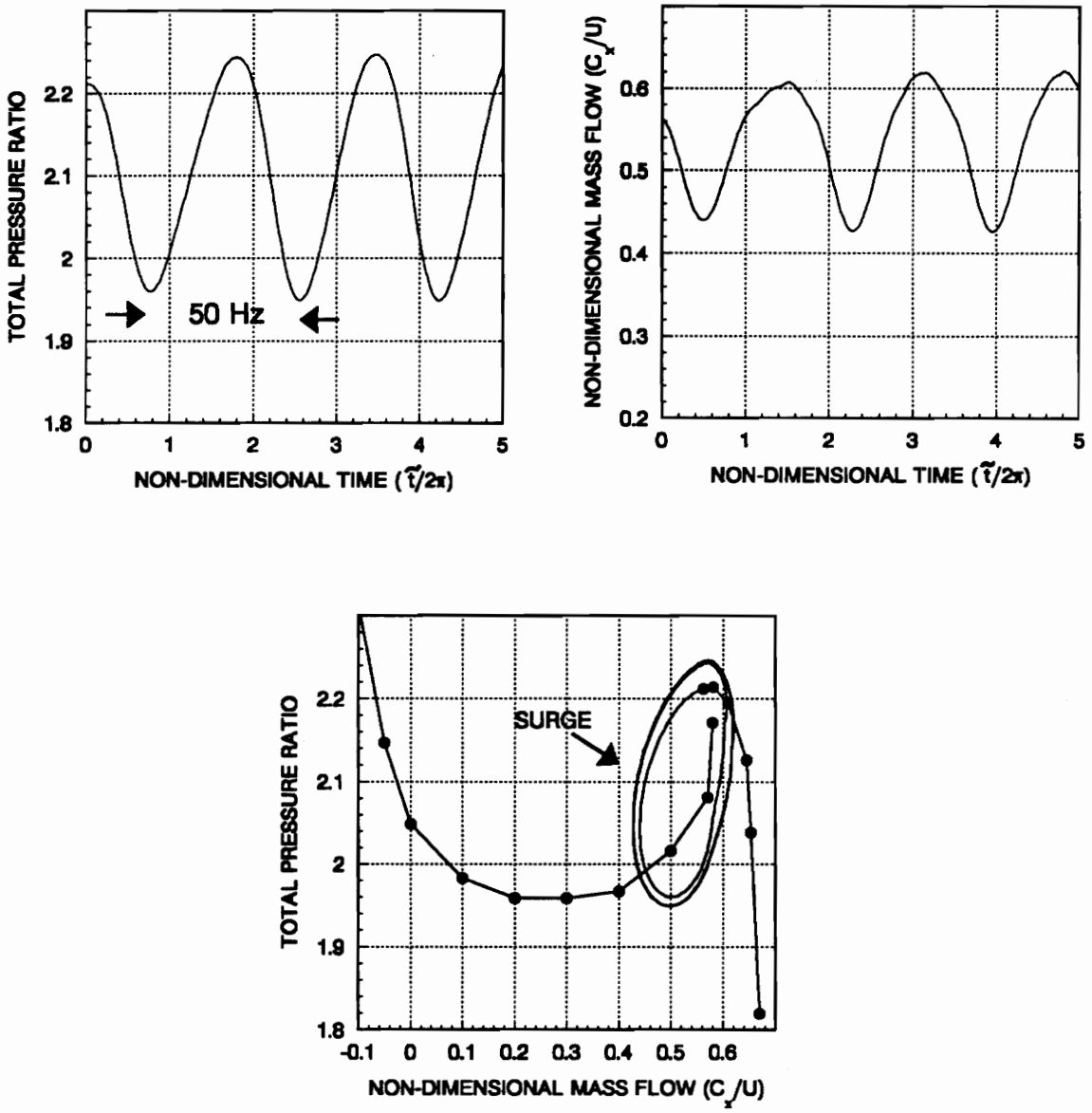

Figure 31. Greitzer's Model - Best Prediction, with B = .787 and $\tilde{t}$ = 1.8.

5.0 Conclusions and Recommendations

This chapter briefly summarizes the results obtained from the transient instability measurements that were taken on the transonic core-compressor rotor. Finally, some recommendations for further research are presented.

5.1 Conclusions

The main thrust of this research was to gain a better understanding of the transient instability flow physics present in a transonic core-compressor rotor. Almost all published literature contains results from low-speed machines only. Thus, the results presented are especially interesting because of the high-speed nature of the machine and the general absence of any similar studies in the open literature.

The unstable transonic flow field at 100% speed was shown to contain both surge and rotating stall phenomena. The stall was shown to rotate at approximately 54% of the wheel speed (286 Hz) and became fully developed after approximately nine rotor

revolutions. Also, the surge frequency (16 Hz) was shown to be an order of magnitude smaller than the rotating stall frequency (155 Hz). These relationships are typical for low-speed machines and were confirmed in this thesis for this transonic machine.

The transonic rotor typically exhibited a fully spanwise, single-cell, large-extent, type rotating stall with a fully developed circumferential extent of 150° (42%) of the compressor annulus. Furthermore, the rotating stall was shown to occur instantaneously across the entire span of the blades. This result is typical for low-speed high hub-tip ratio machines and it is confirmed here for this high-speed high hub-tip ratio machine. The cause of this could be due to the fact that the blades are fully supersonic and it is hypothesized that the shock structure is the driving mechanism for rotating stall in transonic machines (section 2.1). Thus, since the driving mechanism for stall stretches across the entire blade span, it is possible for the machine to exhibit instantaneous fully spanwise stall.

The initial form of the transient instability consisted of a large-extent single rotating stall cell developing only over the first half of the surge cycle. The second half of the surge cycle did not contain rotating stall, rather the compressor was operating with attached, axi-symmetric flow in the stable operating region. This is the typical form of surge/stall coupling that occurred immediately after the machine stalled. These initial surge cycles involved a single-cell large-extent stall with partial operation in both the stable and unstable operating regions. Cycles of this type are widely reported in the literature; however, this was not the only type of surge/stall coupling present on this rotor.

After a few cycles of the typical surge/stall coupling discussed above, surge cycles

changed to the type that contained several smaller-extent rotating stall cells that existed throughout the entire surge cycle. Thus, the compressor was completely operating in the unstable region during these surge cycles. No partial operation in the stable operating region was observed when several small-extent stall cells were present.

This indicates that system recovery from a large-extent single-cell rotating stall will be easier than system recovery from a small-extent multiple-cell type rotating stall. This is apparent because large-extent single-cell stall allows the surge cycle to operate over both the stable and unstable operating regions. However, a small-extent multiple-cell rotating stall causes the surge cycle to operate only in the unstable region. Thus, since no partial operation in the stable operation region occurs the rotor is headed towards a stagnation stall condition. If there was some way to artificially alter the mode of rotating stall present, the chances for recovery would be greatly increased. Furthermore, this indicates that surge cycles are not always characterized by partial operation in the stable and unstable operating regions.

Evidence of coupling between the rotating stall and surge phenomena was discovered and some preliminary attempts at quantification were performed. It was shown that rotating stall and surge are more closely coupled by pressure interactions than by temperature or efficiency interactions. This result was not surprising, because most attempts at modeling unstable operation concentrate on applying fundamental pressure type relationships.

The 100% speed data was dominated by surge; however, the 90% speed data was dominated by rotating stall. The energy content of the surge and rotating stall for the two

speeds was basically reversed. This confirmed the importance of rotational wheel speed upon the form of the transient unstable characteristics present. This effect has been widely documented for low-speed machines and these results extend this behavior to this high-speed rotor.

Attempts made to match the data to Greitzer's non-linear, one-dimensional, lumped-parameter model were unsuccessful in matching the frequency of the predicted surging with that measured during the experiment. This was due to the discrepancy between the ideal system used in the derivation of the governing equations of the model and the actual experimental system that was present. The system present contained no separate compressor duct, downstream plenum or throttle duct. The best match obtained between the measured and calculated surge frequencies was off by more than a factor of three.

5.2 Recommendations

The data presented was taken with a single circumferential probe, this limited the observations and results that could be obtained from the measurements. A second circumferential probe would provide numerous benefits associated with better understanding the transient flow field. A second probe at the same circumferential and axial location, but at different spanwise positions, could resolve questions of whether a noticed phenomena was a spanwise effect or if it was simply an effect of different depths

of system surging during each run. Furthermore, a second probe at a different circumferential location could better analyze stall cell growth studies.

The flow field of rotor 37 was extremely random in nature [29]. Thus, the identification of blade passages was very difficult. It would be very interesting to use the high response probe to measure the transient instability operation of a low speed, nicely behaved rotor. In this case, the flow field would not be so random and blade wakes could be identified. Thus, the time resolved nature of the measurements could be further explored in hopes of finding significant trends in the blade wake patterns at locations just prior to rig stalling. The data presented in this thesis was really not able to take maximum advantage of the high response nature of the measurements because the flow field was so random that blade passage wakes were difficult to locate, much less use to notice trends or changes at the stall inception point.

The position of the downstream throttle should also be digitized during any future experiments of this type. This allows a correlation between trends in the transient unstable operation and the position of the throttle valve. It was impossible to comment upon the effect of the throttle position for the data presented in this thesis.

Also, the mechanism of rotating stall propagation in a transonic rotor should be investigated. All the current theories of rotating stall are based on the flow field properties of low-speed machinery. Transonic rotating stall is indeed a real problem because the current trend in engine design is towards higher and higher blade speeds. Eventually, rotating stall knowledge in low-speed machines must be extended to high-speed machinery.

Appendix A. Raw Transient Stall Data

This appendix presents traces of the raw transient stall data before the averaging technique was applied. All the previous figures in this thesis presented the averaged data. Figures 32, 33, and 34 show plots of raw total pressure ratio traces with the averaged data superimposed. The data is presented in blocks, with each consisting of 4096 data points, 2.34 rotor revolutions, 84 blade passages, or approximately 8 msec. There are also approximately 32 points of averaged data for each block of raw data. The blocks are numbered consecutively from block 62 to block 73 and are denoted by B62 - B73.

The twelve blocks presented constitute more than an entire surge cycle. Blocks 62 and 63 were obtained before the instability occurred. Block 64 contains the first rotating stall passage. The stall then developed during blocks 65, 66, 67, and 68. By block 69, the surge cycle was half complete and the rotating stall began to dissipate. Blocks 70, 71, and 72 represent the second half of the surge cycle, which in this case did not contain rotating stall.

The surge cycle is not as noticeable as the rotating stall. However, it becomes clear if the mean total pressure ratio at block 62 (beginning of cycle) is compared to the

mean total pressure at block 70 (middle of cycle). There is a difference of 0.1 in total pressure ratio which represents the swing associated with the surge cycle. Finally, block 72 is at approximately the same total pressure ratio as block 62, thus the surge cycle was completed. Figure 35 presents a plot of the raw data for the entire surge cycle. The plot indicates the beginning and end of the surge cycle, along with the development of the rotating stall cells. This plot was constructed from the traces shown in figures 32, 33, and 34. The first half of the surge cycle lasted for approximately 49 msec. (74% of the cycle). However, the second half of the surge cycle took only approximately 17 msec. (26 % of the cycle). This indicates a hinderance by the rotating stall to the surge cycle. This is the typical large-extent, single-cell, intermittent rotating stall, surge cycles that were discussed previously.

These plots should give the reader a feel for the difficulty involved in purely presenting and analyzing the raw data. The averaging technique allowed the entire transient instability trace from different spans and speeds to be easily compared for relative flow field content.

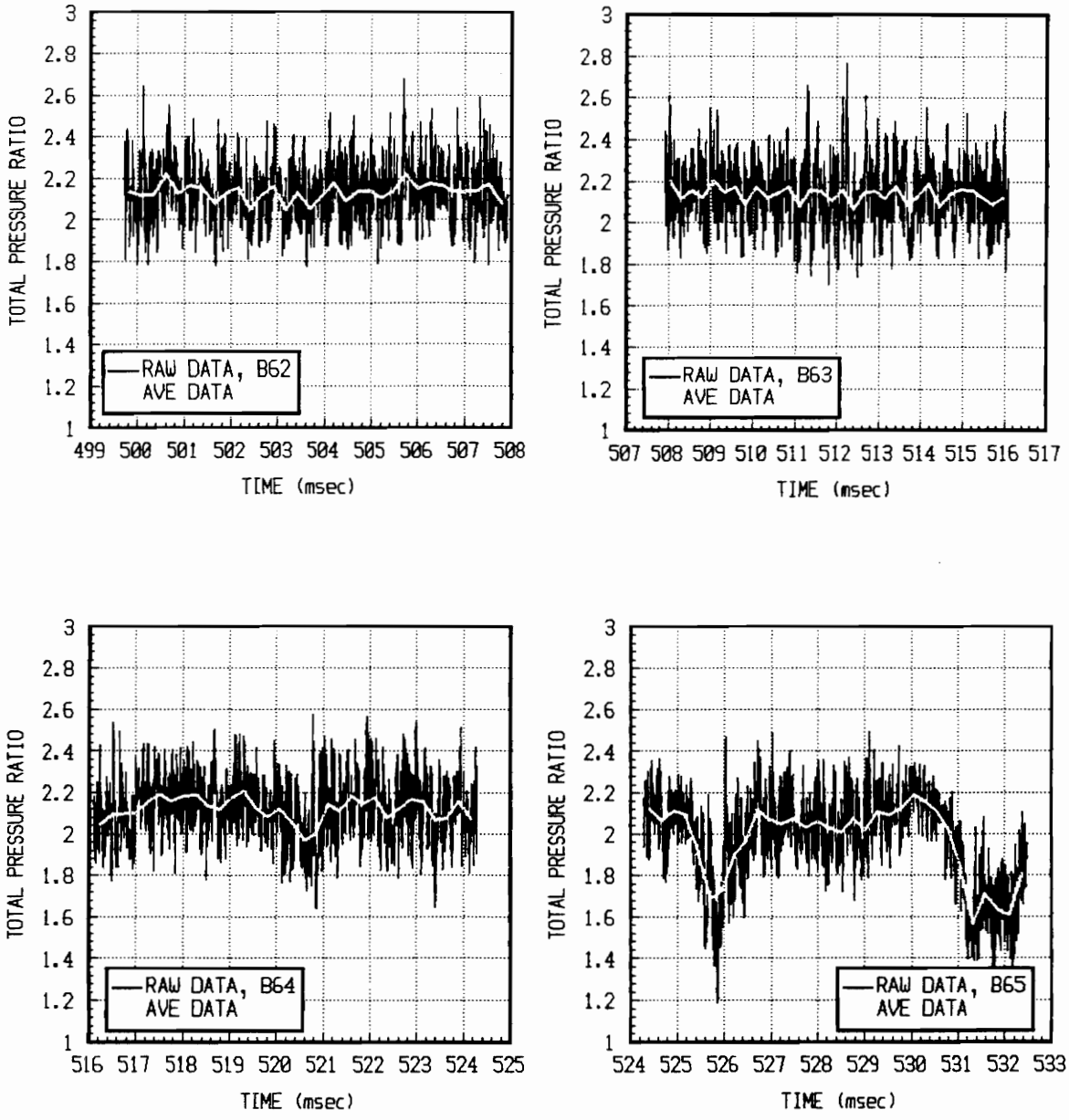

Figure 32. Raw Transient Instability Data - Total Pressure Ratio, B62 - B65.

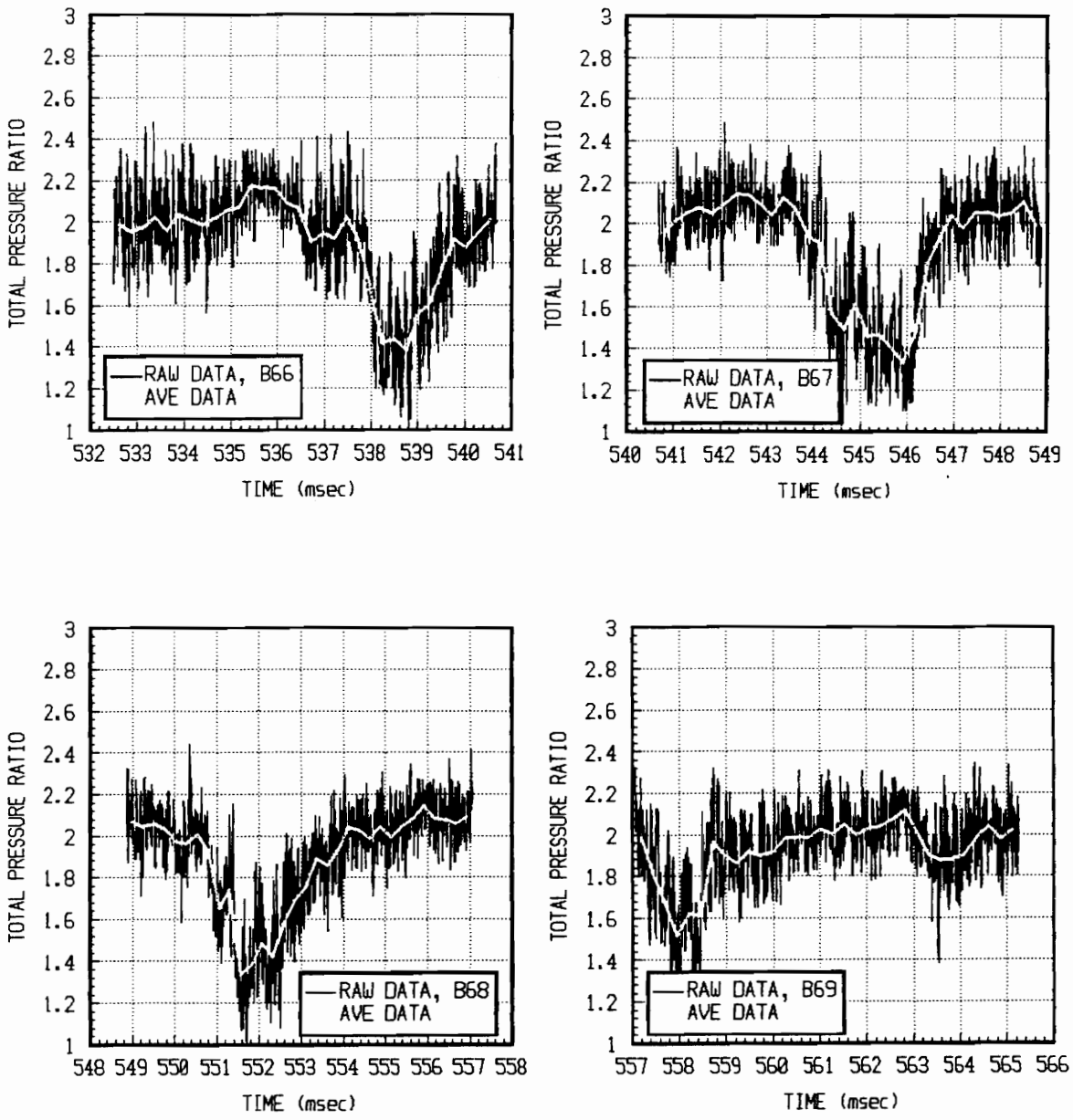

Figure 33. Raw Transient Instability Data - Total Pressure Ratio, B66 - B69.

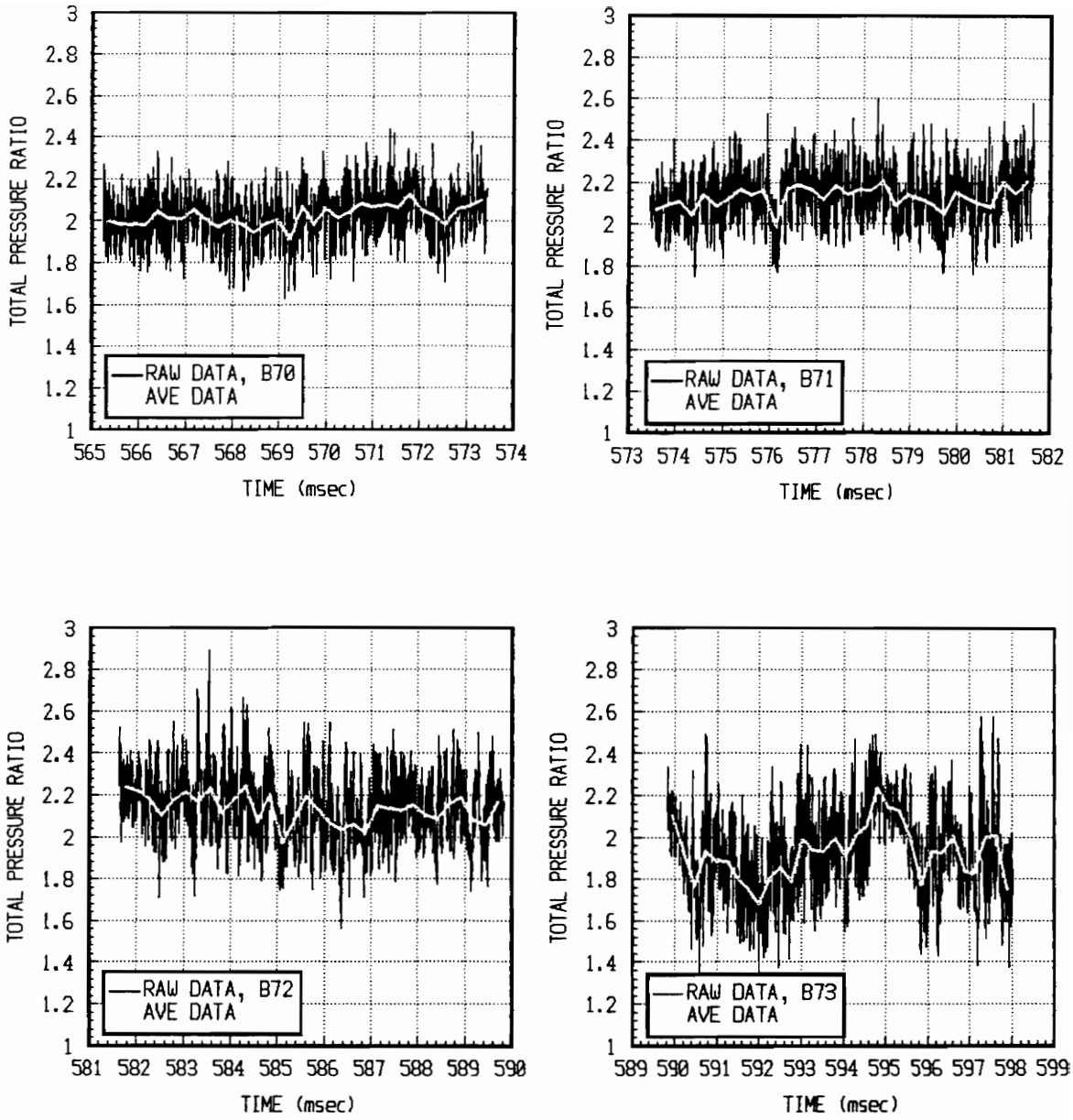

Figure 34. Raw Transient Instability Data - Total Pressure Ratio, B70 - B73.

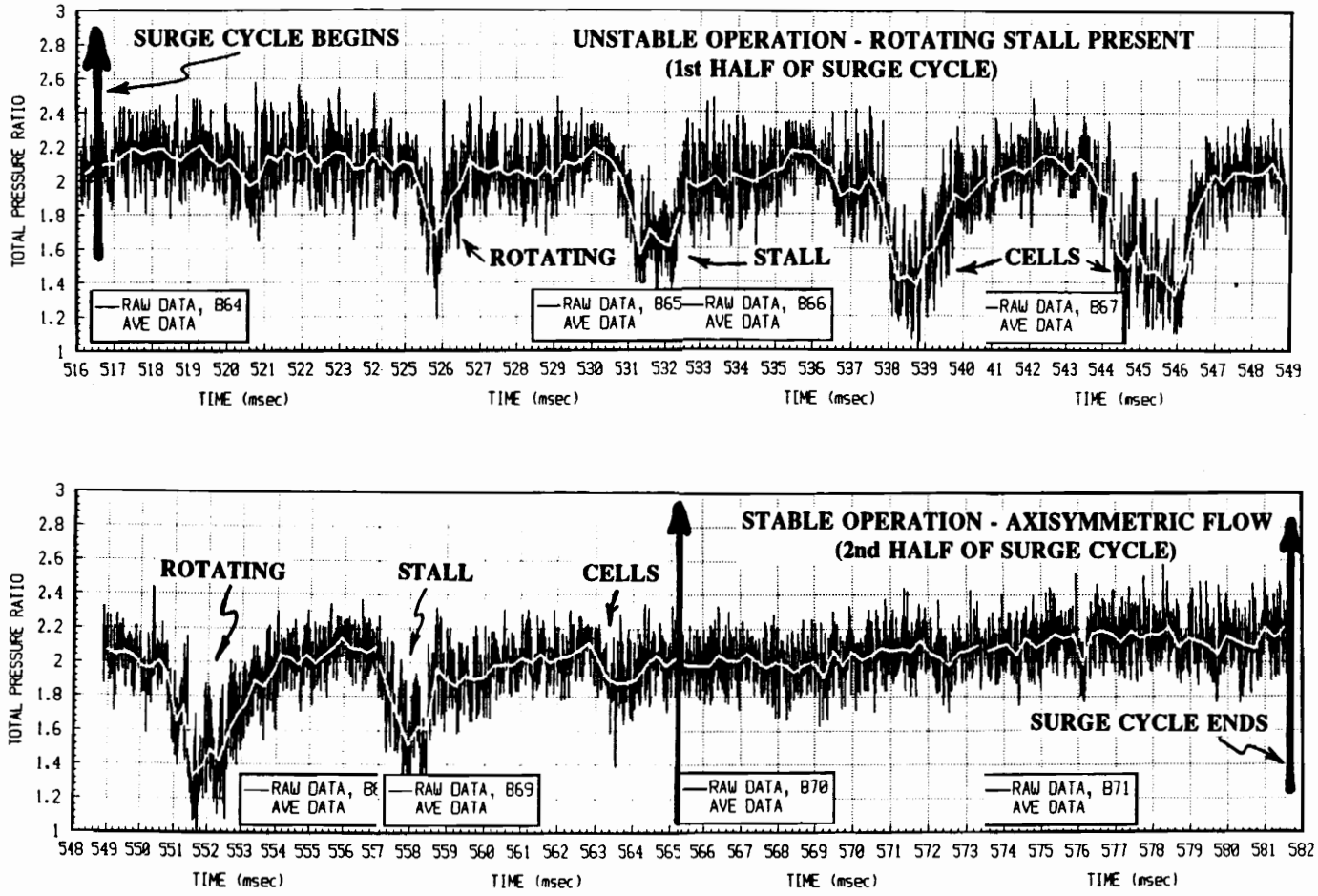

Figure 35. Raw Transient Stall Data - Entire Surge Cycle.

Appendix B. Contour Plots of Transient Instability

This appendix presents some interesting hypothetical contour plots of the transient unstable operation of Rotor 37. Data taken from different spans was ran through a grid generation routine that interpolated intra-span contours. The resulting contour plots contained the full spanwise behavior of the instability versus rotor revolutions in the absolute reference frame. Figures 36 and 37 present contour plots of total pressure and efficiency, respectively.

The data used to generate the grid was taken from consecutive runs to facilitate repeatability. No shifting was involved before the data was entered into the grid generation routine. The surge and rotating stall contents are highlighted on the plot. The surge growth is indicated by an increasingly wider black band that suddenly disappears. The surge content is apparent by the two similar developments and disappearances of rotating stall.

The contour plots further indicate that the entire span of the blade instantaneously undergoes unstable operation. This was expected since the mechanism of rotating stall cells was assumed to be the rotor shock wave (section 2.1); thus, since the blades are

fully supersonic, instantaneous fully spanwise stall is expected. Also, the frequencies from different spans do not change very much over the first surge cycle. There is some frequency shifting between the spans by the second surge cycle. Contour plots of several surge cycles confirms that the rotating stall frequencies vary in time. Furthermore, since the spanwise data was obtained during different times, it was impossible to believe the generated contour plots after a couple of surge cycles.

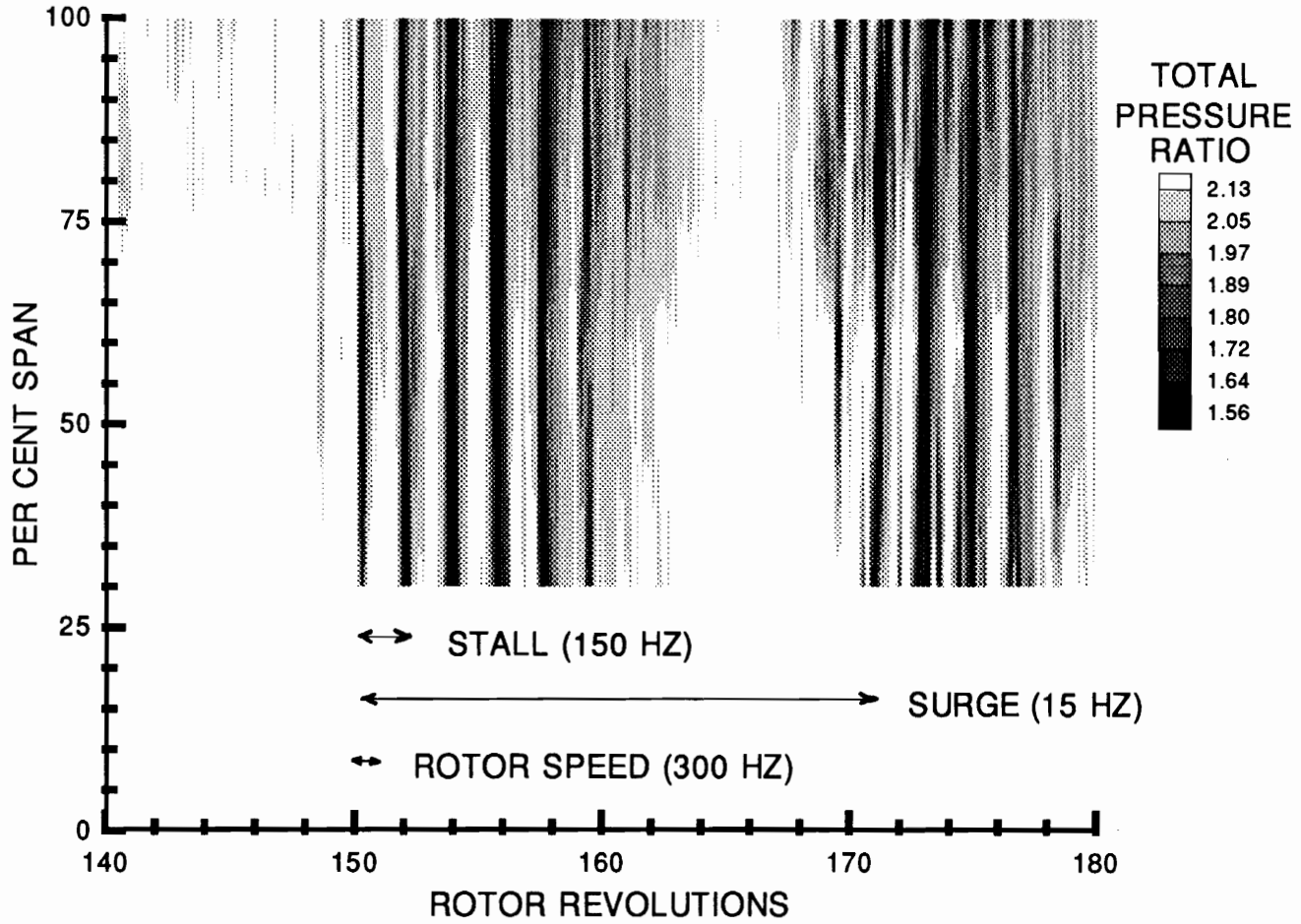

Figure 36. Transient Instability Contour Plots - Total Pressure Ratio.

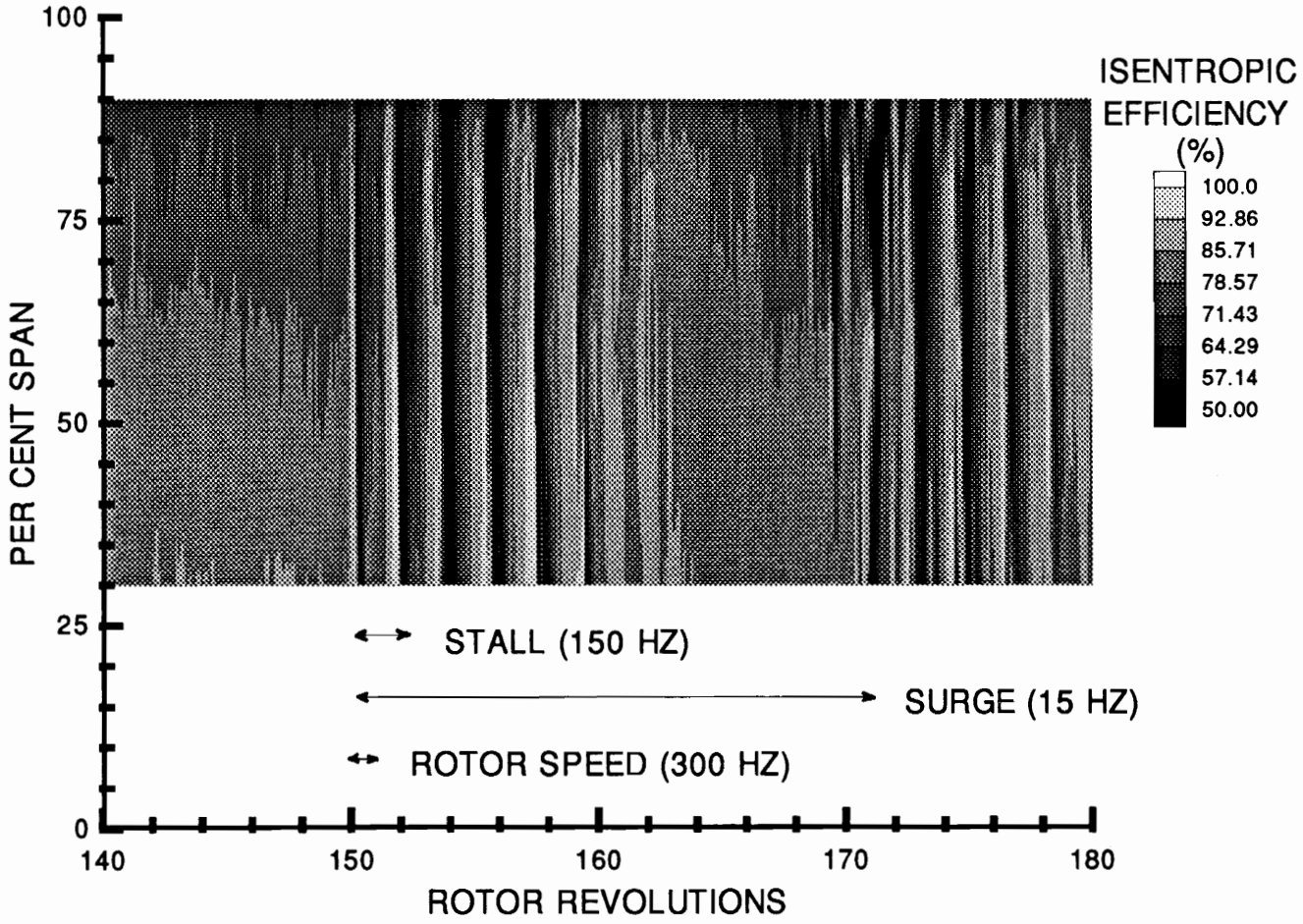

Figure 37. Transient Instability Contour Plots - Isentropic Efficiency.

References

1. Ng, W. F., Epstein, A. H., "A High Frequency Temperature and Pressure Probe for Unsteady Compressible Flows.", *Review of Scientific instruments*, Vol 54, No. 12 Dec. 1983, pp. 1678-1683.

2. Moore, R. D., Reid, L., "Performance of a Single-Stage Axial-Flow Transonic Compressor With Rotor and Stator Aspect Ratios of 1.19 and 1.26, Respectively, and With Design Pressure Ratio of 2.05," NASA Technical Paper 1659, April 1980.

3. Urasek, D. C., Janetzke, D. C., "Performance of Tandem-Bladed Transonic Compressor Rotor with Rotor Tip Speed of 1375 Feet Per Second.", NASA TM X-2484, 1972.

4. Garnier, V. H., Epstein, A. H., and Greitzer, E. M. "Rotating Waves as a Stall Inception Indication in Axial Compressors", *Transactions of the ASME*, Vol. ,1990

5. Moore, F. K., and Greitzer, E. M., "A Theory of Post-Stall Transients in Axial Compression Systems: Part 1 - Development of Equations,"*ASME Journal of Engineering for Gas Turbines and Power*, Vol. 108, 1985, pp. 78-76.

6. Moore, F. K., "A Theory of Rotating Stall of Multistage Axial Compressors: Parts I, II, and III.", *ASME Journal of Engineering for Gas Turbines and Power, Vol. 108*, Vol 106, 1984, pp. 313-335.

7. Greitzer, E. M., "Surge and Rotating Stall in Axial Flow Compressors, Parts I and II.", *ASME Journal of Engineering for Gas Turbines and Power*, Vol. 106, April 1976.

8. Stenning, A. H., "Rotating Stall and Surge", *Journal of Fluids Engineering*, Vol. 102, March 1980, pp. 14-20.

9. Emmons, H. W., Pearson, C. E., Grant, H. P., "Compressor Surge and Stall Propagation", *Transactions of the ASME*, Vol. 77, pp. 455, May 1955.

10. Greitzer, E. M., "Review - Axial Compressor Stall Phenomenon", *Journal of Fluids Engineering*, Vol. 102, June 1980.

11. Iura, T., and Rannie, W. D., "Experimental Investigations of Propagating Stall in Axial-Flow Compressors", *Transactions of the ASME*, April 1954.

12. Bölcs, Albin, Institut de Thermique appliquée, Lausanne, Switzerland, Personal Communication, August 1992.

13. O'Brien, W. F., Professor, Virginia Polytechnic Institute and State University, Blacksburg, Va., Personal Communication, August 1992.

14. Huppert, M. C., and Benser, W. A., "Some Stall and Surge Phenomena in Axial-Flow Compressors", *Journal of the Aeronautical Sciences*, January 1953.

15. Emmons, H. W., Kronauer, R. E., and Rockett, J. A., "A Survey of Stall Propagation - Experiment and Theory", *Transactions of the ASME: Journal Of Basic Engineering*, Sept. 1959.

16. Pearson, C. E., "Surge Behavior in a Three-Stage Compressor", *Journal of the Aeronautical Sciences*, November 1955.

17. Rockett, J. A., "Modulation Phenomena in Stall Propagation", *Transactions of the ASME: Journal Of Basic Engineering*, Sept. 1959.

18. Bullock, R. O., Wilcox, W. W., and Moses, J. J., "Experimental and Theoretical Studies of Surging in Continuous-Flow Compressors", NASA Report 861, NACA Technical Note No. 1213, 1946.

19. Day, I. J., and Cumpsty, N. A., "The Measurement and Interpretation of Flow within Rotating Stall Cells in Axial Compressor", *Journal of Mechanical Engineering Science*, Vol. 20, No. 2, 1978.

20. Day, I. J., "Detailed Flow Measurements During Deep Stall in Axial Flow Compressors", AGARD Conference Proceeding 177, 1976.

21. Day, I. J., "Active Suppression of Rotating Stall and Surge in Axial Compressors", *Transactions of the ASME*, 1991.

22. Day, I. J., "Stall Inception in Axial Flow Compressors", *Transactions of the ASME*, 1991.

23. McDougall, N. M., Cumpsty, N. A., and Hynes, T. P., "Stall Inception in Axial Compressors", *Transactions of the ASME: Journal of Turbomachinery*, Vol. 112, January 1990.

24. Moore, R. D., and Reid, L., "Design and Overall Performance of Four Highly Loaded, High Speed Inlet Stages for an Advanced High-Pressure Ratio Core Compressor," NASA TP-1337, 1978.

25. Hauser, C. H. et al, "Compressor and Turbine Technology," *Journal of Aeronautical Propulsion*, NASA SP-381, 1975, pp. 229-288.

26. Suder, Ken, NASA Lewis Research Center, Cleveland, Ohio, Personal Communication, November 1991.

27. Ng, W. F., "Detailed Time Resolved Measurements and Analysis of Unsteady Flow in a Transonic Compressor," Master of Science Thesis, Department of Mechanical Engineering, Massachusetts Institute of Technology, Cambridge, Mass., Sept. 1980.

28. Ng, W. F., "Review - Simultaneous Measurements of Stagnation Temperature and Pressure Using an Aspirating Probe," International Symposium on Pressure and Temperature Measurement, ASME Winter Annual Meeting, December 1986.

29. Alday, J. H., "The Correlation of Randomness with high Tip Losses in an Axial Flow Fan Stage,", Master of Science Thesis, Department of Mechanical Engineering, Virginia Polytechnic Institute and State University, May 1991.

30. Morris, M. B., Osborne, D. J., Ng, W. F., "Flow Randomness and Tip Losses in Transonic Rotors.", NASA Contractors Report, May 1992.

31. Strazisar, A. J., NASA Lewis Research Center, Cleveland, Ohio, Personal Communication, March 1991.

32. Morris, M. B., "Flow Randomness and Tip Losses in Transonic Rotors.", Master of Science Thesis, Department of Mechanical Engineering, Virginia Polytechnic Institute and State University, May 1991.

33. Moore, R. D., NASA Lewis Research Center, Cleveland, Ohio, Personal Communication, April 1992.

Vita

Denver Jackson Osborne, Jr. was born on October 9, 1967 in Wise, Virginia. He completed his high school education in 1985, graduating with honors from J.J. Kelly High School in Wise, Va. After a year spent at Clinch Valley College taking first year basics, the author moved to Blacksburg, Va. in the fall of 1986 to begin his engineering education at Virginia Tech. After changing his major from chemical to civil and finally to mechanical engineering, the author graduated *cum laude* from Virginia Tech in the spring of 1990. The author spent the summers during his undergraduate years working as a civil engineering assistant at Thompson & Litton Engineering in Wise, Va. The author entered graduate school the fall of 1990 and immediately began building the instrumentation employed in this thesis. November 1991 was spent at the NASA Lewis Research Center in Cleveland Ohio, where the author instrumented the transonic rotor discussed in this thesis. The author defended this thesis on August 17, 1992 and is conducting post-graduate research for Dr. W. F. Ng until a more permanent employment position is secured.

Denver Jackson Osborne, Jr.